MEASUREMENT OF STEADY STATE FUNCTIONAL CONNECTIVITY IN THE HUMAN BRAIN USING FUNCTIONAL MAGNETIC RESONANCE IMAGING

By

ALLEN TIMOTHY NEWTON

Dissertation

Submitted to the Faculty of the

Graduate School of Vanderbilt University

in partial fulfillment of the requirements for

the degree of

DOCTOR OF PHILOSOPHY

in

Biomedical Engineering

May, 2009

Nashville, Tennessee

Approved:

Professor John C. Gore

Professor Victoria L. Morgan

Professor Adam W. Anderson

Professor Ronald R. Price

Professor Richard G. Shiavi

TABLE OF CONTENTS

Page

ACKNOWLEDGEMENTS

Over the course of my graduate studies here at Vanderbilt, there are several people that deserve special acknowledgement for their contributions to my development, and thus to this body of work. Some have supported me on a personal level, while others have clearly contributed to my academic development.

First let me make some personal acknowledgements. I want to start by acknowledging the Lord, who underlies all of my successes. Secondly, my wife Stephanie deserves special recognition. She supports me in the truest sense of the word, and has done so selflessly from the first day of our marriage. Sharing my life as a graduate student with her has made this work more than just interesting, it has made it enjoyable. Finally, my parents deserve special recognition as well. They nurtured me when I was a child, they supported me as a young adult, and they continue to love and advise me as a married man. Their willingness to sacrifice for my education has played a significant role in making this achievement possible.

Academically speaking, there are several people that must be recognized for their contributions to my professional development, and first on that list is Dr. John Gore. His support as a mentor and that of the institution under his direction has been invaluable. His ability to bring a broader perspective to these very specific studies has meant that the right questions were asked, and were then answered. Second is the unsung hero of this work, Dr. Victoria Morgan. It was her monthly, weekly, and (frequently) daily advice that provided me the raw material I needed to learn. Whether her advice came in the form of gentle critiques, collaborative discussions, or outright confrontation, I can

honestly say that her points of view were virtually always correct, and her well intentioned comments always led to my learning something important.

Finally, let me say that separating these special people into groups based on personal or professional contributions is actually unfair. Each of these people has contributed to my development both personally and professionally. Be they mentors, parents, or my wife, I count each of these outstanding people as sincere friends, and they deserve credit as you read the work contained in this thesis.

I also acknowledge the National Institute of Health, who provided the funding of these studies through the following grants: T32 EB03817, R01 EB00461.

LIST OF TABLES

LIST OF FIGURES

LIST OF ABBREVIATIONS AND SYMBOLS

Symbol / Abbreviaiton	Description
θ	flip angle
ANOVA	analysis of variance
AUD	auditory cortex
B_0	static magnetic field
B_1	transient RF magnetic field
BOLD	fMRI
CB	cerebellum
CNR	contrast to noise ratio
EEG	electroencephalography
EPI	echo planar imaging
fMRI	functional magnetic resonance imaging
FMθ	frontal midline theta power
FOV	field of view
FWE	family wise error
GLM	general linear model
H	Shannon entropy
ICA	independent component analysis
IQ	intelligence quotient
LCD	liquid crystal diode
LPFC	left prefrontal cortex
MPC	mean partial correlation

Symbol / Abbreviaiton	Description
MI	mutual information
MRI	magnetic resonance imaging
PAT	percent above threshold
PCA	principal component analysis
PCC	posterior cingulate cortex
PHG	parahippocampal gyrus
PIC	path independent connectivity
PM	primary motor
PMC	primary motor cortex
pSMA	pre-supplementary motor area
r	Pearson's correlation coefficient
ROI	region of interest
RETROICOR	retrospective image based correction of physiological artifacts
ROCC	right occipital cortex
SENSE	sensitivity encoding
SOM	self organizing map
SMA	supplementary motor area
SNR	signal to noise ratio
SPM	statistical parametric map
T_1	longitudinal magnetization time constant
T_2	Transverse magnetization time constant

Symbol / Abbreviaiton	Description
T_2^*	Transverse decay time constant including magnetic field inhomogeneity effects
TE	echo time
TR	repetition time

CHAPTER I

INTRODUCTION

Functional magnetic resonance imaging (fMRI) relies on the detection and analysis of temporal signals that are indirectly sensitive to neuronal activity. Maps of cognitive networks based on these signals may be generated through the construction and analysis of models based on a priori knowledge of carefully designed tasks performed during image acquisition. However similar network maps can be generated through analysis of residual fMRI signal variance in cognitive steady states, absent of changes in the prescribed cognitive task. These analyses are generally referred to as measurements of functional connectivity. While steady state functional connectivity analyses, and in particular resting state functional connectivity analyses, have generated quite a bit of interest, important questions remain regarding their implementation and interpretation. The following body of work is an attempt to address some of these shortcomings in the communal understanding of steady state functional connectivity analyses.

Functional Magnetic Resonance Imaging

Overview

Functional magnetic resonance imaging has become an important and useful tool for observing hemodynamic changes through time in cerebral vasculature, and has been used in neuroimaging for almost 20 years. FMRI is a non-invasive method of generating

and observing contrast between functionally separable regions of gray matter, and is usually used to map cerebral activity tomographically. Simply put, fMRI is used to identify what parts of the brain are being activated during carefully designed cognitive tasks. FMRI has made significant contributions to fields such as neuroscience, psychology, and medicine among others. In order to understand fMRI based measures of functional connectivity, it is important to start with a brief introduction to standard fMRI concepts, as these underlie more complicated functional connectivity analyses.

The central assumption underlying fMRI is that localized hemodynamic changes (vasodilation, increased blood flow and oxygen consumption) are proportional to underlying neuronal tissue electrical activity. (Logothetis, et al. 2001; Mathiesen, et al. 1998) Due to its reliance on sensitivity to hemodynamic changes, fMRI indirectly marks changes in neural activity. Typical fMRI studies employ gradient echo excitations to measure signals produced by the bulk nuclear magnetization of hydrogen protons, whose magnetic moments can be spatially localized via echo planar gradient schemes. (Mansfield 1977; Worthington and Mansfield 1990) Inhomogeneity in the static magnetic field, as is present with the introduction of endogenous paramagnetic agents like deoxyhemoglobin, results in dephasing of nearby nuclear spins, yielding signal decreases. (Ogawa, et al. 1990) When focal regions of gray matter are recruited for the performance of a specific task (performed during image acquisition), the natural hemodynamic response over compensates for increased oxygen consumption, washing out newly formed deoxyhemoglobin, and locally increasing the magnetic field homogeneity, resulting in increased signal. This blood oxygen level dependent (BOLD) contrast results in increased image brightness in regions recruited for the performance of

the given task. BOLD contrast is emphasized in gray matter through choosing echo times approximately equal to the measured T_2^* relaxation time (Bandettini, et al. 1994) of that tissue. While there are incentives to acquire fMRI data in as large of a static magnetic field as is possible, typical fMRI can and has been performed using commonly available clinical hardware. (Constable, et al. 1993; Jack, et al. 1994)

Typical Analysis - Preprocessing

Analysis of fMRI data takes a variety of forms, many serving specific functions, and each with its merits and shortcomings. While the specific methods/algorithms used may vary, many of the goals of typical fMRI analyses remain the same. FMRI data are usually distilled down to maps of activation via a variety of statistical tests. This activation results from performance of some prescribed cognitive task. From this point forward, activation will be used to describe BOLD signal increases, probably associated with increases in neuronal firing, typically during an organized task. Several methods of removing artifacts from, or preprocessing, signals before such analysis have become common. These include motion correction, slice timing correction, and spatial smoothing.

The need for motion correction arises from the fact that in fMRI studies, a series of images are gathered over a period of time on the order of tens to hundreds of seconds, during which the subject may move, thus destroying the registration between image volumes. (Friston, et al. 1996) This can be a particular problem in analysis of some tasks because the task itself can induce head motion. An example of this is when a subject's head moves in step with squeezing a hand held responder. However, more subtle sources

of motion have also been problematic, such as that associated with swallowing of saliva. (Birn, et al. 1999) While motion artifact within the acquisition time of a single image volume is difficult to correct (typically this is minimized by using as short of an acquisition time as possible), motion between image volumes reduces to an image registration problem, commonly solved through maximization of spatial mutual information between images. (Maes, et al. 1997)

Slice timing correction refers to the removal of an artifact resulting from the acquisition of multiple slices, one at a time, to create a volume. (Kneeland, et al. 1986; VandeMoortele, et al. 1997) In this case, each slice is acquired as a separate image, and is temporally separated from the previous slice by at least the time required for one full sampling of k-space, often by more. In an attempt to reduce signal losses arising from magnetization saturation effects, slices are frequently sampled in an interleaved fashion, such that if six slices were acquired, they would be sampled in the following order: 1, 3, 5, 2, 4, and 6, thus increasing the time between adjacent slice acquisitions. If the repetition time for the entire set of slices is 2 seconds, slice 1 and slice 2 may be acquired 1 second apart, though they are collapsed into the same imaging volume that is commonly thought of as being acquired at one point in time. Slice timing correction methods attempt to account for this difference in slice acquisition times, usually by temporal interpolation either of task regressors or of the data. (Friston, et al. 1998; VandeMoortele, et al. 1997)

Spatial smoothing serves to reduce the effects of spatially independent noise in any given image, though it can be used for other purposes as well. (Fransson, et al. 2002) Spatial smoothing commonly involves computing a weighted average of neighboring

voxels via convolution with a filter kernel, thereby reducing very high spatial frequencies in the image. To reduce the effects of high spatial frequencies, one could also decrease the contributions to the image from the edges of k-space, though both approaches risk eliminating weak activations and blurring out focal activations. In the practice of comparing activity maps from individual subjects on a group level, spatial smoothing has been promoted as a method for increasing the overlap between subjects through the blurring of individual differences in activation.

Typical Analysis – The GLM

So far, the methods of data analysis discussed do not address the extraction of activity information from the data. They simply prepare the data for more reliable analysis through removing acquisition artifacts, and thus are considered as 'preprocessing' steps. Once complete, the data may be subjected to several types of further analysis to detect activation.

Extracting activity information is the most common objective of fMRI, and is typically done by assuming that a general linear model (GLM) of the task can be used to fit the data. (Friston, et al. 1995a; Friston, et al. 1995b; Friston, et al. 1994a; Friston, et al. 1994b) This method basically consists of testing the accuracy of a specific hypothesis or model for how the signal is expected to behave. This is done through determining the linear relationship between the model parameters and the data. An example of a simple model is shown in equation 1.1, where y(t) is the time series of a single voxel, x(t) is one regressor being tested, and e(t) is the residual error of the total model. The model is considered to be the sum of all the regressors, each multiplied by its respective beta

$$y(t) = \beta_1 \cdot x_1(t) + c + e(t) \tag{1.1}$$

weight plus the constant term. Estimation of the model parameters β and c is commonly accomplished through implementing an ordinary least squares solution. The term β, or beta weight, is a measure of how well the regressor predicts the data. Construction of regressors is commonly done through use of the time course of a particular stimulus simultaneously presented with data acquisition temporally convolved with a canonical hemodynamic response function. The canonical hemodynamic response can take a variety of forms, with a common one being that of a gamma function. The residual error represents the variance of y(t) that can not be explained by a linear manipulation of the regressor. It is useful to remember that these models are applied on a voxel-by-voxel basis, where the signal and regressors are 1D time courses.

This model is flexible in that multiple regressors can be simultaneously evaluated, with each regressor having its own beta weight, as is shown in equation 1.2. The constant term is usually modeled as a unity time course, thus leaving the β parameters as

$$y(t) = \beta_1 \cdot x_1(t) + \beta_2 \cdot x_2(t) + \beta_3 \cdot x_3(t) + \beta_4 \cdot x_4(t) + c + e(t) \tag{1.2}$$

the only ones needing estimation. So long as each regressor is orthogonal to the others, beta weights represent how well a given regressor fits the data. If any regressors are not orthogonal, then the beta weights may underestimate the true amount of variance explained by those regressors. After estimation of all the model parameters, it then becomes possible to test for effects through interrogation of the beta weights. Here it

becomes useful to change to matrix notation. Equation 1.2 can be rewritten in terms of a two dimensional matrix of regressors (X; rows=model #, columns = time), and a column matrix of beta weights (B) for those regressors, shown in equation 1.3. Regressors can be tested for significance by comparing their beta weights against the standard error of the whole model. In the case

$$y(t) = BX + e \tag{1.3}$$

where one regressor is expected to explain all of the conditions of interest, for example when you only have two conditions and the time course of one condition is the inverse representation of the other (i.e. block designed tasks of stimulation verses rest), interrogation of the beta weight for that one regressor completely tests for significant differences between conditions. This test can be done in matrix form by taking the dot product of *B* with a contrast matrix (called the estimate of the effect), and dividing by the square root of the estimated variance of that product (called the variance of the effect), yielding a t-statistic. This is shown in equation 1.4. The contrast matrix will have one value for each regressor, with zeros for all regressors not being tested, and a one in the place of the regressor being tested. If there are four regressors, and the first one is

$$T = \frac{c'\beta}{\sqrt{est\left(\mathrm{var}\left(c'\beta\right)\right)}} \tag{1.4}$$

tested for significance, then the contrast matrix 'c' is a column matrix c=[1 0 0 0]. If two regressors need to be compared, as is the case when there are multiple conditions and

several may serve as an interesting baseline condition, then the contrast matrix can be manipulated to account for this test as well. If we are contrasting the first regressor against the second, then the contrast matrix becomes c=[1 -1 0 0]. This highlights the flexibility of the general linear model, though the obvious limitation is that your test is only as good as the regressors that are put into the model.

It may be useful to generally discuss some aspects the general linear model and its application to fMRI data. An underlying assumption of general linear models is that the hemodynamic response to changes in neuronal activation is linear. (Dale and Buckner 1997) Because changes in neural activity generally produce changes in signal, and because task performance is related to neural activity, the model of the data used is typically a model of the task, with specific signal regressors representing various task conditions. In addition, the hemodynamic response and its temporal effects must be incorporated into the model because BOLD signals are hemodynamic in origin. This can be accomplished through a convolution of each regressor with an estimate of the hemodynamic response function. The goodness of the fit of the model is used as a surrogate measure of the effect of the task on the signal, and thus neuronal activity from that volume of tissue.

Functional Connectivity Analysis

What is Functional Connectivity?

While typical BOLD fMRI analyses involve detecting potential signal changes using a priori knowledge of the task design, designing tasks for which these predictions

can be made can become extremely difficult and may not be necessary to map functional networks across the brain. Alternatively, fMRI studies of inter-voxel temporal similarities can be used to map functional networks using functional connectiivty. Functional connectivity may be broadly described as measurable similarity between neurophysiologic signals originating from spatially distinct regions of the brain. (Friston, et al. 1993) Similarity between neurophysiologic signals has been used as a measure of functional relationships for decades in electrophysiological studies (Gerstein and Perkel 1969; Perkel, et al. 1967), and most fMRI analyses make use of this idea. The difference between fMRI based functional connectivity analyses and typical fMRI mapping techniques is that measures of functional connectivity, in principal, rely only on signals contained within the data themselves, meaning that knowledge of task design is not necessary. Restating this point, common fMRI activity studies compare a model to the signal from single voxels, whereas functional connectivity studies compare the signal from one voxel to that from another voxel. This point is highlighted by the development of steady-state functional connectivity measures where task related temporal variance in BOLD signals is minimized, with the most popular being measurements made in the resting state (i.e. the subject is asked to lie still with their eyes closed and do nothing). Steady state measurements will be referred to as those made while the subject is instructed to keep their cognitive state constant. Functional connectivity analyses are one of a relatively few methods available for studying functional organization of the brain at rest. Furthermore, the development of reliable steady state measures of functional connectivity allows fMRI mapping techniques to be performed in situations where

subject compliance may be difficult or impossible to achieve, broadening the potential uses of these measurements in a clinical setting.

The above definition of functional connectivity may appear vague, partly because the term 'functional connectivity' has been used by different people to mean different things. (Horwitz 2003) In general, most investigators agree that functional connectivity analyses should focus on analyzing temporal variance that is not related to the performance of a task, and yields only a functional measure of the 'connectedness' of two regions. This is different from anatomic connectivity because these regions need not be directly linked via physical nerve fibers, though it is assumed that they communicate with intermediary regions potentially playing a role between them. Functional connectivity generally does nothing to tell the investigator which region is affecting the other, or said differently, it establishes no cause and effect relationship between brain regions. It simply identifies regions whose neurophysiologic signals are similar, generally identifying functionally related networks of brain regions.

The first fMRI study of functional connectivity in the resting state was performed at the Medical College of Wisconsin illustrating that virtually the same motor network map achieved through analysis of data acquired during a finger tapping task could be generated though measuring the correlations of low frequency BOLD signals at rest. (Biswal, et al. 1995) This study made two important contributions to the greater fMRI community. First, this provided a method for probing functional relationships across the brain in the resting state. Second, this study identified the functional significance of low frequency fluctuations in BOLD signals, which may have gone underappreciated previously.

Steady State Functional Connectivity Analysis

The first step in understanding functional connectivity analyses is clearly identifying what signals we are interested in, what potential confounding covariates are, and how they can be removed. Going back to Biswal's original analysis, it was suggested that low frequency (<0.1Hz) BOLD signals contained the majority of the information needed to construct resting state motor maps. (Biswal, et al. 1995) Studies critically sampling cardiac and respiratory variations confirm that the variance underlying resting state functional connectivity maps (remember this is one subset of steady state experiments) primarily lie in the 0-0.1Hz range. (Cordes, et al. 2001) It has also been shown that these signals are truly of a hemodynamic origin, as opposed to being an artifact of measurement via fMRI, evidenced by studies of BOLD signals in near-infrared data. (Obrig, et al. 2000) These signals have been described as representing 'intrinsic variance' due to their existence in cognitive steady states where task driven signal variance is minimized. However, intrinsic fluctuations are present during task performance as well, and some evidence suggests that they add linearly to task induced variance. (Fox, et al. 2006)

The minimization of artifacts is an important part of steady state functional connectivity analyses. Common practices include temporally low pass filtering steady state data at 0.1Hz to remove the potential for higher frequency noise while preserving necessary variance for construction of functional connectivity maps. Motion artifacts are almost always reduced through the application of registration techniques, though residual motion artifacts frequently exist temporally. As such, linear regression of the six standard

estimated motion parameters (usually estimated during the initial motion correction via coregistration) is common, as is removal of very low signal drifts not uncommon in fMRI data. Finally, because functional networks are presumed to be focal, fluctuations occurring on the spatial scale of the whole brain are commonly assumed to be confounding, thus linear regression of the global time series (the average temporal signal across the whole brain) has become common as well.

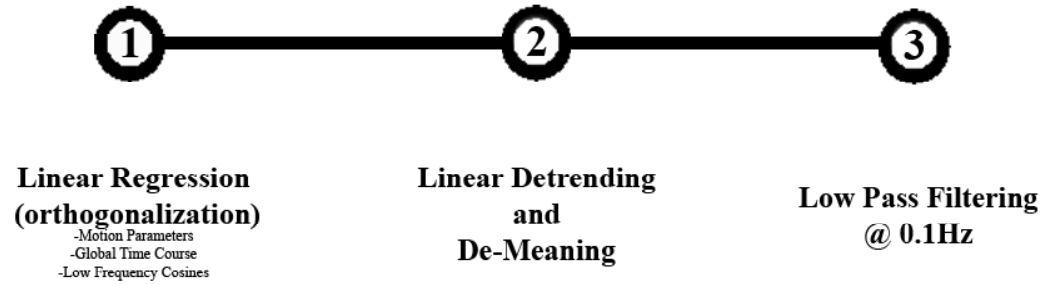

Figure 1.1 - Typical processing steps taken prior to steady state functional connectivity analysis.

The majority of steady state functional connectivity analyses fall into one of two categories. These categories are seed region analyses and data-driven analyses of which independent component analyses are the most commonly used. While these categories differ in several ways, their goals remain the same. Both approaches attempt to identify regions of the brain whose BOLD signals co-vary, thus constructing networks of related, functionally relevant BOLD signals. The two most important differences between these categories of analyses are the a priori information needed and the interpretation of their results.

Independent component analysis of fMRI data began as a solution to the cocktail party problem. (Bell and Sejnowski 1995) Blind source separation of input signals into maximally independent, or minimally redundant, source signals is the process that has become known as independent component analysis (ICA). Similar to less generalized principal component analyses, data are reduced to a set number of components together representing the original signal. If we describe fMRI data as being two dimensional (one spatial dimension representing spatial location and one dimension representing time), ICA analysis of fMRI data must a priori assume spatial independence of the signals (a.k.a spatial ICA, the most common type for fMRI data) (McKeown, et al. 1998; McKeown and Sejnowski 1998), or temporal independence (Calhoun, et al. 2001), or some combination of the two used in conjunction. (Seifritz, et al. 2002) An important feature of ICA techniques is the blind part of blind source separation. This means that sources of variance are identified, and their variance isolated, without any a priori knowledge of the sources required, and it is this feature that has garnered the approach a great deal of attention. The output of a spatial ICA of fMRI data is a number of maps constructed from functional signals on the individual subject level, each potentially representing functionally relevant networks. Each map identifies regions whose signals are similar, which are interpreted as being functionally connected.

However, ICA of fMRI data suffers some significant limitations. The fact that these calculated maps only potentially represent functionally relevant networks is one. The practical reality is that most spatial ICA of human fMRI data typically result in a large number of maps, many of which do not represent any easily identifiable functional network. Thus, identifying what components are most interesting, and assigning

functional significance to those components is a challenge. This amounts to a difficulty in interpreting ICA results. Once spatially independent groups of regions are identified, what groups are important, and what components just represent noise? (Calhoun, et al. 2001) What components have been identified by neuronally driven signals, and what components have been identified using other physiologically driven temporal variance? (Birn, et al. 2008)

The main alternative to independent component analysis is the seed region correlation analysis. In this approach, a region of interest is identified a priori, and correlations between that region and the rest of the brain are calculated as a measure of functional connectivity. (Biswal, et al. 1995; Hampson, et al. 2002; Lowe, et al. 2000) The most general correlation analysis would involve measuring the correlation between every possible pair of voxels within the brain. However, this analysis is too computationally intensive given current resources and results in a large set of results that are difficult to decipher. Generally this approach has not been used. Alternatively, studies have mapped functional connectivity through measuring the correlation between the average time course from a seed region and every individual voxel within the brain, creating whole brain maps of functional connectivity to a specific seed.

The major advantage of seed region functional connectivity analyses is their ease of interpretation. Correlations measured in a target region represent functional connectivity to the seed region. In addition, seed region analyses benefit from the freedom to choose any desired seed region. This supports hypothesis driven studies, where particular interest lies in the connectivity between known regions of the brain. However, the obvious limitation in comparison to ICA is the need for a priori definition

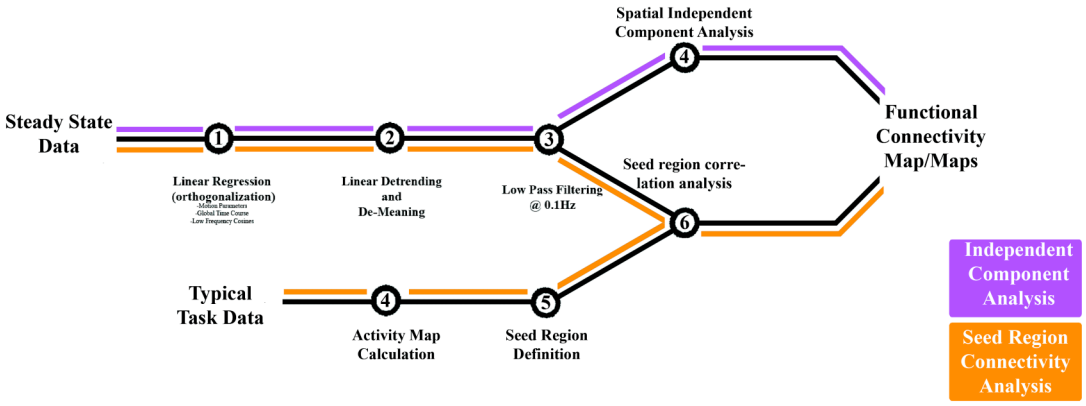

Figure 1.2 - Two common methods for generating steady state functional connectivity maps.

of the seed region. This usually means that additional data need to be acquired in order to spatially define regions of interest (ROIs).

Quantification of Functional Connectivity

When performing seed region functional connectivity analyses, correlation coefficients (Pearson's) are commonly used to measure similarity between functionally relevant signals. Other measures have been used, affecting their interpretation.

Pearson's correlation coefficients, first described by Francis Galton (Galton 1888), are useful for describing linear relationships between normally distributed variables, which approximately describes observed fMRI time series (see Figure 1.3). These measurements are bounded between negative one and one, with identical signals having a correlation coefficient of one. Correlation coefficients are merely a value of the normalized cross correlation function with lag equal to zero (a.k.a. 0^{th} order cross correlation). Because correlation coefficients are bounded, groups of correlation

measures may not be normally distributed, especially if many values are near their inherent limits. For this reason, prior to performing statistical tests, it is common to apply Fisher's z transformation to 'normalize' (i.e. make the distribution of values more nearly normal) the measures of correlation. (Fisher 1928; Hampson, et al. 2006) However, depending on the actual correlations measured, this may not be necessary.

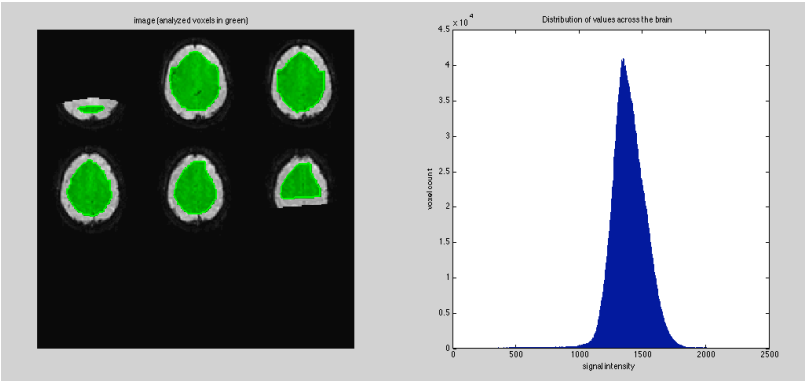

Figure 1.3 - Empirically measured fMRI data have an approximately normal distribution through time. The histogram on the right represents the distribution of signal from all green voxels (left) across 512 image volumes.

Coherence between temporal signals has also been used as a marker of functional connectivity in fMRI data. (Sun, et al. 2004) Coherence can be thought of as the correlation of the frequency spectra of two signals. Likewise, coherence measures are sensitive to linear relationships of frequency components of each signal and trend towards unity as signals become linearly related. (Shiavi 1999) Measures of coherence are insensitive to phase offsets between signals, which can be either an advantage or a disadvantage, depending on the situation. For example, the phase insensitivity of coherence measures may be particularly problematic for some studies of causality, but may be advantageous in observing wide spread networks whose signals have large

temporal lags. Either way, measurement of coherence as a marker of functional connectivity has not become commonplace. As a different measure of connectivity, some studies have instead focused on measuring the lag of the maximum correlation. The phase shift index (PSI) (Xu, et al. 2006) has been shown to have some functional significance, evidenced by its decrease in Alzheimer's patients known to have compromised anatomic connectivity between brain regions. (Xu, et al. 2008) The utility and functional significance associated with both coherence measures and the phase shift index emphasizes the point that important functional information is contained in the frequencies shared by signals, as well as in their phase relative to each other.

Anatomic vs. Functional Connectivity

Suggestions of functional relationships between regions of the brain lead to obvious questions about the underlying structural connections that may facilitate their neuronal communication. The relationship between functional connectivity (measured with fMRI) and structural connectivity (generally measured with tractography analysis of diffusion tensor imaging data) remains unclear. Analysis of typical fMRI data dominated by variance related to task design (i.e. non-steady state data) has informed tractography analyses leading to more reliable mapping of motor, memory, visual, and language networks, though these only represent synergistic fusion of functional and structural information. (Guye, et al. 2003; Jang, et al. 2005; Kim, et al. 2006a; Kim, et al. 2006b; Takahashi, et al. 2007; Takahashi, et al. 2008; Upadhyay, et al. 2007; Vernooij, et al. 2007) We know almost nothing of what one type of connectivity tells us about the other. Effective connectivity analyses, different from functional connectivity in its implication

of causality and its need for an assumed network model, has shown agreement with structural connectivity analyses in their implication of connectivity between primary auditory cortex and the lateral planum polare and anterior superior temporal gyrus. (Upadhyay, et al. 2008) Still this does not inform us as to how structure drives functional connectivity measures. Pathalogic deficits in structural connectivity, measured with water transverse diffusivity in white matter, predict decreases in functional connectivity measured with fMRI (Lowe, et al. 2008), though this pathologic relationship may not be representative of the normal brain. In a recent study done by myself and others, we found that between two functionally and structurally connected regions in the language network, measurements of functional connectivity positively correlated with the bundle thickness of the white matter bundle structurally connecting the regions. Not only do these studies highlight the opportunity for future studies of structural-functional connectivity relationship, these distinctly different types of information suggest the opportunity for development of approaches modeling brain connectivity simultaneously using both types of data. (Rykhlevskaia, et al. 2008)

Physiologic Noise and Related Issues

The art of correlation analyses of fMRI data requires isolation of interesting signals from the pool of potential confounding covariates. Though we have already described in brief the common methods used for noise reduction in functional connectivity analyses, it may be worthwhile to cover this topic in more detail. Covariates can suggest interesting relationships between signals that actually arise from truly unrelated or irrelevant sources. The aims of a particular study govern what

physiologically based signals should be considered as noise, and which should be preserved as signal. As mentioned earlier, most of the information underlying functional connectivity maps lies in the low temporal frequencies, leading us to confine our definition of signal to frequencies below 0.1Hz. Meanwhile, the most common forms of physiological noise include residual motion artifacts, pulsatility related to blood flow, respiratory artifacts (manifested through a variety of mechanisms), among others which can alias into the low frequencies.

Many methods have been adopted for the removal of undesirable physiological noise. A widely used method involves retrospectively correcting image data (RETROICOR) using low order fourier series whose frequencies and phases are dictated by measurements made in separately recorded cardiac and respiratory signals. (Glover, et al. 2000) While proving to be a highly effective method for removing cardiac and respiratory noise, this method relies on signals that are measured simultaneously with image acquisition, a prerequisite that many imaging studies do not meet.

Alternatively, measurements made from specific regions of tissue have been used to represent undesirable noise. For example, variance contained in voxels covering the white matter or cerebral spinal fluid might be assumed to be dominated by noise given the low probability of significant changes in cellular metabolism of their underlying tissue. Assuming that the signal of interest is contained in focal tissue that is small compared to the total size of the brain, the average signal across the brain (a.k.a. the global time course) has also been removed as a method of reducing unwanted physiological noise. (Desjardins, et al. 2001; Macey, et al. 2004) In each of these cases, a signal representing common, uninteresting variance is measured and needs to be removed

prior to functional connectivity mapping.

There are multiple methods for practically calculating residual correlations between time courses after the effects of a third time course have been taken out. Partial correlation coefficients involving three time series (two of interest and one common confound) can be measured in terms of a combination of pair wise correlations. (Spiegel 1972) While this method can be extended to account for the regression of multiple signals (motion parameters in addition to the global time course, for example), this extension becomes cumbersome and is unnecessary. Assuming that covariates add linearly (an underlying assumption of the just mentioned partial correlation coefficient as well), the general linear model can be more easily used to quantify the contribution of a range of noise sources to a given voxel's signal, and the residual error of the model represents the variance remaining unexplained by those covariates. Measuring the correlations using the residual variance of two signals after modeling each using the same set of regressors is an efficient method of calculating partial correlations that yields identical results to the pair wise correlation method.

However, it is important to remember that linearly regressing imaging signals derived from the images themselves (i.e. regressing global time courses from individual within-brain voxel signals) by definition means that the signal and the regressor are not independently measured. It has been argued that this will lead to complications in interpreting maps of correlation coefficients calculated after global time course regression. (Murphy, et al. 2009) Remember that an underlying assumption of using global time courses as models of noise is that the signals of interest are found over focal regions of the brain that are small in comparison to the volume of tissue contributing to

the global time course. Despite this controversy, removal of the global time course via linear regression has been used in a number of studies of functional connectivity, including studies of the default mode hypothesis. (Fox, et al. 2005; Fransson 2005)

Clinical Significance of Functional Connectivity Measurements

Functional connectivity has shown to be predictive of a variety of clinically relevant measures. Behaviorally, resting state functional connectivity between language regions has been shown to predict reading performance across subjects. (Hampson, et al. 2006) Even within a given subject, it has been suggested that intrinsic BOLD variance can explain some trial-to-trial variability in both event related hemodynamic responses (Fox, et al. 2006) and in their behavioral correlates (force of button pressing for example). (Fox, et al. 2007). Differences in resting state functional connectivity also match gender and age differences in IQ. (Schmithorst and Holland 2006)

A variety of studies have demonstrated changes in functional connectivity in the context of known pathology. Just covering a sampling of representative studies, patients suffering from dyslexia show differences in the spatial extent of connectivity between the left and right inferior frontal gyrus and the cerebellum (Stanberry, et al. 2006). Patients with multiple sclerosis have shown deficits in functional connectivity within the frontal and motor cortices (Cader, et al. 2006; Lowe, et al. 2002), while schizophrenic patients have shown differences in prefrontal, parietal, and temporal cortices (Liang, et al. 2006; Whalley, et al. 2005), further highlighting the potential for clinical relevance assigned to measures of functional connectivity.

Where Do We Go Next?

Despite the rapidly growing number of steady state functional connectivity studies, some fundamental questions remain unanswered. The first is whether the low frequency variance measured in resting states is representative of that under other cognitive conditions. Two chapters in this thesis are dedicated to addressing this topic. First we review our earlier study of functional connectivity in the motor network, and then we continue with its extension into the working memory and default mode networks. Second, we explore methods of extending functional connectivity analyses using other functionally relevant signals measured with electroencephalography. Finally, we explore methods by which functional connectivity analyses can be improved through advanced image acquisition and analysis, in the form of ultra high field imaging and measurements of mutual information.

References

Bandettini PA, Wong EC, Jesmanowicz A, Hinks RS, Hyde JS. 1994. Spin-Echo and Gradient-Echo Epi of Human Brain Activation Using Bold Contrast - a Comparative-Study at 1.5 T. Nmr in Biomedicine 7(1-2):12-20.

Bell AJ, Sejnowski TJ. 1995. An Information Maximization Approach to Blind Separation and Blind Deconvolution. Neural Computation 7(6):1129-1159.

Birn RM, Bandettini PA, Cox RW, Shaker R. 1999. Event-related fMRI of tasks involving brief motion. Hum Brain Mapp 7(2):106-14.

Birn RM, Murphy K, Bandettini PA. 2008. The effect of respiration variations on independent component analysis results of resting state functional connectivity. Hum Brain Mapp 29(7):740-50.

Biswal B, Yetkin FZ, Haughton VM, Hyde JS. 1995. Functional connectivity in the motor cortex of resting human brain using echo-planar MRI. Magn Reson Med 34(4):537-41.

Cader S, Cifelli A, Abu-Omar Y, Palace J, Matthews PM. 2006. Reduced brain functional reserve and altered functional connectivity in patients with multiple sclerosis. Brain 129(Pt 2):527-37.

Calhoun VD, Adali T, Pearlson GD, Pekar JJ. 2001. Spatial and temporal independent component analysis of functional MRI data containing a pair of task-related waveforms. Hum Brain Mapp 13(1):43-53.
Constable RT, McCarthy G, Allison T, Anderson AW, Gore JC. 1993. Functional brain imaging at 1.5 T using conventional gradient echo MR imaging techniques. Magn Reson Imaging 11(4):451-9.
Cordes D, Haughton VM, Arfanakis K, Carew JD, Turski PA, Moritz CH, Quigley MA, Meyerand ME. 2001. Frequencies contributing to functional connectivity in the cerebral cortex in "resting-state" data. AJNR Am J Neuroradiol 22(7):1326-33.
Dale AM, Buckner RL. 1997. Selective averaging of rapidly presented individual trials using fMRI. Human Brain Mapping 5(5):329-340.
Desjardins AE, Kiehl KA, Liddle PF. 2001. Removal of confounding effects of global signal in functional MRI analyses. Neuroimage 13(4):751-8.
Fisher RA. 1928. The General Sampling Distribution of the Multiple Correlation Coefficient. Proceedings of the Royal Society of London. Series A, Containing Papers of a Mathematical and Physical Character 121(788):20.
Fox MD, Snyder AZ, Vincent JL, Corbetta M, Van Essen DC, Raichle ME. 2005. The human brain is intrinsically organized into dynamic, anticorrelated functional networks. Proc Natl Acad Sci U S A 102(27):9673-8.
Fox MD, Snyder AZ, Vincent JL, Raichle ME. 2007. Intrinsic fluctuations within cortical systems account for intertrial variability in human Behavior. Neuron 56(1):171-184.
Fox MD, Snyder AZ, Zacks JM, Raichle ME. 2006. Coherent spontaneous activity accounts for trial-to-trial variability in human evoked brain responses. Nat Neurosci 9(1):23-5.
Fransson P. 2005. Spontaneous low-frequency BOLD signal fluctuations: an fMRI investigation of the resting-state default mode of brain function hypothesis. Hum Brain Mapp 26(1):15-29.
Fransson P, Merboldt KD, Petersson KM, Ingvar M, Frahm J. 2002. On the effects of spatial filtering--a comparative fMRI study of episodic memory encoding at high and low resolution. Neuroimage 16(4):977-84.
Friston KJ, Frith CD, Liddle PF, Frackowiak RS. 1993. Functional connectivity: the principal-component analysis of large (PET) data sets. J Cereb Blood Flow Metab 13(1):5-14.
Friston KJ, Frith CD, Turner R, Frackowiak RS. 1995a. Characterizing evoked hemodynamics with fMRI. Neuroimage 2(2):157-65.
Friston KJ, Holmes AP, Poline JB, Grasby PJ, Williams SC, Frackowiak RS, Turner R. 1995b. Analysis of fMRI time-series revisited. Neuroimage 2(1):45-53.
Friston KJ, Holmes AP, Worsley KJ, Poline JP, Frith CD, Frackowiak RSJ. 1994a. Statistical parametric maps in functional imaging: A general linear approach. Human Brain Mapping 2(4):189-210.
Friston KJ, Josephs O, Rees G, Turner R. 1998. Nonlinear event-related responses in fMRI. Magnetic Resonance in Medicine 39(1):41-52.
Friston KJ, P. J, R. T. 1994b. Analysis of functional MRI time-series. Hum Brain Mapp 1(2):153-171.

Friston KJ, Williams S, Howard R, Frackowiak RS, Turner R. 1996. Movement-related effects in fMRI time-series. Magn Reson Med 35(3):346-55.
Galton F. 1888. Co-relations and Their Measurement, Cheifly From Anthropometric Data. Proceedings of the Royal Society of London 45:11.
Gerstein GL, Perkel DH. 1969. Simultaneously recorded trains of action potentials: analysis and functional interpretation. Science 164(881):828-30.
Glover GH, Li TQ, Ress D. 2000. Image-based method for retrospective correction of physiological motion effects in fMRI: RETROICOR. Magn Reson Med 44(1):162-7.
Guye M, Parker GJ, Symms M, Boulby P, Wheeler-Kingshott CA, Salek-Haddadi A, Barker GJ, Duncan JS. 2003. Combined functional MRI and tractography to demonstrate the connectivity of the human primary motor cortex in vivo. Neuroimage 19(4):1349-60.
Hampson M, Peterson BS, Skudlarski P, Gatenby JC, Gore JC. 2002. Detection of functional connectivity using temporal correlations in MR images. Hum Brain Mapp 15(4):247-62.
Hampson M, Tokoglu F, Sun Z, Schafer RJ, Skudlarski P, Gore JC, Constable RT. 2006. Connectivity-behavior analysis reveals that functional connectivity between left BA39 and Broca's area varies with reading ability. Neuroimage 31(2):513-9.
Horwitz B. 2003. The elusive concept of brain connectivity. Neuroimage 19(2 Pt 1):466-70.
Jack CR, Jr., Thompson RM, Butts RK, Sharbrough FW, Kelly PJ, Hanson DP, Riederer SJ, Ehman RL, Hangiandreou NJ, Cascino GD. 1994. Sensory motor cortex: correlation of presurgical mapping with functional MR imaging and invasive cortical mapping. Radiology 190(1):85-92.
Jang SH, You SH, Kwon YH, Hallett M, Lee MY, Ahn SH. 2005. Cortical reorganization associated lower extremity motor recovery as evidenced by functional MRI and diffusion tensor tractography in a stroke patient. Restor Neurol Neurosci 23(5-6):325-9.
Kim M, Ducros M, Carlson T, Ronen I, He S, Ugurbil K, Kim DS. 2006a. Anatomical correlates of the functional organization in the human occipitotemporal cortex. Magn Reson Imaging 24(5):583-90.
Kim MJ, Provenzale JM, Law M. 2006b. Magnetic resonance and diffusion tensor imaging in pediatric white matter diseases. Top Magn Reson Imaging 17(4):265-74.
Kneeland JB, Shimakawa A, Wehrli FW. 1986. Effect of intersection spacing on MR image contrast and study time. Radiology 158(3):819-22.
Liang M, Zhou Y, Jiang T, Liu Z, Tian L, Liu H, Hao Y. 2006. Widespread functional disconnectivity in schizophrenia with resting-state functional magnetic resonance imaging. Neuroreport 17(2):209-13.
Logothetis NK, Pauls J, Augath M, Trinath T, Oeltermann A. 2001. Neurophysiological investigation of the basis of the fMRI signal. Nature 412(6843):150-7.
Lowe MJ, Beall EB, Sakaie KE, Koenig KA, Stone L, Marrie RA, Phillips MD. 2008. Resting state sensorimotor functional connectivity in multiple sclerosis inversely correlates with transcallosal motor pathway transverse diffusivity. Hum Brain Mapp 29(7):818-27.

Lowe MJ, Dzemidzic M, Lurito JT, Mathews VP, Phillips MD. 2000. Correlations in low-frequency BOLD fluctuations reflect cortico-cortical connections. Neuroimage 12(5):582-7.
Lowe MJ, Phillips MD, Lurito JT, Mattson D, Dzemidzic M, Mathews VP. 2002. Multiple sclerosis: low-frequency temporal blood oxygen level-dependent fluctuations indicate reduced functional connectivity initial results. Radiology 224(1):184-92.
Macey PM, Macey KE, Kumar R, Harper RM. 2004. A method for removal of global effects from fMRI time series. Neuroimage 22(1):360-6.
Maes F, Collignon A, Vandermeulen D, Marchal G, Suetens P. 1997. Multimodality image registration by maximization of mutual information. Ieee Transactions on Medical Imaging 16(2):187-198.
Mansfield P. 1977. Multi-Planar Image-Formation Using Nmr Spin Echoes. Journal of Physics C-Solid State Physics 10(3):L55-L58.
Mathiesen C, Caesar K, Akgoren N, Lauritzen M. 1998. Modification of activity-dependent increases of cerebral blood flow by excitatory synaptic activity and spikes in rat cerebellar cortex. Journal of Physiology-London 512(2):555-566.
McKeown MJ, Makeig S, Brown GG, Jung TP, Kindermann SS, Bell AJ, Sejnowski TJ. 1998. Analysis of fMRI data by blind separation into independent spatial components. Human Brain Mapping 6(3):160-188.
McKeown MJ, Sejnowski TJ. 1998. Independent component analysis of fMRI data: Examining the assumptions. Human Brain Mapping 6(5-6):368-372.
Murphy K, Birn RM, Handwerker DA, Jones TB, Bandettini PA. 2009. The impact of global signal regression on resting state correlations: are anti-correlated networks introduced? Neuroimage 44(3):893-905.
Obrig H, Neufang M, Wenzel R, Kohl M, Steinbrink J, Einhaupl K, Villringer A. 2000. Spontaneous low frequency oscillations of cerebral hemodynamics and metabolism in human adults. Neuroimage 12(6):623-39.
Ogawa S, Lee TM, Kay AR, Tank DW. 1990. Brain magnetic resonance imaging with contrast dependent on blood oxygenation. Proc Natl Acad Sci U S A 87(24):9868-72.
Perkel DH, Gerstein GL, Moore GP. 1967. Neuronal Spike Trains and Stochastic Point Processes .2. Simultaneous Spike Trains. Biophysical Journal 7(4):419-&.
Rykhlevskaia E, Gratton G, Fabiani M. 2008. Combining structural and functional neuroimaging data for studying brain connectivity: a review. Psychophysiology 45(2):173-87.
Schmithorst VJ, Holland SK. 2006. Functional MRI evidence for disparate developmental processes underlying intelligence in boys and girls. Neuroimage 31(3):1366-79.
Seifritz E, Esposito F, Hennel F, Mustovic H, Neuhoff JG, Bilecen D, Tedeschi G, Scheffler K, Di Salle F. 2002. Spatiotemporal pattern of neural processing in the human auditory cortex. Science 297(5587):1706-8.
Shiavi R. 1999. Introduction to Applied Statistical Signal Analysis. Bronzino J, editor. San Dieo: Academic Press. 390 p.
Spiegel MR. 1972. Schaum's Outline of Theory and Problems of Statistics in SI Units. RW B, editor. New York: McGraw-Hill International Book Company. 512 p.

Stanberry LI, Richards TL, Berninger VW, Nandy RR, Aylward EH, Maravilla KR, Stock PS, Cordes D. 2006. Low-frequency signal changes reflect differences in functional connectivity between good readers and dyslexics during continuous phoneme mapping. Magn Reson Imaging 24(3):217-29.

Sun FT, Miller LM, D'Esposito M. 2004. Measuring interregional functional connectivity using coherence and partial coherence analyses of fMRI data. Neuroimage 21(2):647-58.

Takahashi E, Ohki K, Kim DS. 2007. Diffusion tensor studies dissociated two fronto-temporal pathways in the human memory system. Neuroimage 34(2):827-38.

Takahashi E, Ohki K, Kim DS. 2008. Dissociated pathways for successful memory retrieval from the human parietal cortex: anatomical and functional connectivity analyses. Cereb Cortex 18(8):1771-8.

Upadhyay J, Ducros M, Knaus TA, Lindgren KA, Silver A, Tager-Flusberg H, Kim DS. 2007. Function and connectivity in human primary auditory cortex: a combined fMRI and DTI study at 3 Tesla. Cereb Cortex 17(10):2420-32.

Upadhyay J, Silver A, Knaus TA, Lindgren KA, Ducros M, Kim DS, Tager-Flusberg H. 2008. Effective and structural connectivity in the human auditory cortex. J Neurosci 28(13):3341-9.

VandeMoortele PF, Cerf B, Lobel E, Paradis AL, Faurion A, LeBihan D. 1997. Latencies in fMRI time-series: Effect of slice acquisition order and perception. Nmr in Biomedicine 10(4-5):230-236.

Vernooij MW, Smits M, Wielopolski PA, Houston GC, Krestin GP, van der Lugt A. 2007. Fiber density asymmetry of the arcuate fasciculus in relation to functional hemispheric language lateralization in both right- and left-handed healthy subjects: a combined fMRI and DTI study. Neuroimage 35(3):1064-76.

Whalley HC, Simonotto E, Marshall I, Owens DG, Goddard NH, Johnstone EC, Lawrie SM. 2005. Functional disconnectivity in subjects at high genetic risk of schizophrenia. Brain 128(Pt 9):2097-108.

Worthington BS, Mansfield P. 1990. The Clinical-Applications of Echo Planar Imaging in Neuroradiology. Neuroradiology 32(5):367-370.

Xu G, Xu Y, Wu G, Antuono PG, Hammeke TA, Li SJ. 2006. Task-modulation of functional synchrony between spontaneous low-frequency oscillations in the human brain detected by fMRI. Magn Reson Med 56(1):41-50.

Xu Y, Xu G, Wu G, Antuono P, Rowe DB, Li SJ. 2008. The phase shift index for marking functional asynchrony in Alzheimer's disease patients using fMRI. Magn Reson Imaging 26(3):379-92.

CHAPTER II

TASK DEMAND MODULATION OF STEADY-STATE FUNCTIONAL CONNECTIIVTY TO PRIMARY MOTOR CORTEX

Overview

The following chapter recounts one of our initial studies of functional connectivity in normal subjects, and is intended to serve as background for the studies discussed in the following chapters. Here we investigated whether steady state measurements of functional connectivity were affected by cognitive load, and we found that they were within the sensorimotor network. It was this study that led to our studies of cognitive load in the working memory and default mode networks, presented in the next two chapters. This study was published shortly after it was presented in connection with my master's thesis work. (Newton, et al. 2007)

Introduction

Interregional correlations between BOLD signals have been identified, even in the absence of a task or stimulus, as possible indicators of functional connectivity between regions in the brain. (Biswal, et al. 1995; Biswal, et al. 1997) Although there has been considerable interest in using such measurements to assess neural circuits, significant questions about how to perform and interpret them remain unanswered. Several studies have shown that functional connectivity can be measured in the resting state, and that maps of some systems and circuits can be reproducibly obtained without performing a task or being subject to a stimulus. (Biswal, et al. 1995; Cordes, et al. 2002; Fransson

2005; Greicius, et al. 2003; Quigley, et al. 2001) Other studies have focused on measuring functional connectivity during continuous task performance. (Kemmotsu, et al. 2005; Lowe, et al. 2000; Sun, et al. 2004) Hampson et al. (Hampson, et al. 2004; Hampson, et al. 2002) and Hirsh et al. (Hirsch, et al. 2004) broadened their scope to include data gathered both during a resting state, as well as during continuous performance of a task or with constant stimulation, and found that functional connectivity in the steady state during stimulation was modified compared to a baseline state. However, as noted recently in a review by Raichle et al. (Raichle and Gusnard 2005), the relationship between functional connectivity and traditional activation patterns has proven to be confusing and difficult to characterize. Studies that quantitatively evaluate the effects of steady-state task performance, in particular the effects of task demand, on interregional correlations in low frequency BOLD fluctuations are still needed.

One system in which functional connectivity has been explored extensively with fMRI is the motor system. This system is particularly appealing because a large body of literature exists, providing information about the major regions of the human brain involved in the execution of many motor tasks, and the influence they have on each other. Finger tapping has been the focus of many fMRI studies because there are known to be large BOLD signal changes in motor cortex during the movement of even a single finger, and finger tapping can be quite easy for subjects to execute reliably.

Several activation studies have been previously performed on the motor system, using a variety of tasks. (Cramer, et al. 2002; Debaere, et al. 2001; Dhamala, et al. 2003) It has been found that the specific design of a task can predictably affect changes in the BOLD signal. For example, Dhamala et al. (Dhamala, et al. 2002) found that when a

subject was allowed to create their own pattern of finger tapping, increases in complexity of the pattern correlated well with increases in activity in the primary motor cortex, supplementary motor area, basal ganglia, thalamus, and cerebellum. However, in this case, tapping patterns were not well controlled, and functional connectivity was not addressed. This type of question has been addressed more broadly in studying the effects of task demand on activity in finger movement tasks [Wexler et. al. 1997], and it was found that finger tapping rate did modulate activity, though only in the contralateral primary motor cortex. Rao et al. (Rao, et al. 1996) recorded activity in a finger tapping task in which subjects were paced at a variety of tapping rates. They found that activity increased with increases in the tapping rate in a variety of motor areas, with subjects tapping at 1, 2, 3, 4, and 5Hz. However, this relied heavily on analysis of only a few specific, selected voxels in each region, and also did not address the subject of functional connectivity. Riecker et al. (Riecker, et al. 2003) published a study intricately mapping how activity changes with the rate of finger tapping in paced tapping, where the subjects were paced at 1, 2,3, 4, 5, and 6Hz. They found that activity increased as finger tapping rate increased in primary motor cortex, supplementary motor area, cerebellum, and thalamus. However, not all regions showed the same pattern of activation increases. Activation in some regions seems to scale linearly with tapping rate, while others follow more complicated relationships. However, these activation studies did not address tapping rate effects on functional connectivity.

Toma et al. (Toma, et al. 2002) investigated the effect of movement rate on both activity and functional coupling using electro-encephalography (EEG). Using measures like EEG band-power and correlation, they found that tapping rate can have an effect on

functional coupling. In slow movements (≤ 1Hz), they reported being able to see the strengthening of coupling between regions followed by uncoupling before the next tap was executed. Fast movements showed continuous coupling. Limitations on spatial resolution constrained their ability to resolve regions within the brain, and also limited the number of regions chosen to study. No strict mapping of the functional data onto anatomical landmarks was done.

In contrast, Jiang et al. (Jiang, et al. 2004) studied the modulation of functional connectivity in a finger tapping task using a network model based on graph theory. They found that it was possible to delineate between the different component tasks contained within the execution of a single finger tap, but they did not look at how connectivity between regions changed as tapping rate was modulated.

The purpose of this study was to evaluate how fMRI measures of functional connectivity, based on steady state interregional correlations, are modulated in an audibly paced finger tapping task by varying the task demand, and to investigate the underlying factors contributing to any such changes. Tapping rate was used as a measure of task demand. If steady-state interregional correlations of BOLD data reflect connectivity, we would expect those correlations to change for some regions as task demand increases, reflecting the recruitment of those areas to a network for completion of the task. (Hampson, et al. 2004; Hampson, et al. 2002; Morgan and Price 2004) Some areas may show strong connectivity regardless of the task demand, while others could display more complicated relationships. A two-fold approach was taken. First, the effects of tapping rate on mean interregional correlations to left primary motor cortex in a steady-state finger tapping task were investigated. Second, the origins of changes in mean

interregional correlations were explored by studying the variations in the number of highly correlated voxels within regions of interest (ROIs).

Methods

Subjects

Eleven normal, right-handed subjects were recruited for participation in this study. All subjects were self identified as right handed, and were in good health. All subjects provided informed consent in accordance with procedures developed by the Institutional Review Board at Vanderbilt University, and were compensated. The subject pool was composed of 4 male and 7 female subjects, and ranged in age from 19 to 34 years (mean=25).

Imaging and Setup

Imaging was performed using on a 3-T whole-body MRI scanner (GE Medical Systems, Milwaukee, WI), using a 'bird cage' head coil. A high resolution T1-weighted scan was performed, using conventional parameters (TE=3.4ms, TR=250ms, 256x256 matrix, 7mm slice thickness, FOV=24cm), and was set up such that both the number of slices and their location coincided with the five functional data sets. All functional images were acquired using 18 slices of 64x64 pixels covering a field of view of 24cm using an acquisition band width of 62.5kHz. Slices were 7mm thick, with no gap between slices. All anatomic and functional image slices were axially oriented. Four volumes were discarded at the beginning to allow the magnetization to reach equilibrium.

Slices were acquired in an interleaved fashion, with TE=25ms, TR=2s, and a flip angle of 90°. All subjects were prepared with a button pad attached to their right wrist, headphones equipped with a microphone, and goggles containing LCD screens for visual cues. Button pads were provided by Rowland Institute of Science, Boston, MA. LCD goggles were produced by Resonance Technologies, Northridge, CA. Head restraints were used to reduce motion.

Functional Scans

Five functional scans were performed in total. The first functional scan consisted of one resting period, lasting 200 seconds, where the subject was visually presented with the word 'REST', no auditory cue was given, and the subject was asked to rest. The second functional scan was a blocked design and lasted 200 seconds, as shown in Figure 2.1. The blocked design consisted of three blocks of 60 seconds each, and a final resting period of 20 seconds. Each block was split into three distinct parts, including a resting period of 20 seconds (silent rest), a passive listening task where the auditory cue was presented at 2Hz (beeping rest), and a 2Hz tapping task lasting for 20 seconds (beeping tapping). For all tapping periods, the word 'TAP' was visually displayed, and the subject was presented with an auditory beep (10kHz, 20ms) that repeated at the desired rate of tapping. The subject was instructed to treat the beeping as a metronome and to pace their tapping with it. The remaining three functional scans were acquired with the subject performing a steady state tapping task, consisting of a 30s resting period, followed by a 200s steady tapping period, and concluding with a 30s resting period. Pre and post task resting periods were removed prior to analysis. Each of these three steady state tasks

used a different auditory cueing rate during tapping, with the three rates being 1, 2, and 4Hz. All four functional scans lasting 200s and not having a blocked design are considered steady-state scans.

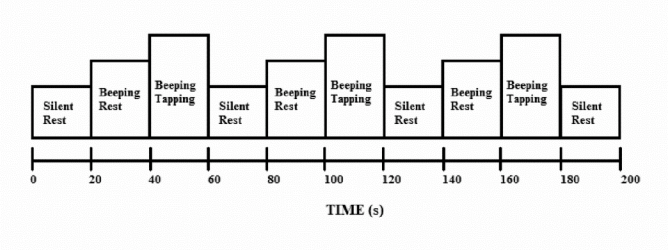

Figure 2.1 - Task design used for the isolation of functionally active motor and auditory voxels during audibly paced finger tapping at two taps per second. 'Silent Rest' refers to a period where the subject was visually presented with the word 'REST', no auditory cue was presented, and no tapping was performed. 'Beeping Rest' refers to the time where the subject was visually presented with the word 'REST', the pacing auditory cue was presented, but the subject did not tap. 'Beeping Tapping' refers to when the subject was visually presented with the word 'TAP', and the subject executed the finger tapping task being paced by the auditory cues.

During all tapping periods, performance was measured by recording timing information for each tap executed. One tap was defined as the depressing and releasing of the button on the button pad with the right index finger. All cues (visual and auditory) were presented with the help of MATLAB version 7 (The Mathworks Inc. Natick, MA), in combination with the Psych Toolbox extensions. (Pelli 1997)

ROI Definition

Preprocessing was performed using *SPM2* fMRI processing software (www.fil.ion.ucl.ac.uk/spm/software/spm2) to realign and reslice data as well as correct for slice timing issues. Realignment parameters were inspected to confirm the absence of

gross head motion. Paired t-tests were used to test for differences between motion parameters gathered during different stimulus frequencies. Spatial smoothing was not performed in order to reduce the likelihood that highly correlated voxels would influence their neighbors.

Regions of interest were defined in a two step process. First, large regions were drawn on high resolution, T1 weighted anatomic images using predetermined landmarks for each region. Regions were allowed to span over multiple slices. Once these regions were defined, they were refined by excluding any voxels that were not significantly activated in the blocked design experiment. This can be thought of as selecting active voxels in the 2Hz stimulus condition, and grouping them into functional groups based on their anatomic location. Defined motor regions included left primary motor (PM), supplementary motor area (SMA), and right cerebellum (CB). An additional ROI was defined in the right auditory cortex (AUD). A control region (CONTROL) was defined as being the entire brain excluding any voxels contained in already defined ROIs. The voxels contained within the brain were identified using an appropriate signal threshold (30.5+/- 5.9% of individual maximum). This threshold was settled upon by visual inspection of whole brain masks of all subjects.

PM anatomical boundaries were defined as those voxels surrounding and including the contralateral central sulcus. This ROI was drawn manually from the edge of the brain, around the tip of the central sulcus, back to the edge of the brain, splitting the space between the central sulcus and neighboring sulci. Superior and inferior limits were defined by the top of the brain and the top of the ventricles respectively. Anatomic landmarks for SMA were the tips of sulci surrounding the midline of the brain, on both

sides, with the superior limits defined by the top of the brain and the inferior limits defined by the top of the ventricles. The anatomic region containing AUD was defined as being contained between the top and the bottom of the ventricles, extending laterally from the midline to the edge of the brain. CB was defined as being contained on slices including the cerebellum, in the hemisphere ipsilateral to the tapping hand.

All anatomically defined ROIs were then refined using functional activation maps. Activation maps used for this refinement were generated using *SPM2*, making use of the general linear model (Friston, et al. 1994), with a threshold for activity set at $p<0.001$ uncorrected for multiple comparisons, and voxel clusters of at least 5 voxels. Activation maps were generated using the blocked design functional data, where periods of 'silent rest' were compared to 'beeping rest' in order to locate auditory activation. This auditory activation map was used for refinement of AUD. PM, SMA, and CB were refined using motor activation maps. Motor activation maps were constructed by comparing 'beeping rest' periods to 'beeping tapping' periods. From this point on, an ROI refers only to the activated voxels within the defined anatomic boundaries.

Partial Correlation Coefficient Map Generation

The focus of this study was to calculate correlations between the signal from one region to the signal in another region. This was accomplished by first generating partial correlation coefficient maps where each voxel has a partial correlation coefficient, 'r' value, associated with it. Partial correlation maps for each subject were calculated making use of equations 2.1 and 2.2. The term 'r_{xy}' refers to the Pearson's correlation coefficient for two time series, *x* and *y*. Both *x* and *y* have *N* time points. The term '$r_{xy \cdot z}$'

refers to the partial correlation coefficient between *x* and *y* with the effects of *z* removed. In this case, *z* has the same number of time points as *x* and *y*. Partial correlation maps were generated for each of the four steady-state functional scans (rest, 1, 2, 4Hz tapping). Prior to their use in equations 1 and 2, all time series were linearly detrended and low pass filtered with a cut off frequency equal to 0.1Hz, using a Chebyshev Type II filter. The filter was implemented in both the forward and the reverse direction in order to prevent phase distortion.

$$r_{xy} = \frac{\sum xy - \frac{\sum x \sum y}{N}}{\sqrt{\left(\sum x^2 - \frac{(\sum x)^2}{N}\right)\left(\sum y^2 - \frac{(\sum y)^2}{N}\right)}} \tag{2.1}$$

$$r_{xy \cdot z} = \frac{r_{xy} - (r_{xz})(r_{yz})}{\sqrt{(1 - r_{xz}^2)(1 - r_{yz}^2)}} \tag{2.2}$$

Partial correlation maps were generated showing the partial correlation between the average PM time course (x) and the time course for every voxel (y), removing the effects of the global time course (z). First, an average time course for PM was calculated by averaging the signal from each PM voxel at each time point. A similar procedure was performed to construct an average time course for the whole brain, which was considered the global time course which may have been influenced by various effects of no specific interest to motor regional connectivity. Voxels within the brain that should be included in this global time course were identified using the before mentioned signal threshold and included voxels within previously defined ROIs. The third time series used in calculating

partial correlation maps was the time course from each voxel, taken individually. Steady-state tapping scans had their resting periods removed before the partial correlation coefficient maps were generated.

Analysis

Two major analyses were applied. Each analysis tested for two different effects using two ANOVAs. The first analysis addresses the question of whether the strength of correlations to PM for each ROI changes as a function of the tapping rate. This consisted of calculating the mean partial correlation (MPC) coefficient within an ROI. The MPC represents the strength of correlation between an ROI and PM. This was done for all steady-state data (rest, 1Hz, 2Hz, and 4Hz tapping) and for each ROI (SMA, CB, AUD, and CONTROL). Statistical analysis was done using *R version 2.0.0* (www.r-project.org). ANOVAs were used to test whether tapping rate affected the MPC of an ROI (i.e. 0Hz vs. 1Hz, 2Hz vs. 4Hz, etc.) and to test whether ROIs had a different MPC at each tapping rate (i.e. SMA vs. CB, AUD vs. CONTROL, etc.). In each case, if the ANOVA was significant with a p-value ≤ 0.05, paired t-tests were performed to determine significant differences between values.

The second analysis addressed the question of whether changes in correlation were due to changes in the number of correlated voxels. This consisted of establishing a correlation threshold for each subject, and calculating the percent of the voxels above that threshold (PAT) within each ROI for that subject. Again, these correlations are between an ROI and PM. Results were then averaged across subjects, and studied for significant differences. The threshold used for each subject was the mean of all the partial

correlations for all voxels throughout the whole brain plus one standard deviation. Again, two ANOVAs were performed, as was done for the MPC, where a p-value of less than 0.05 led to paired t-testing.

Results

ROI Definition and Partial Correlation Coefficient Map Generation

There were three cases where data were found to be unusable for analysis. In each case, only one aspect of the analysis was affected, and thus the remaining data from that subject could be included in the appropriate analyses. Analysis of intertap intervals and number of executed taps were used to evaluate tapping performance. During 1Hz cueing for 200s, subjects averaged 203+/-4 taps (mean +/- stdev, target 200 taps). During 2Hz cueing for 200s, subjects averaged 401+/-3 taps (target 400 taps). During 4Hz cueing, subjects averaged 782+/-25 taps (target 800 taps). It was seen that performance was most accurate across subjects at the 2Hz tapping rate, with the poorest accuracy at the 4Hz tapping rate. One subject's 4Hz tapping data were discarded based on several extended intertap intervals attributed to reported fatigue, in addition to a tap count (750 taps) falling outside of the mean minus one standard deviation across subjects. Analysis of motion parameters showed no effect of stimulus frequency on maximum displacements or rotations ($p<0.05$), as well as no displacements greater than 1mm or rotations greater than 0.03 radians in any direction.

Activation maps were generated for each subject, for motor activation and auditory activation separately. Sample ROIs and their relation to auditory and motor

activation maps of the same subject can be seen in Figure 2.2 and Figure 2.3. ROIs were defined for each subject, and the number of voxels in each refined ROI was counted. The mean of the number of voxels in each region across subjects can be seen in Table 2.1. Two cases were discarded due to lack of detectable activation within the anatomical boundaries of an ROI.

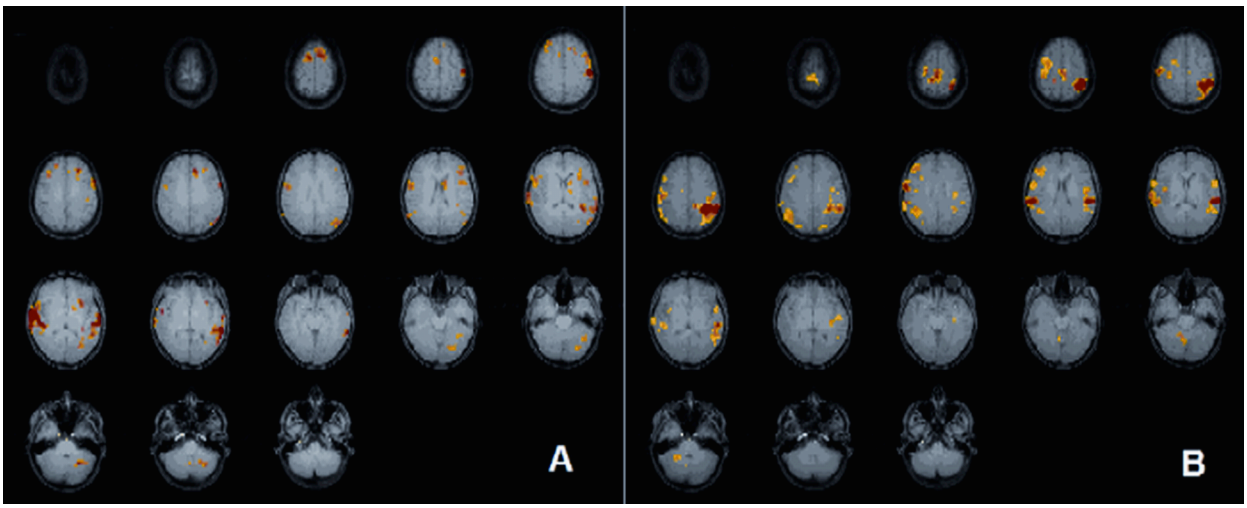

Figure 2. 2 - Activation maps generated from the blocked task design overlaid on T1 weighted anatomic images. Activity thresholds were calculated without accounting for multiple comparisons,with $p \leq 0.001$, and a minimum cluster size of 5. (A) Auditory activation calculated by comparing 'beeping rest' periods with 'silent rest' periods. (B) Motor activation maps calculated from comparing 'beeping tapping' periods with 'beeping rest' periods.

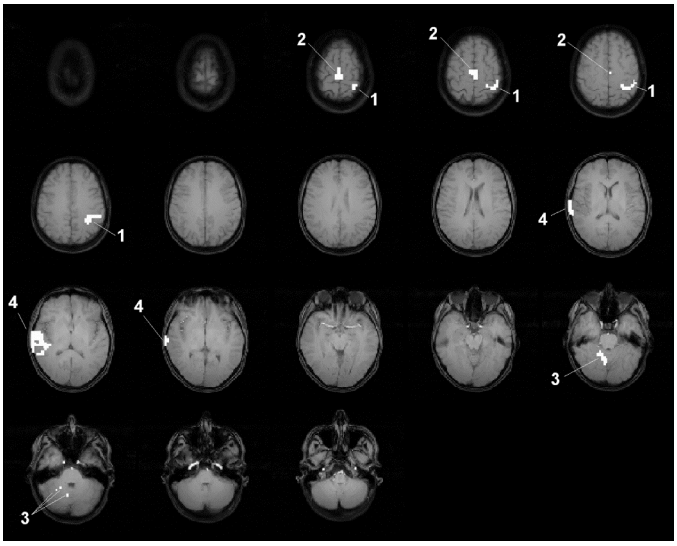

Figure 2. 3 - Location of ROIs on a representative subject. These ROIs were identified by establishing anatomical boundaries and then refining the ROI within those boundaries by keeping only significantly activated voxels within them. The activation maps from Figure 2.2 were used for this refinement. 1=left primary motor (PM) 2=supplementary motor area (SMA), 3=right cerebellum (CB), 4=right auditory cortex (AUD).

TABLE 2.1: Number of voxels per ROI across subjects

	PM	SMA	CB	AUD	Control
Mean	47	30	57	67	1.77E+04
Std dev.	17	46	18	50	2.00E+03

For all subjects, ROIs were distinct from each other, with no overlaps. Maps of partial correlation coefficients between each voxel and the average PM signal, accounting for the global time course, were successfully constructed for all subject's steady-state scans. An example of a map of partial correlation coefficients can be seen in Figure 2.4. This example was taken from the same subject as Figures 2.2 and 2.3, and the 2Hz steady-state tapping data were again used.

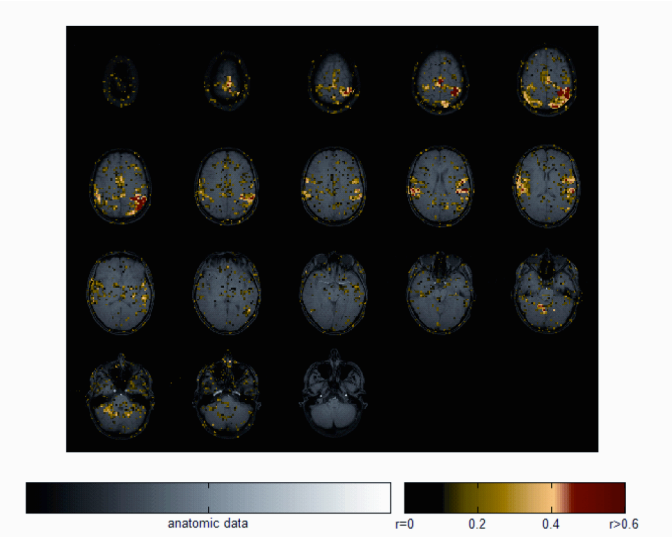

Figure 2. 4 - A map of partial correlation coefficients between each voxel and the average time course from PM (see Figure 2.3, #1) overlaid on a high resolution, T1 weighted image. These partial correlations represent the correlation of each voxel to the average time series from PM, removing the effects of the global time course. These correlations were calculated from steady-state tapping data, with the subject tapping at 2Hz. Steady-state scans imaged the subject with TR=2s over a scan time of 200s. Maps of this nature were generated for each subject during rest and steady-state finger tapping at 1, 2, and 4Hz. Note that significant correlation clusters exist in and around the ROIs identified in Figure 2.3.

MPC Analysis

Figure 2.5 shows the MPC of each ROI averaged across subjects at each tapping rate. Note that correlations in the control region are uniformly low, while correlations in other ROIs are much higher. ANOVA showed that MPC was modified by tapping rate in all regions except SMA (SMA: p=0.23;CB: p=0.01; AUD: p=7.4e-5; CONTROL: p=0.001). Paired t-tests between rates can be seen for each ROI in Table 2.2.

TABLE 2.2: Paired t-test results between tapping rates within ROI

	SMA		CB		AUD		CONTROL	
	MPC p-value	PAT p-value	MPC p-value	PAT p-value	MPC p-value	PAT p-value	MPC p-value	PAT p-value
0Hz-1Hz	0.05*	0.03*	0.05*	0.03*	7.4e-3*	0.01*	0.28	0.41
0Hz-2Hz	0.66	0.56	0.01*	0.01*	3.3e-4*	1.8e-4*	0.02*	0.77
0Hz-4Hz	0.11	0.02*	0.07	0.07	4.9e-3*	4.1e-3*	2.8e-3*	0.45
1Hz-2Hz	0.16	0.07	0.26	0.71	0.05*	0.03*	0.13	0.67
1Hz-4Hz	0.44	0.35	0.34	0.84	0.21	0.26	0.08	0.11
2Hz-4Hz	0.90	0.56	0.61	0.93	0.74	0.71	0.33	0.22

* denotes p-values ≤ 0.05

ANOVA also showed that within a tapping rate, MPCs were different between ROIs ($p \leq 0.01$ for all rates). CB correlations to PM were not found to be different from CONTROL at rest, but were different during tapping. Similarly, correlations between AUD and PM were not statistically different from correlations between CONTROL and PM at rest, but were different during cued finger tapping. At rest, PM correlations to AUD and SMA were significantly different from each other, but as tapping rate increased, their difference lost significance. The t-test results for differences between ROIs correlation to PM, at each tapping rate, are summarized in Table 2.3. P-values were not corrected for multiple comparisons.

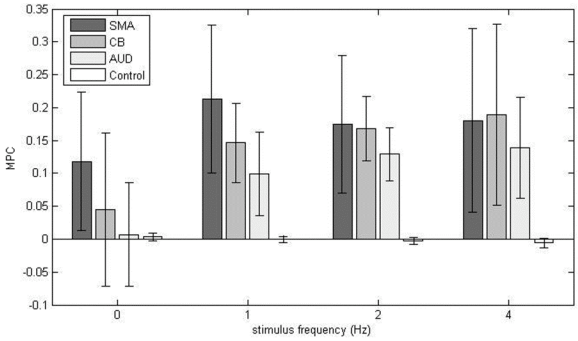

Figure 2. 5 - Across subjects average of the Mean Partial Correlation (MPC) of each region during a given steady-state task demand. Error bars represent the standard deviation between subjects. Paired t-tests for significant differences between regions can be seen in Table 2.3. 0Hz is the resting state data. Notice that some ROIs were significantly correlated to PM at all task demands (SMA), while others showed modulation (CB and AUD). The control region consistently showed low correlation.

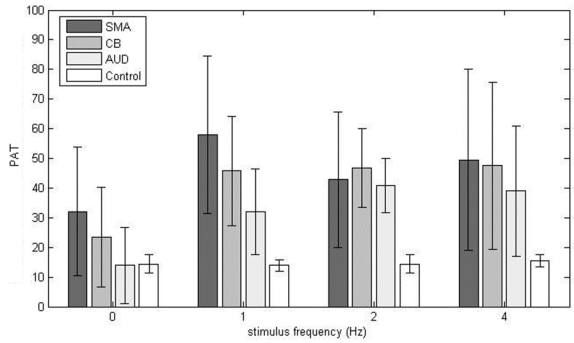

Figure 2. 6 - When looking at the voxels within a given ROI, the Percent Above Threshold (PAT) is shown to closely mirror results of the ROIs MPC. This suggests that changes in the percent of correlated voxels within a region drives changes in the MPC. Tests for significant differences between the ROIs and between tapping rates can be seen in Tables II and III. Error bars represent the standard deviation between subjects.

TABLE 2.3: Paired t-test results between ROIs within tapping rate

	REST: 0Hz		TAPPING: 1Hz		TAPPING: 2Hz		TAPPING: 4Hz	
	MPC p-value	PAT p-value	MPC p-value	PAT p-value	MPC p-value	PAT p-value	MPC p-value	PAT p-value
SMA-CB	0.16	0.19	0.18	0.37	0.51	0.33	0.77	0.57
SMA-AUD	0.02*	0.04*	6.5e-3*	0.01*	0.68	0.82	0.33	0.42
SMA-Control	2.1e-3*	0.01*	7.3e-5*	2.1e-4*	3.9e-3*	6.6e-3*	2.4e-3*	6.4e-3*
CB-AUD	0.54	0.27	0.06	0.14	0.17	0.37	0.25	0.57
CB-Control	0.28	0.14	1.7e-5*	3.5e-4*	8.7e-7*	6.6e-5*	2.9e-3*	8.7e-3*
AUD-Control	0.96	0.86	1.3e-3*	2.8e-3*	2.3e-6*	7.9e-6*	5.8e-7*	1.1e-3*

* denotes p-values ≤ 0.05

PAT Analysis

Figure 2.6 shows that finger tapping rate can affect the percent of the voxels in a given ROI above a given correlation threshold. These results represent the average PAT across subjects. ANOVA confirmed that rate affected the PAT in CB (p=0.01) and AUD (p=0.18e-3), but not in SMA (p=0.06) or CONTROL (p=0.44). In general, as the tapping rate increased, all regions except the control region increased in the percent of voxels above the correlation threshold, though not all these increases were statistically significant. The results of paired t-tests are reported in Table 2.2. ANOVA confirmed that within a tapping rate, ROIs had significantly different PATs ($p \leq 0.02$ for all rates). Corresponding results for t-tests looking for differences between ROIs at each tapping rate can be seen in Table 2.3.

Discussion

The data presented here supports the idea that task demand can affect measures of functional connectivity made during the execution of a task. This is significant because many studies until now have not considered the effect of task demand on measures of functional connectivity. In addition, it is interesting that changes in the number of voxels within ROIs that were significantly correlated to PM mirrored changes in mean correlation of the regions. This suggests the underlying cause for mean correlation changes within a region is the recruitment of additional voxels rather than changes in a fixed set of voxels.

The data presented here supports the assertion that resting state correlations reflect functional networks, and that steady state correlations can change in both magnitude and pattern when a task is executed. In order to complete a given task, it may be expected that some regions must become recruited into a functional network. If interregional correlations truly measure functional connectivity, it may also be expected that those correlations should change for some brain regions when going from a resting state to task performance. These data show that mean correlations to PM at rest are different from mean correlations during finger tapping. In addition, it has been shown that different states of activity can affect connectivity differently, even when the nature of the task is similar. This can be seen by comparing SMA and CB in Figure 2.5. SMA is highly connected to PM at all levels of activity, including rest. CB behaves differently in that it has weak connectivity to PM at rest, but strong connectivity while tapping, though CB connectivity with PM is not affected by the rate of tapping. Conversely, AUD correlation to PM is significantly changed at each tapping rate. Failure to see changes in

connectivity between tapping rates may be due to a saturation effect. This may apply to SMA-PM correlations, which are always high, or to CB-PM correlations which are high when the task is performed.

There is an overall trend of the data to become more variant during 4Hz tapping. However, despite the increased variance, paired t-tests yield significant results. The increased variance at 4Hz tapping could have a variety of explanations. Because the 4Hz tapping scan occurred last, there was a higher likelihood that the subjects had moved significantly with respect to the blocked design scan, as well as the T1-weighted scan, on which the ROIs were based. Also, 4Hz tapping was reported to be significantly more difficult than 1 or 2Hz tapping. Thus, motion artifacts were more likely. Some subjects also reported wrist cramping and muscle fatigue. Though most subjects tapped accurately at all tapping rates, it was observed that there was more variation in the tapping rates when the cuing rate was 4Hz.

The construction of partial correlation coefficient maps from steady state acquisitions revealed functional networks that closely coincided with regions of activation in a block design experiment, as can be seen in comparing Figure 2.2 and Figure 2.4. This adds to the body of evidence showing that steady state low frequency correlations can be used to reveal functional networks. Particularly high correlations were observed in and around the seed region, PM, which should be expected because the voxels in PM each contributed to the signal being used as the base for all correlations. It should be noted that all ROIs were created through refining anatomical regions using functional data acquired during 2Hz tapping. It is likely the precise extent of this activation would change with tapping rate, and that some of those voxels significantly

active during 2Hz tapping would not be detected during 1Hz, tapping. Similarly, some voxels not active during 2Hz tapping might have been activated during 4Hz tapping. This was necessary to keep the size of ROIs constant across tapping rates.

Given that interregional correlations change with task demand during a finger tapping task, a question arises whether those changes are due to changes in the correlation of a fixed set of voxels to PM, or due to changes in the number of correlated voxels contained within the ROI. Figure 2.6 suggests that increases in the number of correlated voxels account for average increases in interregional correlations. This figure mirrors the mean correlation analysis seen in Figure 2.5. This evidence argues that it is the number of correlated voxels which drives observed changes in overall functional connectivity, though it can not be ruled out that magnitude changes in correlation contribute as well.

It has been seen that in an audibly cued finger tapping task, auditory activation can be found even when attempting to generate motor contrast from a blocked design task consisting of cuing without tapping and cuing with tapping. (Woodruff, et al. 1996) This unexpected auditory activation was attributed to attentional modulation. It can be observed in the mean ROI correlation analysis that AUD appears to behave in a similar fashion to motor ROIs as tapping rate is increased. One hypothesis explaining this is that both AUD and PM are being stimulated at the same frequency, which creates inherent correlations in their BOLD responses. Though all three stimulus frequencies may be aliased to 0Hz when sampled in 2 second intervals, and thus pass through the applied low pass filter, aliasing effects are unlikely to explain increases in correlation as the stimulus frequency increases, as is seen in AUD-PM correlations. Furthermore, uniformly high

SMA-PM correlations across stimulus frequencies, including rest, argue against aliasing being the source of changes in correlations when comparing rest to task performance in AUD and CB.

Aliasing of physiological noise has been a topic of recent study, and potentially could confound studies such as those reported here. Sampling at 0.5Hz, respiratory and cardiac frequencies may be aliased into the low frequency spectrum. Of these, aliasing of the respiratory signal is less troublesome because it will likely be resolved in some or all subjects. Even so, both cardiac and respiratory effects are present over the entire brain, and will contribute to the global time course whose effects have been removed via the partial correlation approach. Furthermore, their residual influence should not change with tapping rate.

A second hypothesis regarding the behavior of AUD is that it is being recruited to complete the given task. This increase in correlation between PM and AUD may represent the creation and refinement of a network of cortical regions used together to perform a given task. Close inspection of Table 2.3 reveals a pattern that emerges as tapping rate increases. It is shown that CB-PM correlations and AUD-PM correlations become different from the control region only when the task is performed, and that AUD-PM correlations become more like SMA-PM correlations as the tapping rate and the auditory cue rate increased. This might be explained by attentional modulation in an auditory cued task, or may provide evidence of an effective connection between motor cortex and auditory cortex used to complete the task. However, this question must be more directly addressed. Figure 2.7 summarizes the trend in interregional correlations that develops as tapping rate increases.

Implicit in our study design, it was hypothesized that activity during conventional block design can predict regions that are correlated. This study requires the establishment of a seed ROI, but it is possible that a self-organizing map (SOM) could be used to eliminate the need to define a seed region. (Peltier, et al. 2003) This may illuminate other regions, or networks of regions, at work that have not been anticipated. Though self identification of handedness is thought to be less reliable than standardized testing, the effects of handedness on this study are likely to be minimal due to the consistent choice of the seed ROI contralateral to the tapping hand. (Jancke, et al. 1998) Better control of handedness may have allowed for additional analysis of ipsilateral primary motor cortex. However, despite these limitations, this study has shown that task demand can modulate functional connectivity in the motor system.

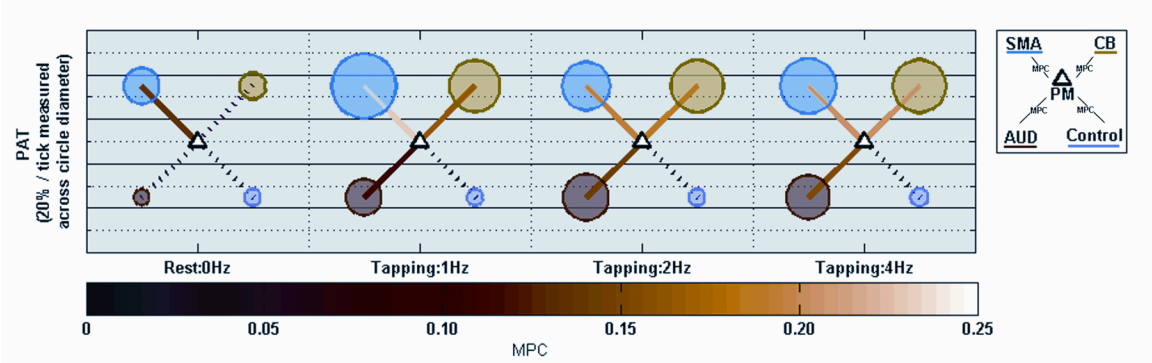

Figure 2. 7 - A visualization summarizing the significant results from Table 2.3, Figure 2.5 and Figure 2.6. Colored lines projecting from PM represent the average MPC across subjects of each region to PM, as shown in Figure 2.5, with color of the line denoting the specific value. The MPC color scale is given by the color bar located at the bottom of the figure. Looking within each tapping rate, solid MPC lines indicate that the ROI's correlations to PM are significantly different from those in the control region, as shown in Table 2.3. Dotted MPC lines mean that the correlations are not significantly different from those in the control region. The mean PAT across subjects, as shown in Figure 2.6, is proportional to the diameter of each ROI's circle. A general trend can be seen where ROIs develop correlations that are increasingly different from those in the control region

as tapping rate increases. This could reflect that tighter coupling of the system may be required at higher task demands.

Conclusions

The present study has shown that in a finger tapping task, the rate of finger tapping affects interregional correlations in the motor cortex. Furthermore, evidence has been presented here that the source of these correlation changes is likely to be changes in the fraction of significantly correlated voxels in an ROI, as opposed to magnitude changes of the same significantly correlated voxels. Finally, evidence has been provided that interregional correlations can illuminate connections made to complete a task which are not strong at rest.

References

Biswal B, Yetkin FZ, Haughton VM, Hyde JS. 1995. Functional connectivity in the motor cortex of resting human brain using echo-planar MRI. Magn Reson Med 34(4):537-41.

Biswal BB, Van Kylen J, Hyde JS. 1997. Simultaneous assessment of flow and BOLD signals in resting-state functional connectivity maps. NMR Biomed 10(4-5):165-70.

Cordes D, Haughton V, Carew JD, Arfanakis K, Maravilla K. 2002. Hierarchical clustering to measure connectivity in fMRI resting-state data. Magn Reson Imaging 20(4):305-17.

Cramer SC, Weisskoff RM, Schaechter JD, Nelles G, Foley M, Finklestein SP, Rosen BR. 2002. Motor cortex activation is related to force of squeezing. Hum Brain Mapp 16(4):197-205.

Debaere F, Swinnen SP, Beatse E, Sunaert S, Van Hecke P, Duysens J. 2001. Brain areas involved in interlimb coordination: a distributed network. Neuroimage 14(5):947-58.

Dhamala M, Pagnoni G, Wiesenfeld K, Berns GS. 2002. Measurements of brain activity complexity for varying mental loads. Phys Rev E Stat Nonlin Soft Matter Phys 65(4 Pt 1):041917.

Dhamala M, Pagnoni G, Wiesenfeld K, Zink CF, Martin M, Berns GS. 2003. Neural correlates of the complexity of rhythmic finger tapping. Neuroimage 20(2):918-26.

Fransson P. 2005. Spontaneous low-frequency BOLD signal fluctuations: an fMRI investigation of the resting-state default mode of brain function hypothesis. Hum Brain Mapp 26(1):15-29.

Friston KJ, Holmes AP, Worsley KJ, Poline JP, Frith CD, Frackowiak RSJ. 1994. Statistical parametric maps in functional imaging: A general linear approach. Human Brain Mapping 2(4):189-210.

Greicius MD, Krasnow B, Reiss AL, Menon V. 2003. Functional connectivity in the resting brain: a network analysis of the default mode hypothesis. Proc Natl Acad Sci U S A 100(1):253-8.

Hampson M, Olson IR, Leung HC, Skudlarski P, Gore JC. 2004. Changes in functional connectivity of human MT/V5 with visual motion input. Neuroreport 15(8):1315-9.

Hampson M, Peterson BS, Skudlarski P, Gatenby JC, Gore JC. 2002. Detection of functional connectivity using temporal correlations in MR images. Hum Brain Mapp 15(4):247-62.

Hirsch JG, Lowe MJ, Schwenk S, Rossmanith C, Hennerici MG, Gass A. Functional connectivity in the motor and auditory systems: a reproducibility study at 3T; 2004. p 1072.

Jancke J, Peters M, Schlaug G, Posse S, Steinmetz H, Muller-Gartner HW. 1998. Differential magnetic resonance signal change in human sensorimotor cortex to finger movements of different rate of the dominant and subdominant hand. Cognitive Brain Research 6(4):279-284.

Jiang T, He Y, Zang Y, Weng X. 2004. Modulation of functional connectivity during the resting state and the motor task. Hum Brain Mapp 22(1):63-71.

Kemmotsu N, Villalobos ME, Gaffrey MS, Courchesne E, Muller RA. 2005. Activity and functional connectivity of inferior frontal cortex associated with response conflict. Brain Res Cogn Brain Res 24(2):335-42.

Lowe MJ, Dzemidzic M, Lurito JT, Mathews VP, Phillips MD. 2000. Correlations in low-frequency BOLD fluctuations reflect cortico-cortical connections. Neuroimage 12(5):582-7.

Morgan VL, Price RR. 2004. The effect of sensorimotor activation on functional connectivity mapping with MRI. Magn Reson Imaging 22(8):1069-75.

Newton AT, Morgan VL, Gore JC. 2007. Task demand modulation of steady-state functional connectivity to primary motor cortex. Hum Brain Mapp 28(7):663-72.

Pelli d. 1997. The Video Toolbox softare for visual psychophysics: transforming numbers into movies. Spatial Vision 4:5.

Peltier SJ, Polk TA, Noll DC. 2003. Detecting low-frequency functional connectivity in fMRI using a self-organizing map (SOM) algorithm. Human Brain Mapping 20(4):220-226.

Quigley M, Cordes D, Wendt G, Turski P, Moritz C, Haughton V, Meyerand ME. 2001. Effect of focal and nonfocal cerebral lesions on functional connectivity studied with MR imaging. AJNR Am J Neuroradiol 22(2):294-300.

Raichle ME, Gusnard DA. 2005. Intrinsic brain activity sets the stage for expression of motivated behavior. J Comp Neurol 493(1):167-76.

Rao SM, Bandettini PA, Binder JR, Bobholz JA, Hammeke TA, Stein EA, Hyde JS. 1996. Relationship between finger movement rate and functional magnetic resonance signal change in human primary motor cortex. J Cereb Blood Flow Metab 16(6):1250-4.

Riecker A, Wildgruber D, Mathiak K, Grodd W, Ackermann H. 2003. Parametric analysis of rate-dependent hemodynamic response functions of cortical and subcortical brain structures during auditorily cued finger tapping: a fMRI study. Neuroimage 18(3):731-9.

Sun FT, Miller LM, D'Esposito M. 2004. Measuring interregional functional connectivity using coherence and partial coherence analyses of fMRI data. Neuroimage 21(2):647-58.

Toma K, Mima T, Matsuoka T, Gerloff C, Ohnishi T, Koshy B, Andres F, Hallett M. 2002. Movement rate effect on activation and functional coupling of motor cortical areas. J Neurophysiol 88(6):3377-85.

Woodruff PW, Benson RR, Bandettini PA, Kwong KK, Howard RJ, Talavage T, Belliveau J, Rosen BR. 1996. Modulation of auditory and visual cortex by selective attention is modality-dependent. Neuroreport 7(12):1909-13.

CHAPTER III

THE EFFECTS OF COGNITIVE LOAD ON FUNCTIONAL CONNECTIVITY IN THE WORKING MEMORY AND DEFAULT MODE NETWORKS

Introduction

Steady-state correlations in low frequency blood oxygen level dependent (BOLD) magnetic resonance imaging (MRI) signals have been interpreted as revealing functional connectivity between regions within the human brain (Biswal, et al. 1997; Biswal, et al. 1995; Hampson, et al. 2006b; Lowe, et al. 2000). Most studies have examined interregional correlations in the resting state in which no task or stimulus effects are specifically encoded into the temporal variance of BOLD signals (Cordes, et al. 2001; Lowe, et al. 1998; Prohovnik, et al. 1980; Rogers, et al. 2007; van de Ven, et al. 2004), though functional connectivity can also be measured during steady state tasks.

Measurements of functional connectivity have been shown to vary with cognitive load in some networks. In previous studies of the motor system, we have shown that measures of functional connectivity scale with the rate of finger tapping in some regions and not in others (Newton, et al. 2007). We and others have established that connectivity measured during performance of steady state tasks may be greater than at rest (Fox, et al. 2005; Hampson, et al. 2004; Hampson, et al. 2001; Hampson, et al. 2006b; Lowe, et al. 2000; Newton, et al. 2007). In the working memory system specifically, path analysis has shown that effective connectivity increases under increased cognitive loads (Honey, et al. 2002). Correlation analysis focusing on the trial-by-trial variance in event related working memory responses (as a different measure of steady state functional

connectivity) has shown decreasing functional connectivity during delay periods between the hippocampus, the fusiform face area, and the inferior frontal gyrus (Rissman, et al. 2004; Rissman, et al. 2008). Principal component analysis (PCA) has also been used to examine working memory systems, showing different networks with load dependent connectivity for the encoding and maintenance periods of an event related task (Woodward, et al. 2006). However, none of these studies specifically addressed how working memory load changes some typical fMRI measures of functional connectivity across the brain during steady-state working memory tasks.

Analyses of steady state fMRI data, specifically resting state data, have also revealed a variety of networks including one which has become known as the default mode network (Fox, et al. 2005; Greicius, et al. 2003; Raichle, et al. 2001) comprised of brain regions that are more active during rest periods, absent of directed attention demanding tasks. Various data analysis techniques have shown that this default mode network can be identified in the resting conscious state in most subjects (Arfanakis, et al. 2000; Beckmann, et al. 2005; Meyer-Baese, et al. 2004; van de Ven, et al. 2004). It has been recently shown that these default mode regions are functionally connected not only in conscious awake states but during light stages of sleep (Horovitz, et al. 2007), and under light anesthesia (Greicius, et al. 2008). However, the specific role played by these regions in the resting state remains a topic of increased debate, as does their relationship to those networks recruited for specific cognitive tasks. While changes in functional connectivity within a network have been measured between the resting state (when the default-mode network may be most active) and during task performance (Esposito, et al. 2006; Hampson, et al. 2004; Hampson, et al. 2006b), relatively few studies have looked

closely at changes in functional connectivity between networks that may have separate functions. Fransson et al., (Fransson 2006) describes a change in correlations between a recruited cognitive network and the default mode network, in response to a known task. However, it remains unclear whether the connectivity between working memory regions and those in the default mode network scales over a range of cognitive loads.

There are two aims of this study. The first aim is to quantify the degree to which functional connectivity within the working memory network is modulated by cognitive load. Secondly, we aim to identify whether the functional connectivity of the default mode network (either within itself or between it and the working memory network) changes as a function of cognitive load. We hypothesize that increasing cognitive load may cause gradual decreases in synchronization within the default mode network. These analyses provide further insight into the underlying factors affecting typical measurements of functional connectivity using fMRI, and increase our understanding of the default mode network and its role in the normal brain.

Materials and Methods

Subjects

Ten healthy subjects were recruited for participation in this study. All were right handed by self report. The subject pool consisted of 8 female and 2 male volunteers, with an age range of 20-36 years (median=27 years). All subjects provided informed consent in accordance with procedures approved by the Institutional Review Board at Vanderbilt University, and were compensated for their participation. Two of the ten subjects were

removed from the study for failure to complete all necessary tasks, yielding data from eight subjects which are presented here.

Imaging and Initial Processing

All subjects were imaged using a Philips Achieva 3T MR scanner, using an eight channel SENSE coil. Four functional data sets were acquired in each subject using a single shot, gradient-echo echo planar imaging (EPI) pulse sequence (TR=2s, TE=35ms) with a SENSE acceleration factor of 1.8. The multi-slice images covered 12.2 cm of brain and were acquired axially (matrix size: 64x64), using a field of view of 240mm. Voxels measured 3.75mm x 3.75mm x 3.5mm. All functional data had slice timing and motion artifacts corrected, were co-registered within each subject, and were normalized to the MNI 152 template using the SPM5 software (http://www.fil.ion.ucl.ac.uk/spm/software/spm5/). High resolution T1 weighted anatomic images were acquired using conventional parameters, and were used in normalization.

Cognitive Tasks

Each subject completed four fMRI runs: three N-back, and one resting state run. The resting state run consisted of 100 images of each slice acquired over 200 seconds, and subjects were instructed to lie still with eyes closed. Each N-back run was performed with a verbal identity working memory N-back task (1-back, 2-back, and 3-back tasks in random order). These N-back runs each consisted of a 300-second (150 image volumes) block-design portion with N-back and 0-back conditions in alternating 30-second blocks

(15 letters, 3 targets per 30s block), followed by a 200-second steady-state portion of the N-back task only containing 20 targets (Figure 3.1). Stimuli were a single letter presented at the beginning of the acquisition of each image volume.

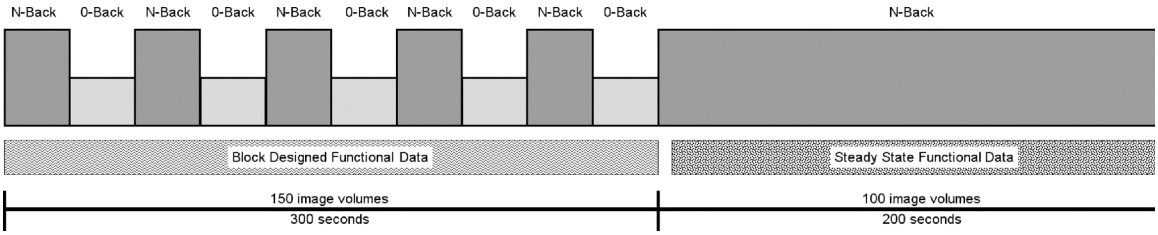

Figure 3.1 - General task description for data acquired during N-back task performance. Note that data were separated into two types of data: blocked-designed task data and steady-state task data.

Regions of Interest

Regions of interest (ROIs) were defined based on statistical parametric mapping of the block-design portions of the N-back runs, and were classified into in three separate groups: task positive regions, activated by the working memory task; task negative regions, deactivated by the working memory task; and control regions, where signal showed no significant response to the task manipulation. These definitions were made using the results of fitting a general linear model to the block-design data of all N-back tasks at the individual subject level, and entering the results into a second level random effects analysis across subjects. Regions of significant activation and deactivation during working memory performance were identified from the group-level statistical contrast of average N-back signal versus 0-back. To identify positively activated clusters, an uncorrected one-tailed voxel-level threshold of $p<0.001$ was applied, followed by a

cluster size threshold to achieve correction for multiple comparisons at a false discovery rate (FDR) of 0.001. (Curran-Everett 2000; Genovese, et al. 2002) Positive activations generally coincided with previously reported working memory regions (D'Esposito, et al. 1995; McCarthy, et al. 1994; Owen, et al. 2005). For negatively activated clusters, FDR was held to 0.005; deactivations generally coincided with the default mode network (Greicius, et al. 2003; Raichle, et al. 2001). The statistical threshold applied to task negative regions was raised in order to capture weaker deactivation in left parietal cortex, a known default mode region. (Fransson 2005) Control regions were defined using maps showing voxels with no significant positive or negative activation with respect to the task (voxel-level $p>0.05$ uncorrected). ROIs were defined from these clusters by retaining all significant voxels within 8 mm of the cluster peak, except for control ROIs which contained all voxels within 8mm of their cluster peaks. Table 3.1 lists all eleven ROIs, their locations (MNI coordinates), and abbreviations of our nomenclature.

Functional Connectivity Analysis

Functional connectivity measures were calculated based on the steady-state data after discarding the first 5 volumes. All time series had a discrete cosine basis high-pass filter with period of 100 seconds applied to remove very low frequency trends and drifts, and residual correlates of motion remaining in the data after image realignment and normalization had their effects minimized through linear regression of the first-order estimated motion parameters. Cardiac, respiratory, and global trends were minimized through regression of the average signal across the entire brain. A 0.1 Hz Chebyshev Type II low-pass filter was also applied. The connectivity measure used was the Pearson

correlation coefficient, converted to an approximately normal random variable via the Fisher Z transformation (Fisher 1928; Hampson, et al. 2006b) according to Equation 3.1, where r is the Pearson's correlation and N denotes the degrees of freedom (estimated as being equal to the number of acquired images here).

Table 3.1: ROI Locations

#	Location	MNI coordinates			Description
		X	Y	Z	
1	Right parietal	33	-45	39	Working memory (Task positive)
2	Right Frontal	33	12	63	Working memory (Task positive)
3	Pre-SMA (pSMA)	0	12	60	Working memory (Task positive)
4	Left Frontal	-24	3	54	Working memory (Task positive)
5	Right Prefrontal	45	42	24	Working memory (Task positive)
6	Left Prefrontal (LPFC)	-45	9	39	Working memory (Task positive)
7	Prefrontal Dorsal	-6	63	30	Default mode (Task negative)
8	Left Parietal	-48	-72	36	Default mode (Task negative)
9	Posterior Cingulate (PCC)	-3	-39	33	Default mode (Task negative)
10	Right occipital cortex (ROCC)	10	-90	2	Visual (Control)
11	Left occipital cortex	-10	-90	2	Visual (Control)

$$z = \operatorname{atanh}(r) \cdot \sqrt{N - 3} \tag{3.1}$$

Four separate analyses of connectivity were performed. In the first, a mean time series was calculated for each ROI at each load, and these representative time courses were tested for significant effects of load on their pair-wise correlation using a one way ANOVA through the R statistical package. (http://www.r-project.org/) All possible pairs of ROIs were tested (# of tests = 54). Load effects were considered significant at $p<0.05$, uncorrected for multiple comparisons across paths.

In the second connectivity analysis, within network changes in functional connectivity were measured by calculating the average correlation across all paths within a given network. This measurement was termed the path independent connectivity (PIC). The distribution of values across subjects was tested for effects of load within the working memory, default mode, and control networks.

In the third analysis, a modified seed region approach was used. Focusing again on individual paths (i.e. pairs of regions) and identifying only those paths showing significant effects of load, one region was defined as being the seed, while the other was defined as the target. Connectivity maps to the seed were constructed for the entire brain by correlating each individual voxel's time course with the mean seed region time course. These maps were entered into a 2nd level ANOVA with four levels (i.e. four different cognitive loads) using SPM5, testing for effects of load on these voxel-wise functional connectivity maps across the brain. Clusters of voxels showing significant effects of load

($p<0.05$ uncorrected) across subjects on functional connectivity bordering or within the target region were interpreted as supporting evidence of load effects in these paths.

The fourth functional connectivity analysis stemmed from inspection of the results from the previous analyses. Preliminary results from a variety of working memory seed regions showed load related changes in functional connectivity to a region of the posterior cingulate cortex not currently covered by any ROI. To summarize these observations, a new seed region (See Figure 3.6A) was identified by selecting a connected cluster of voxels in the posterior cingulate cortex showing significant load effects ($p<0.001$ uncorrected) across all functional connectivity maps employing a working memory (task positive) seed region (6 maps/subject/load, 48 total maps/load). Functional connectivity maps were calculated across the entire brain using this new seed region, and these maps were tested on a voxel-by-voxel basis for significant effects of steady state cognitive load across subjects ($p<0.01$ uncorrected), as was done previously. For comparative purposes, the location of voxels within the PCC showing load related changes in activation during performance of block designed N-back tasks was calculated as well.

Results

In five subjects, performance was measured during steady state N-back acquisitions as the percent of targets correctly identified (1 back: 98 +/- 2.7 %; 2 back: 79 +/- 11%; 3 back: 52 +/-15%), suggesting the increase in task difficulty. Signal changes as a percent of the total signal were measured during the block designed portion of each N-back task for each ROI, and are plotted in Figure 3.2. Load related increases in

activity were qualitatively identified in all working memory regions, with negligible increases occurring when increasing load from 2 Back to 3 Back conditions. (Figure 3.3A and B). Functional connectivity within both the working memory and default mode networks were modulated by cognitive load in steady state working memory tasks, which is illustrated in Figures 3.3C and D. Changes in connectivity occur with N-back conditions in regions identified in the GLM analysis of block designed task data.

Between pairs of ROIs, six paths were found to have significant changes in functional connectivity related to cognitive load, shown in Figure 3.4. These included paths within the working memory network (Left Frontal - Left Prefrontal; PreSMA – Right Frontal; PreSMA – Left Prefrontal), within the default mode network (Prefrontal Dorsal – Posterior Cingulate), and between the working memory and the default mode network (Right Parietal – Posterior Cingulate). One path showed significant load effects between left frontal task positive region and left occipital cortex.

Analyzing full connectivity maps, the load effect on each path was confirmed through the presence of clusters of voxels having load dependent functional connectivity bordering the target regions, the locations of which are reported in Figure 3.4. In each case, significant but relatively weak ($p<0.05$ uncorrected) load effects were observed.

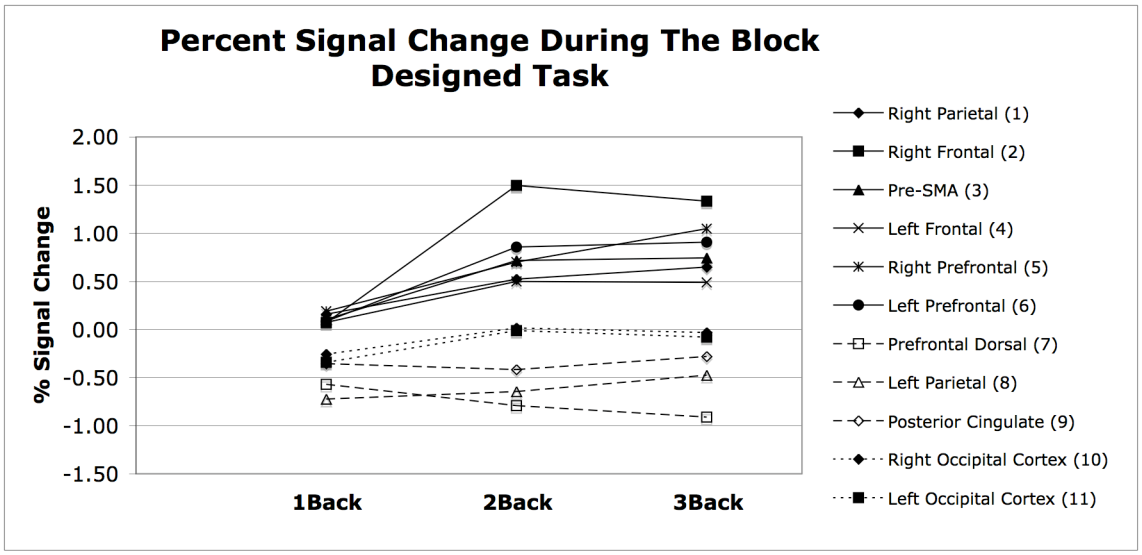

Figure 3. 2 - Percent signal changes were measured during the block designed portion of each N-back task. The numbers listed alongside ROI names correspond to ROI #s in Table 3.1.

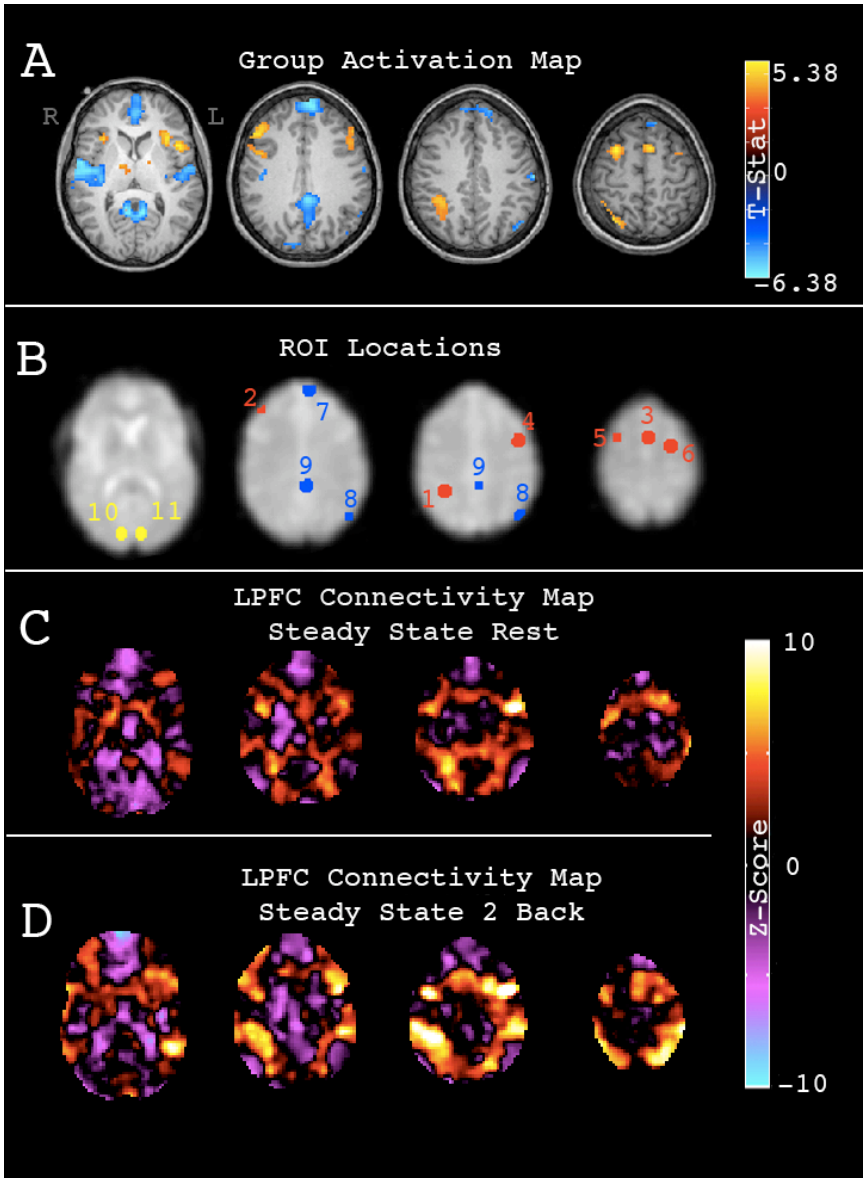

Figure 3. 3 - (A) Group activity map, showing the main effect of task across loads. (B) ROI locations. Red: Task Positive Network, Blue: Task Negative Network, Yellow: Control regions. ROI number key is in Table 1. (C) Resting state functional connectivity map to region 6. (D) Steady State 2 back functional connectivity map to region 6. Note the qualitative increase in connectivity in task positive regions when compared to the resting state, and a decrease in connectivity in task negative regions.

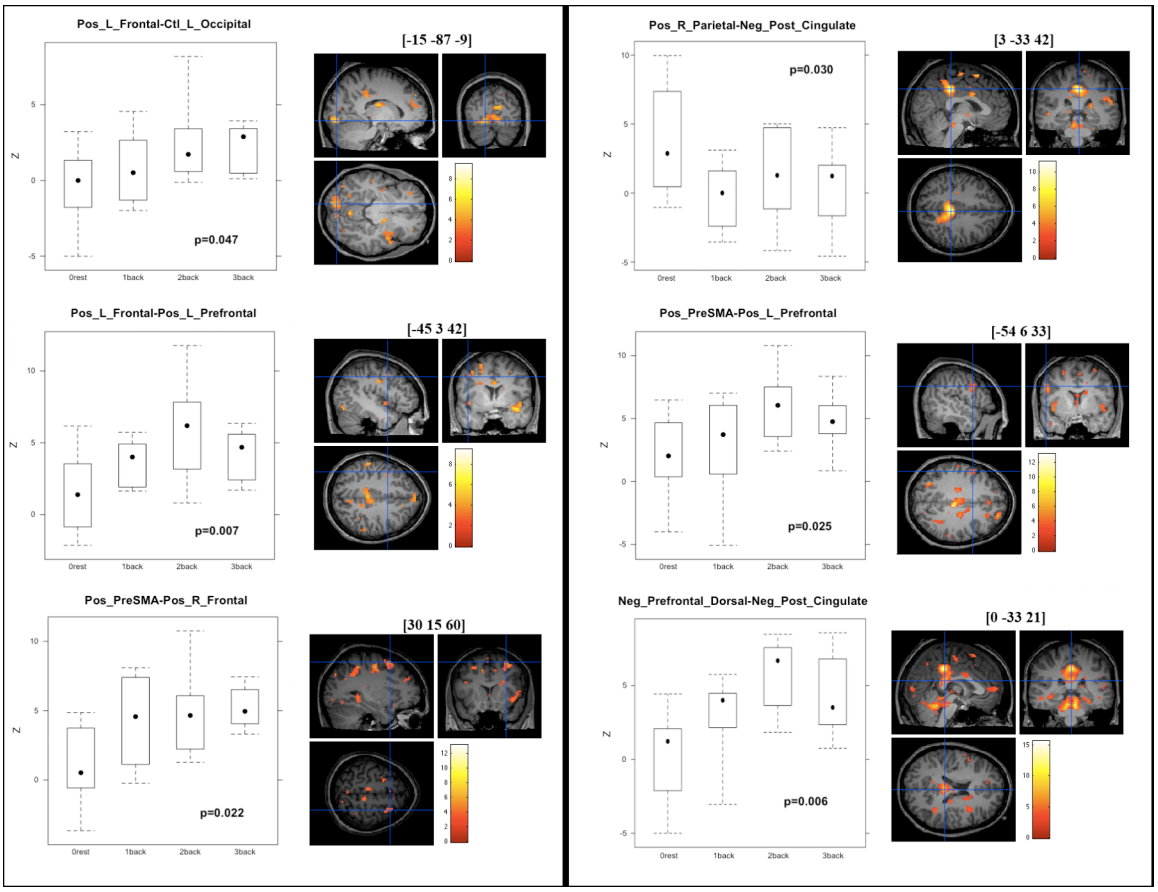

Figure 3.4 - Standard box plots showing the six paths containing significant effects of cognitive load on steady state functional connectivity. Defining each path as containing a seed region and a target region (seed-target as showin in each path's title), clusters of load affected voxels were located near each target region when analyzing seed region connectivity maps (coordinates of cluster shown for comparison with ROI centers listed in Table 1).

Analyzing average within network changes in functional connectivity, Figure 3.5 shows that the networks showing both positive changes and negative changes with the task exhibited load related increases in PIC (p=0.063 & p-0.037 respectively), with no such load effect within the control network (p=0.12).

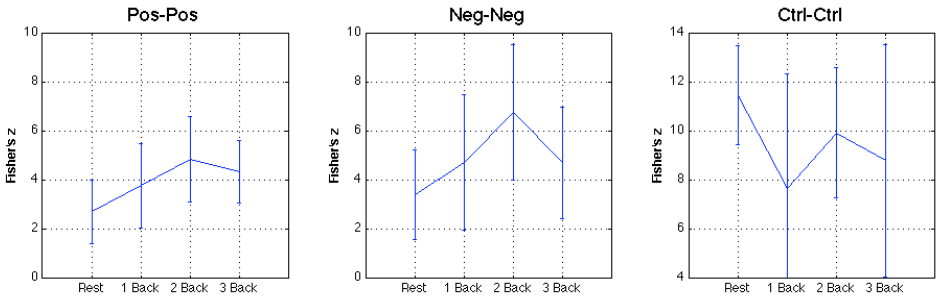

Figure 3.5 - Mean +/- standard deviation across subjects of the path independent connectivity (PIC) measure within networks. The PIC was calculated as the mean connectivity across all possible pairs of ROIs within each specified network (i.e. Pos – Pos reflects the average connectivity of every working memory ROI to every other working memory ROI. Results show increases in functional connectivity within the working memory and within the default mode network as load increases. Pos = task positive; Neg = task negative; Ctrl = control network

Analysis of all working memory functional connectivity maps together showed a cluster of voxels with load dependent functional connectivity in the posterior cingulate cortex ($p<0.001$ corrected for multiple comparisons at the cluster peak, Figure 3.6A), though they only partially overlapped with the PCC region defined in Table 3.1, which was a definition based on task activation (see Figure 3.6B). Comparing voxels with load dependent functional connectivity (to the working memory network) to those having load dependent activity during the blocked design task again separated the posterior cingulate cortex into at least two distinct regions, one superior and anterior to the other (Figure

3.6A). This superior and anterior portion of the PCC was analyzed as a new seed region of load effects in functional connectivity, similar to that performed for previously defined regions. Maps of load effects showed significant clusters ($p<0.01$ uncorrected) in all originally defined working memory and default mode ROIs (Figure 3.6C).

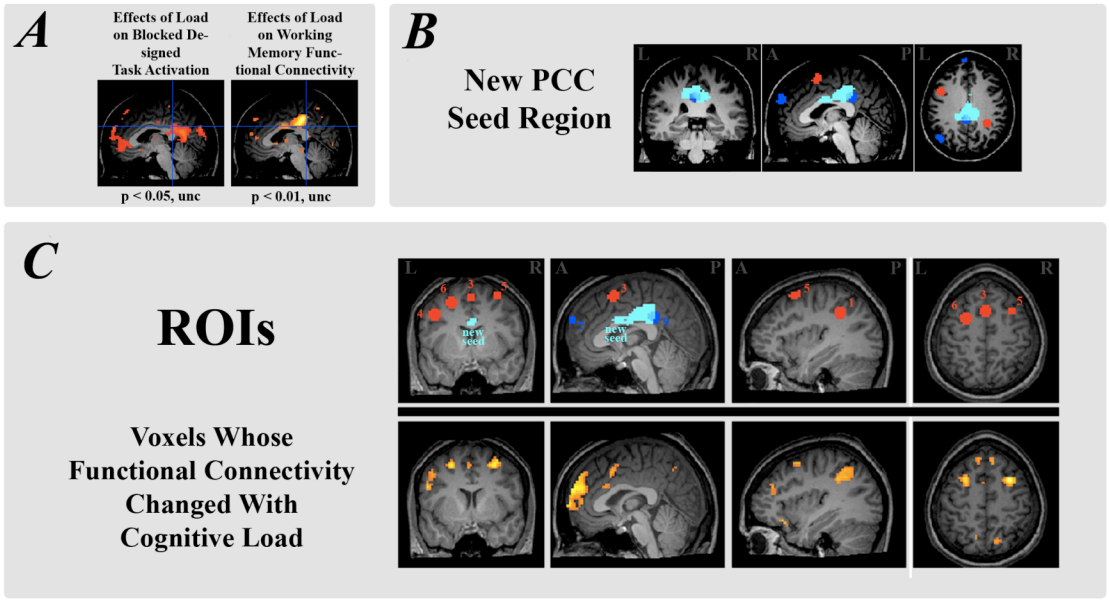

Figure 3.6 - (A) Differences between load effects on block designed task activation and load effects in functional connectivity to the working memory network. Crosshairs identify the same location in both images, highlighting the differences in cluster locations within the posterior cingulate cortex. (B) The new posterior cingulate seed region (cyan) used for stage 3 functional connectivity analysis. Red and blue ROIs correspond to those shown in Figure 3.3. (C) Results showing the effects of cognitive load on functional connectivity to the new seed region. The location of regions from Table 1 are shown on top for reference, as is the location of the seed region. The newly defined region of the posterior cingulate cortex shows significant load effects ($p<0.01$ unc) in most task positive and task negative regions listed in Table 1.

Discussion

We have presented results from four analyses of steady state functional connectivity in the working memory and default mode networks. As prior work demonstrated graded load effects in the motor network (Newton, et al. 2007), this study has demonstrated a similar effect in a cognitive domain (working memory) across a range of cognitive loads. Comparing connectivity measured in the resting state to that measured during steady-state task performance, these data confirm previously reported increases in steady-state connectivity within the working memory network across a wider range of conditions. (Hampson, et al. 2006a) Our data also demonstrate that functional connectivity is not modulated in a binary fashion (representing a 'turning on' or a 'turning off' of the synchronization within a given network), but rather functional connectivity is modulated in a gradual fashion as cognitive load changes.

Whether or not these changes are subject to a ceiling effect (as might be evidenced by the smaller changes in connectivity accompanying the transition from 2back to 3back steady state tasks) remains unclear. Figure 3.2 suggests that working memory regions experience load related increases in the mean BOLD signal that taper off at very high loads (N=2 - N=3), an effect that was relatively uniform across working memory regions. This may be the result of drops in the accuracy of task performance. Load related changes in the mean BOLD signal was not observed among most default mode regions (prefrontal dorsal being the only potential exception), while load related changes in functional connectivity were observed in the posterior cingulate cortex. This suggests that load related changes in task activity does not necessarily dictate the presence of load related changes in functional connectivity, though this could be better

supported by more rigorous comparisons of block designed activation and steady state functional connectivity.

The second goal of this work was to determine how connectivity changes within the default mode network as well as between the default mode network and the working memory network in the context of a continuous working memory task. When we focus on average connectivity measured between all pairs of regions belonging to the same network, load related increases in functional connectivity (the PIC) are significant for both the working memory and the default mode network. This significance potentially represents a convergence of the within network steady functional connectivity, supporting the view that functional connectivity dynamically changes within and between cognitive networks according to the cognitive demands present. We report increased synchrony within the default mode network as working memory load increases, contrary to some previous reports (Fransson 2006) that suggest that correlations within the default mode network trend towards zero as cognitive load increases. However, our data do replicate previously reported findings of negative correlations between working memory regions and default mode regions (Fox, et al. 2005; Greicius, et al. 2003). We expand on those results by suggesting that the relationship between the networks is affected not just by task prescence but by task load, particularly in the posterior cingulate cortex where we report decreasing correlations. Functional connectivity measured under conditions other than rest may provide new information augmenting that obtained from passive subjects alone.

The potential for differences between the behavior of functional connectivity measures and conventional task responses is emphasized by our results from the posterior

cingulate cortex. We found that distinctly different regions show load related changes in traditional task activation than show load related changes in functional connectivity to working memory regions (Figure 3.6A). This suggests that there are functional subdivisions within the large region of deactivation generally covering the posterior cingulate cortex, a region implicated as playing a particularly complex role in the default mode network. (Buckner, et al. 2008) There is evidence that at least two areas are encompassed in this deactivation including the posterior cingulate cortex and restrosplenial cortex, with the latter lying more posterior and inferior to the other. (Buckner, et al. 2008; Kobayashi and Amaral 2007) However, continued subdivision anteriorly along the cingulate gyrus may be possible as well, evidenced by studies of the anterior cingulate cortex. (Margulies, et al. 2007)

The continuous, dynamic nature of changes in our measured functional connectivity may have particular relevance for interpreting the behavior of the default mode network. The basic default mode hypothesis distinguishes between those brain regions that are primarily engaged in the resting state (default mode), and those that are not. Speculations on the underlying cognitive differences between the resting state and other 'active' conditions have focused on classifying thoughts into different types. For example, it has been posited that task related (default mode) deactivations may be related to switching from introspective, self-oriented thought to attention demanding, goal-oriented thought (Gusnard, et al. 2001; Raichle, et al. 2001). Fransson suggests that there may be more than one type of cognition being accomplished by the default mode network, with example functions being self representation and self-referential mental events (Fransson 2006), or self-reflective and self-referential thought (Fransson 2005),

though these hypotheses still operate under the assumption that the default mode network is either active or not depending on the type of thought. Our data suggest that the default mode network does not simply 'switch off' as if operating in a binary fashion, but that it gradually changes its activity according to the current cognitive demands. This may also argue against a simple cessation of one type of thought in favor of another. It is also possible that this changing synchrony between brain regions represents inhibition modulated by a third region of the brain (Greicius, et al. 2003), though the role of BOLD synchrony in measuring inhibition is beyond the scope of this study.

Our finding that functional connectivity changes as a function of cognitive demand may be important for studies developing methods for connectivity measurement in traditional fMRI data, as the temporal dynamics of these connectivity changes remain unclear. Measuring connectivity during traditional fMRI protocols would be useful because successful techniques could greatly increase the amount of candidate data available for connectivity analysis. One method (Fair, et al. 2007) uses short segments of steady-state data from within larger blocks of a condition acquired during a block designed experiment. In this case, our results suggest that functional connectivity would not remain constant throughout these blocked tasks. If the demand induced changes in functional connectivity occur slowly compared to the length of task blocks (i.e. blocks were short relative to the time required for connectivity changes to occur), then estimating connectivity over the entire length of those blocks may produce poor estimates of the true condition dependant functional connectivity. The temporal dynamics of these changes remain unclear.

The possible influence of global time course regression on the results and interpretation of functional connectivity analyses has recently been highlighted. It has been argued that negative correlations between the default mode network and the working memory network may be an artifact of removing the global signal. (Murphy, et al. 2009) However, our study places no particular importance on the sign of measured correlations, merely on whether they change across loads. Given this fact along with the potential for beneficial removal of artifacts and global baseline correlations, we chose to include global time course regression. Measurement of load effects with and without global signal removal in future studies may provide insight into the possible effects of this preprocessing tool.

The present study is limited in several ways. First, the complicated functional connectivity of the posterior cingulate cortex, and the potential for functional subdivision along the cingulate gyrus needs further investigation. Second, the relatively low number of subjects used in this study and the low accuracy of the three back performance necessitates further work to confirm whether these are ceiling effects in functional connectivity. Lastly, investigating the functional connectivity between typical 'default mode' regions and those of various other cognitive networks may lead to a better understanding of the functional role played by the default mode network.

Conclusions

In conclusion, we have demonstrated that functional connectivity within the working memory network modulates gradually with working memory load (i.e. task condition), culminating in increased synchrony between signals from various working

memory regions. Furthermore, the functional connectivity between working memory regions and default mode regions changes with load as well, a finding highlighted by our results in the posterior cingulate cortex.

References

Arfanakis K, Cordes D, Haughton VM, Moritz CH, Quigley MA, Meyerand ME. 2000. Combining independent component analysis and correlation analysis to probe interregional connectivity in fMRI task activation datasets. Magn Reson Imaging 18(8):921-30.

Beckmann CF, DeLuca M, Devlin JT, Smith SM. 2005. Investigations into resting-state connectivity using independent component analysis. Philos Trans R Soc Lond B Biol Sci 360(1457):1001-13.

Biswal B, Hudetz AG, Yetkin FZ, Haughton VM, Hyde JS. 1997. Hypercapnia reversibly suppresses low-frequency fluctuations in the human motor cortex during rest using echo-planar MRI. J Cereb Blood Flow Metab 17(3):301-8.

Biswal B, Yetkin FZ, Haughton VM, Hyde JS. 1995. Functional connectivity in the motor cortex of resting human brain using echo-planar MRI. Magn Reson Med 34(4):537-41.

Buckner RL, Andrews-Hanna JR, Schacter DL. 2008. The brain's default network: anatomy, function, and relevance to disease. Ann N Y Acad Sci 1124:1-38.

Cordes D, Haughton VM, Arfanakis K, Carew JD, Turski PA, Moritz CH, Quigley MA, Meyerand ME. 2001. Frequencies contributing to functional connectivity in the cerebral cortex in "resting-state" data. AJNR Am J Neuroradiol 22(7):1326-33.

Curran-Everett D. 2000. Multiple comparisons: philosophies and illustrations. Am J Physiol Regul Integr Comp Physiol 279(1):R1-8.

D'Esposito M, Detre JA, Alsop DC, Shin RK, Atlas S, Grossman M. 1995. The neural basis of the central executive system of working memory. Nature 378(6554):279-81.

Esposito F, Bertolino A, Scarabino T, Latorre V, Blasi G, Popolizio T, Tedeschi G, Cirillo S, Goebel R, Di Salle F. 2006. Independent component model of the default-mode brain function: Assessing the impact of active thinking. Brain Res Bull 70(4-6):263-9.

Fair DA, Schlaggar BL, Cohen AL, Miezin FM, Dosenbach NUF, Wenger KK, Fox MD, Snyder AZ, Raichle ME, Petersen SE. 2007. A method for using blocked and event-related fMRI data to study "resting state" functional connectivity. Neuroimage 35(1):396-405.

Fisher RA. 1928. The General Sampling Distribution of the Multiple Correlation Coefficient. Proceedings of the Royal Society of London. Series A, Containing Papers of a Mathematical and Physical Character 121(788):20.

Fox MD, Snyder AZ, Vincent JL, Corbetta M, Van Essen DC, Raichle ME. 2005. The human brain is intrinsically organized into dynamic, anticorrelated functional networks. Proc Natl Acad Sci U S A 102(27):9673-8.

Fransson P. 2005. Spontaneous low-frequency BOLD signal fluctuations: an fMRI investigation of the resting-state default mode of brain function hypothesis. Hum Brain Mapp 26(1):15-29.

Fransson P. 2006. How default is the default mode of brain function? Further evidence from intrinsic BOLD signal fluctuations. Neuropsychologia 44(14):2836-45.

Genovese CR, Lazar NA, Nichols T. 2002. Thresholding of statistical maps in functional neuroimaging using the false discovery rate. Neuroimage 15(4):870-8.

Greicius MD, Kiviniemi V, Tervonen O, Vainionpaa V, Alahuhta S, Reiss AL, Menon V. 2008. Persistent default-mode network connectivity during light sedation. Hum Brain Mapp 29(7):839-47.

Greicius MD, Krasnow B, Reiss AL, Menon V. 2003. Functional connectivity in the resting brain: a network analysis of the default mode hypothesis. Proc Natl Acad Sci U S A 100(1):253-8.

Gusnard DA, Akbudak E, Shulman GL, Raichle ME. 2001. Medial prefrontal cortex and self-referential mental activity: relation to a default mode of brain function. Proc Natl Acad Sci U S A 98(7):4259-64.

Hampson M, Driesen NR, Skudlarski P, Gore JC, Constable RT. 2006a. Brain connectivity related to working memory performance. J Neurosci 26(51):13338-43.

Hampson M, Olson IR, Leung HC, Skudlarski P, Gore JC. 2004. Changes in functional connectivity of human MT/V5 with visual motion input. Neuroreport 15(8):1315-9.

Hampson M, Peterson B, Gore J. 2001. Detection of low frequency temporal correlations in steady state and block design data. Neuroimage 13(6):S144-S144.

Hampson M, Tokoglu F, Sun Z, Schafer RJ, Skudlarski P, Gore JC, Constable RT. 2006b. Connectivity-behavior analysis reveals that functional connectivity between left BA39 and Broca's area varies with reading ability. Neuroimage 31(2):513-9.

Honey GD, Fu CH, Kim J, Brammer MJ, Croudace TJ, Suckling J, Pich EM, Williams SC, Bullmore ET. 2002. Effects of verbal working memory load on corticocortical connectivity modeled by path analysis of functional magnetic resonance imaging data. Neuroimage 17(2):573-82.

Horovitz SG, Fukunaga M, de Zwart JA, van Gelderen P, Fulton SC, Balkin TJ, Duyn JH. 2007. Low frequency BOLD fluctuations during resting wakefulness and light sleep: A simultaneous EEG-fMRI study. Hum Brain Mapp.

Kobayashi Y, Amaral DG. 2007. Macaque monkey retrosplenial cortex: III. Cortical efferents. J Comp Neurol 502(5):810-33.

Lowe MJ, Dzemidzic M, Lurito JT, Mathews VP, Phillips MD. 2000. Correlations in low-frequency BOLD fluctuations reflect cortico-cortical connections. Neuroimage 12(5):582-7.

Lowe MJ, Mock BJ, Sorenson JA. 1998. Functional connectivity in single and multislice echoplanar imaging using resting-state fluctuations. Neuroimage 7(2):119-32.

Margulies DS, Kelly AM, Uddin LQ, Biswal BB, Castellanos FX, Milham MP. 2007. Mapping the functional connectivity of anterior cingulate cortex. Neuroimage 37(2):579-88.

McCarthy G, Blamire AM, Puce A, Nobre AC, Bloch G, Hyder F, Goldman-Rakic P, Shulman RG. 1994. Functional magnetic resonance imaging of human prefrontal cortex activation during a spatial working memory task. Proc Natl Acad Sci U S A 91(18):8690-4.

Meyer-Baese A, Wismueller A, Lange O. 2004. Comparison of two exploratory data analysis methods for fMRI: unsupervised clustering versus independent component analysis. IEEE Trans Inf Technol Biomed 8(3):387-98.

Murphy K, Birn RM, Handwerker DA, Jones TB, Bandettini PA. 2009. The impact of global signal regression on resting state correlations: are anti-correlated networks introduced? Neuroimage 44(3):893-905.

Newton AT, Morgan VL, Gore JC. 2007. Task demand modulation of steady-state functional connectivity to primary motor cortex. Hum Brain Mapp 28(7):663-72.

Owen AM, McMillan KM, Laird AR, Bullmore E. 2005. N-back working memory paradigm: A meta-analysis of normative functional neuroimaging. Human Brain Mapping 25(1):46-59.

Prohovnik I, Hakansson K, Risberg J. 1980. Observations on the functional significance of regional cerebral blood flow in "resting" normal subjects. Neuropsychologia 18(2):203-17.

Raichle ME, MacLeod AM, Snyder AZ, Powers WJ, Gusnard DA, Shulman GL. 2001. A default mode of brain function. Proc Natl Acad Sci U S A 98(2):676-82.

Rissman J, Gazzaley A, D'Esposito M. 2004. Measuring functional connectivity during distinct stages of a cognitive task. Neuroimage 23(2):752-63.

Rissman J, Gazzaley A, D'Esposito M. 2008. Dynamic adjustments in prefrontal, hippocampal, and inferior temporal interactions with increasing visual working memory load. Cereb Cortex 18(7):1618-29.

Rogers BP, Morgan VL, Newton AT, Gore JC. 2007. Assessing functional connectivity in the human brain by fMRI. Magn Reson Imaging 25(10):1347-57.

van de Ven VG, Formisano E, Prvulovic D, Roeder CH, Linden DE. 2004. Functional connectivity as revealed by spatial independent component analysis of fMRI measurements during rest. Hum Brain Mapp 22(3):165-78.

Woodward TS, Cairo TA, Ruff CC, Takane Y, Hunter MA, Ngan ET. 2006. Functional connectivity reveals load dependent neural systems underlying encoding and maintenance in verbal working memory. Neuroscience 139(1):317-25.

CHAPTER IV

BOLD CORRELATES OF THETA POWER ACROSS WORKING MEMORY LOADS

Introduction

Neural activity manifests as electrical discharges within brain circuits that stimulate changes in blood flow and tissue oxygenation measurable by blood oxygen level dependent (BOLD) MRI. Although electrical activity and the subsequent hemodynamic response are coupled, there precise relationship is not well understood, and their have been few studies that quantitatively relate their features. Moreover, while electrical events occur on a timescale of milliseconds, we are unable to noninvasively identify their spatial locations very accurately, whereas BOLD signal changes occur over several seconds and may be resolved to millimeter accuracy. Thus, approaches that can combine the favorable aspects of both types of information synergistically are of potential importance.

Electrophyiological measurements made in concert with functional imaging may be useful in functional connectivity analyses. Most functional connectivity analyses based on seed regions require additional imaging runs to aid in the definition of those seed regions. As has already been discussed, one method involves performing a conventional fMRI experiment whose activation map can localize functionally relevant tissue. Alternatively, studies have used high resolution structural images to define seed regions anatomically. Measurement of electroencephalographic (EEG) oscillations provides another functionally relevant signal that may be used to map related regions

across the brain using techniques common to most fMRI functional connectivity analyses, potentially identifying regions which are appropriate to be entered into subsequent connectivity analyses. (Hampson, et al. 2002)

EEG is a method of measuring two dimensional distributions of functionally relevant electrical potentials across the scalp. EEG studies make use of arrays of electrodes organized along standardized grids covering the scalp, where voltage differences between each electrode and a common reference electrode (EEG voltage) are recorded. Typical EEG data are simply the spatial maps of EEG voltage measured repetitively through time, with the spatial location of each electrode either being measured or inferred from the placement scheme used. This leads to data that are three dimensional with two spatial dimensions and one temporal dimension. EEG voltages on the scalp are produced by electrical changes associated with neuronal activity. The surface potential represents the integrated effect of diverse sources of currents within the volume conductor of the brain and head. Voltage changes on the scalp arise primarily from graded synaptic potentials of the pyramidal neurons, both excitatory and inhibitory in nature, though less significant contributions may be made from synchronous fast action potentials (either calcium or sodium mediated), and dendritic calcium spikes following hyperpolarization. (Olejniczak 2006) Current flow between within-brain neuronal sources and scalp electrodes, referred to as volume conduction, is affected by the conductive properties of all tissues traversed including at least the scalp, fat, skull, and brain tissue (Gevins, et al. 1995), though the complications associated with volume conduction may be different for each study based on the specific analyses performed.

There is evidence that local field potentials are related to the BOLD response underpinning fMRI. (Lauritzen and Gold 2003; Logothetis, et al. 2001) Based on this, EEG and fMRI have been measured and/or analyzed simultaneously in an attempt to identify regions of the brain that are functionally related to various types of EEG signals. One example of this is the spatial localization of epileptic foci using timing information measured with EEG (Cunningham, et al. 2008; Gotman, et al. 2004). In this case, temporal changes in EEG voltage itself (e.g. timing of epileptic spikes) informs the analysis of fMRI data. Another example is the co-analysis of event related potentials measured with EEG and BOLD signal changes measured with fMRI. This novel method of combining EEG data with BOLD sensitive images was developed by Horovitz et al (Horovitz, et al. 2004; Horovitz, et al. 2002), who looked at correlated BOLD signal changes measured inside the scanner with electrophysiological changes in event related potentials measured while subjects performed the same task outside the scanner. This method has also been used to identify those regions throughout the brain that may contribute to the measured electrical potentials recorded at the scalp.

Functional significance has also been attributed to changes in cortical rhythms, leading to studies that have focused instead on measuring the hemodyanamic correlates of various frequency bands within EEG data. These studies also attempt to marry the advantages of both modalities, namely the high temporal resolution of EEG measured over long imaging runs (allowing for frequency analysis of its data across multiple intervals of time), and high spatial resolution of tomographic fMRI data allowing for more specific localization than is achievable by EEG measurements alone. By separating the EEG data into several segments (i.e. epoching), and estimating the power spectrum of

each segment, time courses of power across a range of frequencies in EEG data can be used for modeling fMRI signals using the general linear model. Examples include studies of the 8-12Hz alpha band (Goldman, et al. 2002; Laufs, et al. 2003), the 17-23Hz beta band (Laufs, et al. 2003), the 1-3Hz delta band (Lu, et al. 2007), and the 3-8Hz theta band (Scheeringa, et al. 2007; Scheeringa, et al. 2009). Changes in power within given EEG frequency bands have been studied during task performance in some cases, though studies of the resting state have continued to become more common. Simultaneous measurements of EEG and fMRI signals allow the identification of those BOLD signals that covary with electrophyiological measurements across increasing cognitive loads.

A key cognitive network that may be amiable to studies utilizing simultaneous EEG and fMRI is working memory. Working memory is the temporary storage of information that plays a supportive role in the performance of a variety of cognitive tasks (Baddeley 1981), and changes in theta power along the frontal midline (FMθ) have been correlated with changes in working memory load. (Basar-Eroglu, et al. 1992; Klimesch 1996a; Klimesch 1999; Roschke and Fell 1997; Yordanova, et al. 2003) Dipole source modeling suggests that FMθ power arises from anterior cingulate cortex (Gevins, et al. 1997; Onton, et al. 2005; Reischies, et al. 2005), though some have hypothesized that these results may mask a more diffuse source located closer to the surface of the brain. (Scheeringa, et al. 2007) It has been shown that frontal midline theta is correlated with hippocampal glutamate concentrations during performance of some difficult cognitive tasks (Gallinat, et al. 2006), though the question of whether hippocampal theta (electrical oscillations measured via single cell recordings in the theta band) drives FMθ remains unclear. (Miller 1991) Analysis of theta power and functional connectivity in

simultaneously acquired EEG and fMRI data may provide a method of evaluating this proposed interaction between cingulate cortex and the hippocampus.

This study has two goals. First, we attempt to illustrate a method of spatially locating regions of cortex associated with specific features of the EEG utilizing load modulated correlations between BOLD signals band power estimates from EEG data. Second, we apply this method to a study of functional connectivity during steady state working memory tasks, with a particular interest in the cingulate cortex, hippocampus and related structures.

Methods

Functional Tasks

EEG and fMRI data were simultaneously recorded during a series of 24 experiments spanning six subjects. FMRI and EEG data were analyzed under four steady state conditions and during one block designed task. Not all tasks were completed by all subjects. Each run consisted of some variation on a verbal identity working memory task using letters presented every 2s. A block designed task consisted of 120 images covering alternating blocks of 0 back and 2 back tasks (15 letters/block, 20% were targets). Blocked task images were analyzed with a standard general linear model to identify voxels significantly activated and deactivated within each subject (2 back vs. 0 back, $p<0.005$, no minimum cluster size). (Ragland, et al. 2002) Each steady state run consisted of 100 images, and corresponded to one of a range of working memory loads. Working memory load was controlled by the number of letters required to be held in

working memory, with loads of zero, one, two, or three being used for a given run (0 back, 1 back, 2 back, 3 back). All subjects completed the block designed task. Out of six subjects completing steady state tasks, images were acquired in four subjects under the 0 back condition, in six subjects under the 1 back condition, in five subjects under the 2 back condition, and in three subjects under the 3 back condition.

Imaging and Initial Processing

All MRI images were acquired on a 3T Philips Achiva scanner with a volume transmit and an eight channel SENSE receive coil. Each subject had high resolution T_1 weighted images gathered for use in normalizing images to the MNI 152 template. All functional images were acquired using single shot, gradient echo, echo planar imaging acquired axially covering the full cerebrum, with the following imaging parameters: field of view = 200x200mm in plane, voxel dimensions = 2.5x2.5x3.5mm, 35 slices, TR/TE=2s/35ms, SENSE factor = 1.8, flip angle = 79°. Functional images had slice timing and motion artifacts corrected, were co-registered within subject, and were spatially normalized (final voxel dimensions: 3x3x3mm) using SPM5. (http://www.fil.ion.ucl.ac.uk/spm/software/spm5/)

EEG Acquisition

EEG data were recorded outside the MR scanner as well as simultaneously with functional images inside the scanner using a 64 channel Neuroscan MagLink Cap in combination with a Synamps 2 amplifier and a PC running Neuroscan's 'Scan' software (version 4.4). All EEG data were recorded from each electrode with a 10kHz sampling

rate, and were separated into epochs of 2s each. Those data, recorded simultaneously with image acquisition, underwent two artifact removal processes. Artifacts resulting from switching of magnetic gradient coils were removed by subtracting the average artifact measured across any given epoch and that on either side of it. (Allen, et al. 2000) Following gradient artifact removal, signals were resampled at 1kHz and low pass filtered at 30Hz.

Ballistocardiogram artifacts were removed through analysis of pulse oximetery data simultaneously recorded with fMRI and EEG data. Pulse oximeter signals were high pass filtered and voltage thresholded in order to identify the timing of heart beats. The corresponding EEG data surrounding each detected heartbeat were separated into epochs. Epochs were corrected for baseline drifts and averaged together, creating an average ballistocardiogram artifact for each EEG channel. A spatial singular value decomposition was performed on those average artifacts, the output of which was input to a spatial filtering algorithm to remove ballistiocardiogram artifacts from each channel's full time course. A high pass filter with a cutoff frequency of 0.6Hz was then applied to each channel's full time course

Calculation of Theta Power Time Courses

Trigger pulses output by the MR scanner were used to synchronize EEG and fMRI data acquisitions for each functional run in order that EEG data could be separated into epochs corresponding to the acquisition of each full fMRI image volume. For each epoch, frequency spectra were estimated over the first 1.8s, leaving a 200ms gap between measurements. The average power across the frequency band of 3-8Hz was calculated

for each electrode and all epochs, resulting in a time course of theta band power for each electrode. The average theta time course was calculated across all 20 frontal electrodes, resulting in one theta time course per experiment (i.e. for each functional imaging run). These theta time courses were convolved with a canonical hemodynamic response function prior to their use in the analysis of fMRI data.

Estimation and Analysis of Theta Correlations to BOLD Signals

Analysis of partial correlation to theta power in steady state fMRI data was accomplished through use of a general linear model. The theta power time course was used as a regressor along with estimated motion parameters and a global fMRI time course as confounds, resulting in a map of steady state correlations to theta power across the brain (theta power maps) in each subject at each load. Theta power maps from the zero back, one back, two back, and three back conditions were entered into an unbalanced repeated measures ANOVA with two factors covering subjects and loads as factors. The positive and negative effects across loads (i.e. those voxels that were positive or negative across loads) were estimated with significance set at $p<0.05$ uncorrected for multiple comparisons. Those regions whose theta power changed from load to load (i.e. the main effect of load) were identified through an F-contrast of values at adjacent loads, with a significance threshold of 0.005 uncorrected for multiple comparisons.

In order to generally describe those regions in which BOLD signals were correlated to theta power across all loads, or those whose correlation to theta power changed with load, the locations of the three most significant local maxima within each

cluster were converted to Talairach coordinates, and input to Talairach Daemon (Lancaster, et al. 2000). The results were then summarized to describe the cluster. In order to decrease the number of clusters needing identification, the p-value thresholds were relaxed and/or the minimum number of voxels in a cluster was increased. The specific thresholds used can be found in Tables 4.1-4.3. These different thresholds were used only for generally describing clusters, and the threshold of $p<0.005$ uncorrected for multiple comparisons with no minimum cluster size was used for all other results presented here.

ROI Definition and Analysis

Three regions of interest were defined around voxels found to significantly change their steady state correlation to theta power across N-back loads. These regions corresponded to the connected cluster of voxels significantly affected by load within the supplementary motor area (SMA), the posterior cingulate cortex (PCC), and along the parahippocampal gyrus (PHG). Beta weights for theta power from the general linear model analyses were averaged within each region of interest for each subject at each load.

Analysis of Steady State Functional Connectivity to the PHG

Steady state functional connectivity under all four N-back conditions (0, 1, 2, and 3) was calculated across the brain to the PHG using a seed region connectivity analysis. Prior to connectivity analysis, functional images had their global time course, six estimated motion parameters, and low frequency cosine basis functions regressed out.

Each voxel's time course was linearly detrended and demeaned, and was filtered at 0.1 Hz using a Chebychev Type II low pass filter. Functional connectivity analysis of the PHG consisted of estimating the average time course across the seed region and calculating the correlation of that time course to that of every within-brain voxel, yielding one map of functional connectivity across the brain for each subject and load. These maps were entered into an unbalanced repeated measures ANOVA identifying those voxels positively correlated with the seed on average across loads, those negatively correlated with the seed on average across loads, and those whose correlation to the seed changed as a function of load. In each of these cases, the significance threshold was set to $p<0.005$ uncorrected for multiple comparisons, with no minimum cluster size. A visualization of this overall analysis strategy is outlined in Figure 4.1.

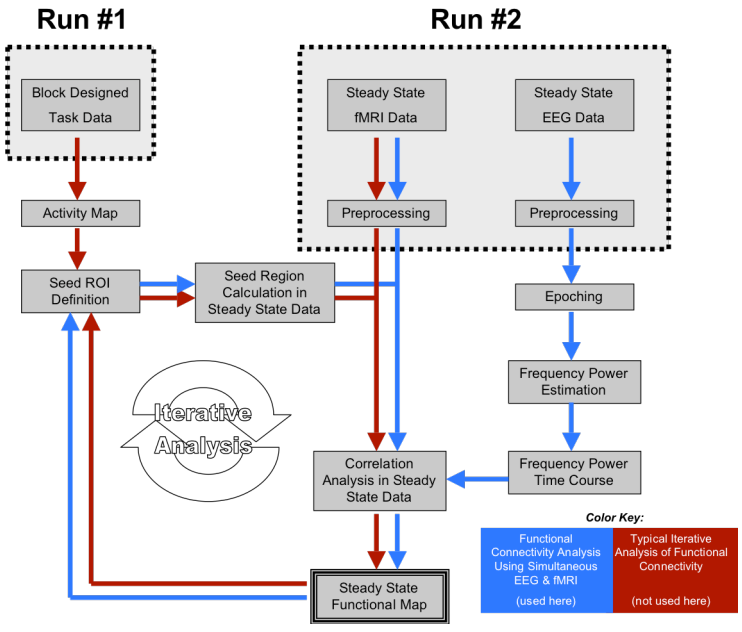

Figure 4.1 - Schematic description of functional connectivity analyses, where seed regions are either defined from activity maps based on another run or from maps of correlation to theta power in the steady state.

Steady State Correlations to Theta Power

Significant positive and negative correlations to theta power were measured on average across all steady state working memory conditions, some of which match regions identified by activation maps calculated from the block designed task data (shown in Figure 4.2). Positive correlations were measured in the supplementary motor area and the left primary motor cortex (Brodmann's areas 4 & 6), among other regions. Negative correlations were measured in the posterior cingulate cortex, and the medial frontal cortex, among other regions.

Significant changes in correlation to theta power were measured in regions overlapping those just described, though the most significant effects were not predicted by what regions were most correlated across conditions (either positively or negatively). The most significant regions found to have changing correlation to theta power across loads were the visual cortex, the supplementary motor area, the cingulate cortex, and the parahippocampal gyrus. Locations and descriptions of all these regions are found in Table 4.1-4.3. Shading identifies local maxima within the same cluster. The top three local maxima are listed for each cluster, unless fewer than three exist. Clusters were omitted from the report if they resided along major contrast boundaries (e.g. the edge of the brain), rising suspicion of residual motion artifacts.

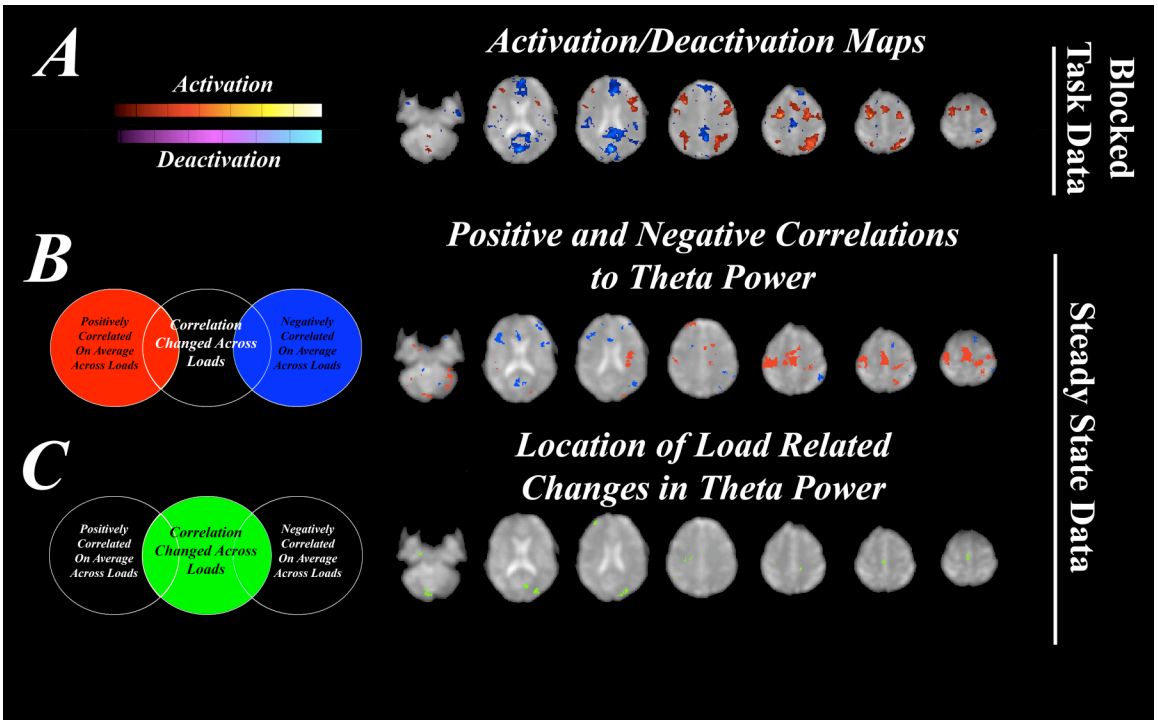

Figure 4.2 - (A) Typical Activation/Deactivation in response to performance of the block designed task. (B) Average correlations to theta power across the 0 back, 1 back, 2 back, and 3 back steady state tasks. Thresholds correspond to those used in Table 4.1 and 4.2. (C) Regions whose correlations to theta power changed with steady state cognitive load. Thresholds used correspond to those from Table 4.3.

Table 4.1 - Average Positive Correlation to Theta Power Across Loads (Positive Effect Of Load, p<0.05 unc, minimum cluster size=50)

Voxel Level			MNI 152 Coordinates			Description of Cluster
T	equivZ	p(unc)	X	Y	Z	
5.99	4.15	1.65E-05	-15.00	15.00	50.00	
5.56	3.97	3.54E-05	40.00	-22.50	72.50	Medial Frontal Gyrus, Brodmann Area 6
4.98	3.72	1.01E-04	5.00	-12.50	67.50	
4.98	3.72	1.00E-04	-62.50	0.00	-2.50	
4.11	3.27	5.34E-04	-55.00	7.50	2.50	Superior Temporal Gyrus, Brodmann Area 22
3.12	2.67	3.76E-03	-57.50	10.00	-12.50	
4.76	3.61	1.51E-04	45.00	-37.50	-5.00	
4.34	3.40	3.39E-04	60.00	-52.50	2.50	Middle Temporal Gyrus
4.15	3.30	4.86E-04	35.00	-7.50	-5.00	
4.66	3.56	1.83E-04	2.50	-87.50	-27.50	Left Lingual Gyrus
3.61	2.99	1.41E-03	-5.00	-90.00	-17.50	
4.06	3.24	5.90E-04	-22.50	-27.50	70.00	
3.91	3.16	7.83E-04	-30.00	-27.50	50.00	Left Precentral Gyrus, Brodmann Area 4
3.24	2.75	2.98E-03	-40.00	-15.00	67.50	
3.98	3.20	6.86E-04	-45.00	-47.50	-22.50	
3.37	2.83	2.30E-03	-35.00	-47.50	-15.00	Left Parahippocampal Gyrus, Brodmann Area 36
2.40	2.16	1.52E-02	-40.00	-30.00	-25.00	
3.85	3.12	8.90E-04	-22.50	-77.50	7.50	
2.52	2.25	1.23E-02	-30.00	-80.00	0.00	Left Middle Occipital Gyrus
2.45	2.20	1.39E-02	-22.50	-87.50	22.50	
3.79	3.09	9.90E-04	-42.50	-77.50	-12.50	
3.68	3.03	1.23E-03	-42.50	-70.00	2.50	Left Middle Occipital Gyrus, Brodmann Area 18
3.38	2.84	2.23E-03	-50.00	-70.00	-10.00	
3.72	3.05	1.13E-03	-45.00	-22.50	-5.00	
3.16	2.70	3.48E-03	-57.50	-37.50	7.50	Left Middle Temporal Gyrus
2.79	2.45	7.21E-03	-55.00	-47.50	7.50	
3.68	3.03	1.22E-03	27.50	-67.50	-5.00	
3.40	2.85	2.16E-03	12.50	-45.00	-10.00	Right Lingual Gyrus
3.03	2.62	4.46E-03	20.00	-55.00	0.00	
3.64	3.00	1.34E-03	-32.50	-25.00	27.50	
3.35	2.82	2.39E-03	-37.50	-7.50	22.50	Left Insula, Brodmann Area 13
3.15	2.69	3.57E-03	-40.00	0.00	25.00	
3.32	2.81	2.51E-03	-20.00	-57.50	60.00	
2.98	2.58	4.94E-03	-17.50	-60.00	75.00	Superior Parietal Lobule, Brodmann Area 7
2.81	2.46	6.89E-03	-32.50	-40.00	72.50	

Table 4.2 - Average Negative Correlation to Theta Power Across Loads (Positive Effect Of Load, p<0.05 unc, minimum cluster size=50)

Voxel Level			MNI 152 Coordinates			Description of Cluster
T	equivZ	p(unc)	X	Y	Z	
5.07	3.76	8.49E-05	45.00	27.50	10.00	
4.25	3.35	4.00E-04	-30.00	25.00	-5.00	Inferior Frontal Gyrus
4.15	3.30	4.87E-04	27.50	42.50	32.50	
4.24	3.34	4.16E-04	20.00	-65.00	-30.00	
3.40	2.85	2.16E-03	27.50	-40.00	-32.50	Right Cerebellum
2.97	2.57	5.04E-03	42.50	-40.00	-30.00	
3.95	3.19	7.23E-04	-30.00	-52.50	-32.50	
2.98	2.58	4.92E-03	-32.50	-67.50	-37.50	Left Cerebellum
2.39	2.15	1.56E-02	-22.50	-65.00	-25.00	
3.73	3.06	1.11E-03	-20.00	45.00	30.00	
2.07	1.90	2.85E-02	-10.00	37.50	27.50	Superior Frontal Gyrus, Brodmann Area 10
1.83	1.72	4.31E-02	-25.00	52.50	30.00	
3.57	2.96	1.54E-03	30.00	15.00	0.00	
3.13	2.68	3.69E-03	20.00	32.50	-7.50	Medial Frontal Gyrus
2.61	2.32	1.03E-02	25.00	32.50	-17.50	
3.56	2.96	1.56E-03	-7.50	-62.50	15.00	
3.40	2.85	2.16E-03	7.50	-65.00	12.50	Posterior Cingulate, Brodmann Area 23
2.29	2.08	1.87E-02	2.50	-55.00	17.50	
3.33	2.81	2.48E-03	-27.50	62.50	0.00	
3.20	2.73	3.20E-03	-37.50	57.50	12.50	Superior, Middle, and Medial Frontal Gyri
3.18	2.71	3.33E-03	-17.50	55.00	7.50	
3.21	2.73	3.12E-03	-42.50	20.00	-7.50	
3.15	2.69	3.54E-03	-42.50	17.50	5.00	Inferior Frontal Gyrus
2.94	2.55	5.34E-03	-45.00	17.50	15.00	
3.07	2.64	4.12E-03	-60.00	-50.00	42.50	
2.90	2.53	5.78E-03	-52.50	-47.50	55.00	Inferior Parietal Lobule, Brodmann Area 40
2.44	2.19	1.41E-02	-47.50	-40.00	40.00	
2.95	2.56	5.29E-03	-42.50	-65.00	27.50	
2.91	2.53	5.71E-03	-35.00	-72.50	27.50	Middle Temporal Gyrus, Brodmann Area 39
2.52	2.25	1.21E-02	-35.00	-67.50	35.00	
2.89	2.52	5.92E-03	-15.00	17.50	70.00	
2.38	2.15	1.58E-02	-12.50	12.50	62.50	Superior Frontal Gyrus
1.86	1.74	4.11E-02	-5.00	22.50	70.00	

Table 4.3 - Main Effect Of Load p<0.005 unc c20

Voxel Level			MNI 152 Coordinates			Description of Cluster
F	equivZ	p(unc)	X	Y	Z	
25.91	4.39	5.64E-06	0.00	-67.50	12.50	
16.13	3.77	8.06E-05	-5.00	-60.00	0.00	Posterior Cingulate, Brodmann Area 30
15.37	3.71	1.04E-04	-12.50	-65.00	7.50	
20.25	4.07	2.32E-05	20.00	-2.50	-20.00	Right Parahippocampal Gyrus, Amygdala
19.69	4.04	2.72E-05	-27.50	-77.50	22.50	
19.36	4.01	2.99E-05	-32.50	-85.00	12.50	Left Middle Occipital Gyrus
18.04	3.92	4.40E-05	-20.00	-85.00	20.00	
16.56	3.81	7.00E-05	5.00	-37.50	32.50	Right Cingulate Gyrus, Brodmann Area 31
13.99	3.58	1.70E-04	32.50	-20.00	47.50	
9.57	3.07	1.08E-03	35.00	-17.50	40.00	Right Precentral Gyrus, Brodmann Area 4
9.03	2.99	1.40E-03	27.50	-17.50	35.00	
13.10	3.49	2.38E-04	-40.00	27.50	-2.50	Left Inferior Frontal Gyrus
11.84	3.36	3.93E-04	25.00	-25.00	50.00	
9.22	3.02	1.28E-03	20.00	-17.50	45.00	Right Cingulate Gyrus, Brodmann Area 24
9.04	2.99	1.40E-03	20.00	-10.00	40.00	
11.80	3.35	3.99E-04	35.00	57.50	22.50	Right Middle Frontal Gyrus, Brodmann Area 10
11.75	3.35	4.09E-04	-15.00	-32.50	52.50	Left Cerebrum,Frontal Lobe,Sub-Gyral
10.38	3.18	7.41E-04	0.00	-20.00	62.50	
9.64	3.08	1.04E-03	2.50	-10.00	72.50	Inter-Hemispheric, Frontal, Medial Gray Matter
9.88	3.11	9.31E-04	57.50	-47.50	45.00	Right Inferior Parietal Lobule, Brodmann area 40

Region of Interest Analysis

Beta weights were plotted as a measure of correlation to theta power in the regions of interest (posterior cingulate cortex, supplementary motor area, and parahippocampal gyrus). These data can be seen in Figure 4.3. Generally decreasing correlation to theta power was observed in the SMA, while correlations measured in the PCC were generally increasing. Correlations in the PHG showed a less consistent pattern across loads, with 1 back and 3 back conditions possessing the highest correlation to theta power.

Functional Connectivity to PHG

The PHG region of interest was significantly correlated with known regions of the default mode network including the posterior cingulate cortex, the medial frontal cortex, and the lateral parietal regions. PHG also was significantly negatively correlated with regions associated with working memory performance, as shown in Figure 4.4.

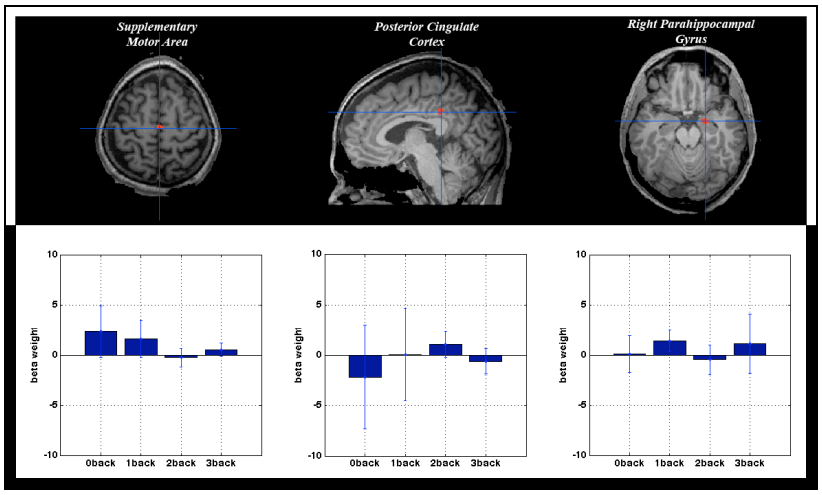

Figure 4.3 - Average correlation to frontal theta power measured in three regions of interest. Regions were identified through measurement of significant changes in their correlation to theta power across loads ($p<0.005$ uncorrected). Solid bars represent the average across subjects, with error bars marking the standard deviation across subjects.

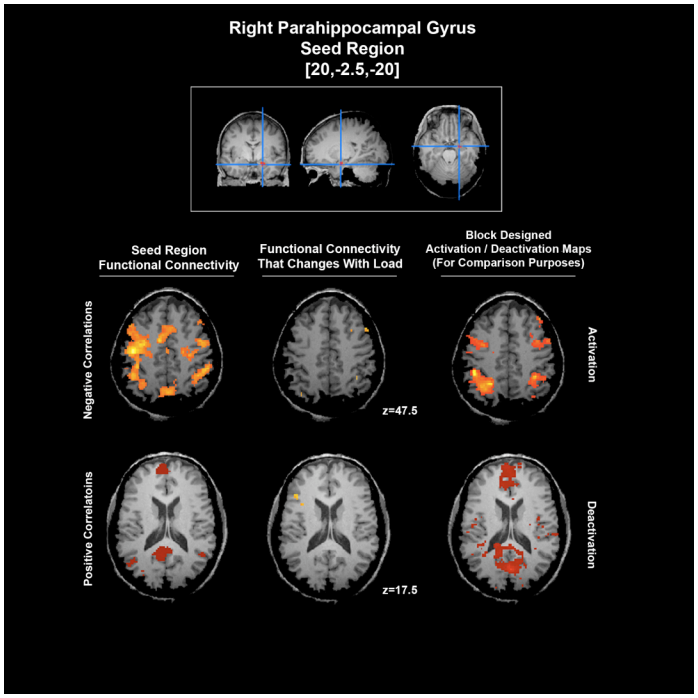

Figure 4.4 - Functional connectivity to the ROI in the parahippocampal gyrus. Note the positive functional connectivity within the default mode network, negative functional connectivity within the working memory network, and relative lack of changes in functional connectivity across loads in most areas. Statistical thresholds were set at an uncorrected $p<0.005$ keeping all clusters regardless of size for all maps.

Discussion

The results presented here demonstrate that measurements of theta power can be used to inform the analysis of steady state fMRI data. Our study suggests that frontal midline theta power is related to the parahippocampal gyrus, and thus to the default mode network. This was shown by our ability to identify the parahippocampal gyrus by mapping those voxels whose BOLD signal's correlation to frontal theta power changes with working memory load (Table 4.3) and then mapping its functional connectivity across loads in the whole brain (Figure 4.4). We have provided new evidence that there are regions whose BOLD signals are positively correlated to theta power in the steady state including bilateral primary motor cortex and the supplementary motor area. This correlation may suggest that those regions play a role in the production of frontal midline theta power, though this would be a topic needing further investigation. Our data support previous studies that suggest that frontal theta power is negatively correlated with default mode regions (specifically the posterior cingulate cortex), and we have shown that significant changes in theta power occur in a variety of regions in addition to the parahippocampal gyrus.

The underlying source of changes in frontal midline theta has been difficult to identify. A number of studies have shown that theta power is related to performance of working memory tasks. (Klimesch 1996b; Klimesch, et al. 1997a; Klimesch, et al. 1997b; Klimesch, et al. 1996; Weiss, et al. 2000) The positive correlations across N-back loads observed here suggest a possible role for sensory motor cortex, in particular the supplementary motor area which may relate to attention. (Coull 2004) These regions have not been identified in previous studies of steady state correlations between BOLD

signals and frontal theta power, though only a handful of studies have investigated BOLD correlates of theta power in the steady state. Negative correlations have been identified in the default mode network by at least two studies (Scheeringa, et al. 2007; Scheeringa, et al. 2009), however these studies focused on either data acquired in the resting state or data acquired during the Sternberg working memory task. Both of these conditions are significantly different from the steady state N-back conditions focused on here. The Sternberg task is a paradigm which requires much less frequent updating of working memory content, instead providing extended maintenance intervals which may themselves be interesting. Another difference between this study and those previously reported is the way in which theta power time courses were calculated. Those studies by Sheeringa et al. used spatial independent component analysis to estimate independent sources with frontal midline topology prior to frequency band analysis. This blind source separation may exclude temporal variance that is not ignored by other studies of theta power.

Another topic of debate is whether the hippocampus plays a role in driving production of frontal midline theta power measured at the scalp and what that role may be. While direct measurements of theta oscillations have been recorded from the hippocampus in rodents, cats, dogs, non-human primates and humans, attributing a specific function to these signals has proven difficult (thoroughly discussed by (Buzsaki 2005)). Frontal midline theta power measured on the scalp has more consistently been liked to attention, memory encoding, memory maintenance, among other functions, which are all involved with accurate performance of the N-back task. Our data suggest the right parahippocampal cortex may be functionally linked to those regions responsible

for observed theta power at the scalp. It is unlikely that parahippocampal cortex plays a direct role in generating FMθ due to its location and weak BOLD correlations under some N-back conditions, though its load dependent changes in correlations to theta, its association with the default mode network during steady state N-back tasks (shown in Figure 4.4), and its established role in some working memory paradigms (Ranganath and Rainer 2003; Stern, et al. 2001) support the view that the parahippocampal gyrus is functionally related to FMθ. With some studies suggesting that frontal midline default mode regions directly generate FMθ, the strong functional connectivity between parahippocampal gyrus and these regions across N-back loads may be significant.

Conclusions

We have shown that frontal midline theta power measured at the scalp has both postive and negative BOLD correlations across a range of steady state N-back tasks. Regions whose BOLD correlates of theta power change with cognitive load include the parahippocampal gyrus, p which has high functional connectivity with the default mode network across the N-back conditions presented here. This latter finding may have implications for how the hippocampus and related regions are associated with those regions generating theta rhythms observed at the scalp.

References

Allen PJ, Josephs O, Turner R. 2000. A method for removing imaging artifact from continuous EEG recorded during functional MRI. Neuroimage 12(2):230-9.

Baddeley A. 1981. The concept of working memory: A view of its current state and probable future development. Cognition 10(1-3):17-23.

Basar-Eroglu C, Basar E, Demiralp T, Schurmann M. 1992. P300-response: possible psychophysiological correlates in delta and theta frequency channels. A review. Int J Psychophysiol 13(2):161-79.

Buzsaki G. 2005. Theta rhythm of navigation: link between path integration and landmark navigation, episodic and semantic memory. Hippocampus 15(7):827-40.

Coull JT. 2004. fMRI studies of temporal attention: allocating attention within, or towards, time. Brain Res Cogn Brain Res 21(2):216-26.

Cunningham CJ, Zaamout Mel F, Goodyear B, Federico P. 2008. Simultaneous EEG-fMRI in human epilepsy. Can J Neurol Sci 35(4):420-35.

Gallinat J, Kunz D, Senkowski D, Kienast T, Seifert F, Schubert F, Heinz A. 2006. Hippocampal glutamate concentration predicts cerebral theta oscillations during cognitive processing. Psychopharmacology (Berl).

Gevins A, Leong H, Smith ME, Le J, Du R. 1995. Mapping cognitive brain function with modern high-resolution electroencephalography. Trends Neurosci 18(10):429-36.

Gevins A, Smith ME, McEvoy L, Yu D. 1997. High-resolution EEG mapping of cortical activation related to working memory: effects of task difficulty, type of processing, and practice. Cereb Cortex 7(4):374-85.

Goldman RI, Stern JM, Engel J, Jr., Cohen MS. 2002. Simultaneous EEG and fMRI of the alpha rhythm. Neuroreport 13(18):2487-92.

Gotman J, Benar CG, Dubeau F. 2004. Combining EEG and FMRI in epilepsy: methodological challenges and clinical results. J Clin Neurophysiol 21(4):229-40.

Hampson M, Peterson BS, Skudlarski P, Gatenby JC, Gore JC. 2002. Detection of functional connectivity using temporal correlations in MR images. Hum Brain Mapp 15(4):247-62.

Horovitz SG, Rossion B, Skudlarski P, Gore JC. 2004. Parametric design and correlational analyses help integrating fMRI and electrophysiological data during face processing. Neuroimage 22(4):1587-95.

Horovitz SG, Skudlarski P, Gore JC. 2002. Correlations and dissociations between BOLD signal and P300 amplitude in an auditory oddball task: a parametric approach to combining fMRI and ERP. Magn Reson Imaging 20(4):319-25.

Klimesch W. 1996a. Event-related power shifts in the theta and alpha bands during encoding and retrieval. Psychophysiology 33:S8-S8.

Klimesch W. 1996b. Memory processes, brain oscillations and EEG synchronization. International Journal of Psychophysiology 24(1-2):61-100.

Klimesch W. 1999. EEG alpha and theta oscillations reflect cognitive and memory performance: a review and analysis. Brain Research Reviews 29(2-3):169-195.

Klimesch W, Doppelmayr M, Pachinger T, Ripper B. 1997a. Brain oscillations and human memory: EEG correlates in the upper alpha and theta band. Neuroscience Letters 238(1-2):9-12.

Klimesch W, Doppelmayr M, Pachinger T, Russegger H. 1997b. Event-related desynchronization in the alpha band and the processing of semantic information. Cognitive Brain Research 6(2):83-94.

Klimesch W, Doppelmayr M, Russegger H, Pachinger T. 1996. Theta band power in the human scalp EEG and the encoding of new information. Neuroreport 7(7):1235-1240.

Lancaster JL, Woldorff MG, Parsons LM, Liotti M, Freitas CS, Rainey L, Kochunov PV, Nickerson D, Mikiten SA, Fox PT. 2000. Automated Talairach atlas labels for functional brain mapping. Hum Brain Mapp 10(3):120-31.

Laufs H, Krakow K, Sterzer P, Eger E, Beyerle A, Salek-Haddadi A, Kleinschmidt A. 2003. Electroencephalographic signatures of attentional and cognitive default modes in spontaneous brain activity fluctuations at rest. Proc Natl Acad Sci U S A 100(19):11053-8.

Lauritzen M, Gold L. 2003. Brain function and neurophysiological correlates of signals used in functional neuroimaging. J Neurosci 23(10):3972-80.

Logothetis NK, Pauls J, Augath M, Trinath T, Oeltermann A. 2001. Neurophysiological investigation of the basis of the fMRI signal. Nature 412(6843):150-7.

Lu H, Zuo Y, Gu H, Waltz JA, Zhan W, Scholl CA, Rea W, Yang Y, Stein EA. 2007. Synchronized delta oscillations correlate with the resting-state functional MRI signal. Proc Natl Acad Sci U S A 104(46):18265-9.

Miller R. 1991. Cortico-hippocampal interplay and the representation of contexts in the brain. Berlin; New York: Springer-Verlag.

Olejniczak P. 2006. Neurophysiologic basis of EEG. J Clin Neurophysiol 23(3):186-9.

Onton J, Delorme A, Makeig S. 2005. Frontal midline EEG dynamics during working memory. Neuroimage 27(2):341-56.

Ragland JD, Turetsky BI, Gur RC, Gunning-Dixon F, Turner T, Schroeder L, Chan R, Gur RE. 2002. Working memory for complex figures: an fMRI comparison of letter and fractal n-back tasks. Neuropsychology 16(3):370-9.

Ranganath C, Rainer G. 2003. Neural mechanisms for detecting and remembering novel events. Nat Rev Neurosci 4(3):193-202.

Reischies FM, Neuhaus AH, Hansen ML, Mientus S, Mulert C, Gallinat J. 2005. Electrophysiological and neuropsychological analysis of a delirious state: The role of the anterior cingulate gyrus. Psychiatry Research-Neuroimaging 138(2):171-181.

Roschke J, Fell J. 1997. Spectral analysis of P300 generation in depression and schizophrenia. Neuropsychobiology 35(2):108-114.

Scheeringa R, Bastiaansen MC, Petersson KM, Oostenveld R, Norris DG, Hagoort P. 2007. Frontal theta EEG activity correlates negatively with the default mode network in resting state. Int J Psychophysiol.

Scheeringa R, Petersson KM, Oostenveld R, Norris DG, Hagoort P, Bastiaansen MC. 2009. Trial-by-trial coupling between EEG and BOLD identifies networks related to alpha and theta EEG power increases during working memory maintenance. Neuroimage 44(3):1224-38.

Stern CE, Sherman SJ, Kirchhoff BA, Hasselmo ME. 2001. Medial temporal and prefrontal contributions to working memory tasks with novel and familiar stimuli. Hippocampus 11(4):337-46.

Weiss S, Muller HM, Rappelsberger P. 2000. Theta synchronization predicts efficient memory encoding of concrete and abstract nouns. Neuroreport 11(11):2357-61.

Yordanova J, Rosso OA, Kolev V. 2003. A transient dominance of theta event-related brain potential component characterizes stimulus processing in an auditory oddball task. Clin Neurophysiol 114(3):529-40.

CHAPTER V

METHODOLOGICAL ADVANCES FOR FMRI MEASUREMENTS OF FUNCTIONAL CONNECTIVITY

Introduction

Overview

Although steady state functional connectivity measurements by fMRI are in routine use, there is continuing interest in improving the methods used and the quality of information obtained. In practice, the methods of image acquisition and analysis used today are very similar to those originally described 14 years ago. (Biswal, et al. 1995) Both image acquisition and image analysis present potential opportunities for improvement. The goal of this chapter is to demonstrate two methodological developments that can improve seed region based functional connectivity analyses of steady state data. The first development focuses on improving spatial resolution through acquiring images at 7T using smaller voxels than are commonly used at 3T. This may decrease partial volume effects that blur and dilute BOLD activity to the benefit of functional connectivity measurements. The second advance is to consider alternative approaches to image analysis. Here we will investigate the utility of mutual information as a nonlinearly sensitive marker of steady state functional connectivity in place of simple linear correlations.

Imaging at 7T to Diminish Partial Volume Averaging

The opportunities for improving fMRI measurements of functional connectivity start at image acquisition. Recent advances in MRI scanners such as using higher fields can provide higher resolution images than are in currently common use. Most fMRI experiments gather relatively low resolution images by echo planar imaging. However, higher resolution images with an adequate signal to noise ratio (SNR) and significant BOLD contrast can be acquired through imaging at higher field strengths, as has been shown at 7T. (Yacoub, et al. 2001) Typical voxel volumes in images acquired at 3T are $27mm^3$, while useful fMRI images can be acquired at 7T with voxel volumes as small as $1mm^3$. As voxel volumes increase, so does the likelihood that the tissue within a voxel is functionally heterogeneous. If only part of the voxel volume contributes to the expected BOLD signal, the rest of the voxel may bring contributions that obfuscate the signal of interest, or at least dilute it. This problem is generally referred to as partial volume averaging. Studying BOLD based functional connectivity at 7T with smaller voxel volumes may decrease partial volume effects and may reveal activation changes more accurately. The question then becomes whether increases in spatial resolution that decrease partial volume averaging affect the estimates of connectivity.

Acquiring fMRI images in larger static magnetic fields (B_0) brings several advantages as well as some disadvantages, and it is important to understand the associated tradeoffs. As B_0 increases, the frequency at which spins precess also increases linearly, meaning increased signal measured via Faraday induction. Increases in signal can be used to decrease voxel volume while maintaining SNR. The common metaphor is that increased SNR is "spent" on decreasing voxel volume.

The benefit of increased SNR is coupled with faster dephasing due to local field inhomogeneities (the basis for the BOLD contrast), improving typical fMRI contrast. However, phase accumulation due to any inhomogeneity in the static magnetic field is also increased, resulting in extraordinary degradation of echo planar images in regions of the brain near large changes in magnetic susceptibility. Also increased are T_1 relaxation times, specific absorption rates (SAR), B_1 inhomogeneities, and dielectric effects, each of which may present significant challenges. These serve only as examples of a wide variety of issues associated with performing fMRI in increasing static field strengths. However, the possibilities presented by working with more potential signal as well as more BOLD contrast from any given tissue make a compelling case for addressing the possible difficulties and acquiring fMRI data at 7T.

Carefully designed studies may be able to avoid some of the problems associated with imaging at 7T while providing an opportunity to assess the benefits of decreasing voxel volume on measurements of functional connectivity. Imaging over a limited number of slices placed in the superior portion of the brain (covering motor cortex, for example) will avoid the large B_0 inhomogeneities that are likely to be present lower in the brain, where the sinuses and the ear canals present large susceptibility borders. Decreasing the through plane coverage at any given in plane resolution also decreases the minimum repetition time between image volumes, compensating for limited gradient performance. Gradient echo imaging schemes reduce the effects of B_1 inhomogeneities compared to spin echo schemes because those B_1 inhomogeneities are not allowed to compound over several refocusing pulses. Single shot EPI schemes also reduce the deposited energy, minimizing the dangers associated with increased SAR. Finally, using

parallel receive coils will reduce the time required for each planar image, reducing distortion associated with remaining B_0 inhomogeneities.

Measuring Connectivity with Mutual Information

Beyond image acquisition, new methods of image analysis may yield improved measurements of functional connectivity. Common measures of connectivity based on correlation are sensitive only to linear relationships between signals. Simple linear measures of connectivity have been used to identify relevant functional networks,. (Biswal, et al. 1995; Cordes, et al. 2000; Hampson, et al. 2002; Kiviniemi, et al. 2004; Lowe, et al. 2000; Lowe, et al. 1998) However, a priori there is little justification for assuming only a linear relationship between signals, yet nonlinear couplings have not been extensively explored. Mutual information may be an improved or complementary marker of functional connectivity due to its sensitivity to both linear and nonlinear relationships between signals (Eckhorn and Popel 1974; Pereda, et al. 2005; Wang, et al. 2005), and has recently been applied to fMRI data. (Salvador, et al. 2007; Salvador, et al. 2005)

Mutual information measured between two signals, as might be measured in calculating functional connectivity between two fMRI time courses, is defined as the difference between their summed individual entropies and their joint entropy, shown in equation 5.1.

$$\mathrm{MI}(X,Y) = \mathrm{H}(X) + \mathrm{H}(Y) - \mathrm{H}(X,Y) \tag{5.1}$$

From a conceptual point of view, the Shannon entropy of a signal is inversely proportional to the certainty with which it can be predicted. (Shannon 1948) Joint entropy can be thought of as the uncertainty in predicting one signal given knowledge of the other. For example, uniformly distributed random signals have higher entropy than normally distributed random signals, which in turn contain more entropy than Poisson distributed random numbers (Pereda, et al. 2005), as is shown in Figure 5.1 where 'H' is Shannon entropy.

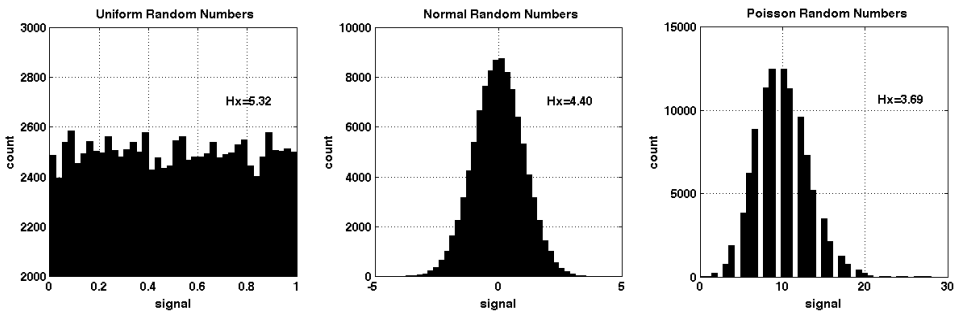

Figure 5. 1 - Histograms of three signals with different probability density functions, and their associated Shannon entropy (mirroring results shown in Pereda E *et al*, 2005, Figure 3).

Mutual information and Pearson's correlation coefficients are conceptually similar. Like Pearson's correlation coefficients, mutual information is essentially a measurement of one signal's relationship to the other scaled by some property of both signals individually. In the case of mutual information, this relationship is defined in terms of individual entropies and joint entropy. In the case of Pearson's correlation coefficients, this relationship is defined in terms of individual variances and covariance.

Equations 5.2 and 5.3 highlight this similarity, where equation 5.3 is identical to equation 5.1 but written in a way to highlight this similarity.

$$r = \frac{\text{covariance between x and y}}{(\text{individual standard deviation of x})(\text{individual standard deviation of y})} \tag{5.2}$$

$$MI(X,Y) = (\text{individual entropy of x}) + (\text{individual entropy of y}) - (\text{joint entropy of x and y}) \tag{5.3}$$

In order to calculate mutual information, the entropy of both signals, and their joint entropy, must be estimated. The most common method for accomplishing this is through estimation of probability density functions for each signal and their joint probability density function via histogram approximation. (Kraskov, et al. 2004) A thorough explanation of how mutual information is calculated via histogram approximation can be found elsewhere (Pereda, et al. 2005), as are more general properties of mutual information (Aczél J. 1975). The definitions of individual entropies and joint entropy in terms of probability density functions (p) are shown here in equations 5.4 and 5.5, with the resulting definition of mutual information being shown in equation 5.6. 'B' refers to the bins used to approximate the probability density functions. For the purposes of this study, we will consider mutual information estimated only with uniform bin widths, though other methods have been described. (Darbellay 1999; Darbellay and Vajda 1999)

$$H(X) = -\sum_{i=1}^{B_X} p_i \ln(p_i) \tag{5.4}$$

$$H(X,Y) = -\sum_{i=1}^{B_X}\sum_{j=1}^{B_Y} p_{ij} \ln(p_{ij}) \tag{5.5}$$

$$MI(X,Y) = \sum p_{ij} \ln\left(\frac{p_{ij}}{p_i p_j}\right) \tag{5.6}$$

Mutual information has been shown to be useful in studying neurophysiologic signals apart from fMRI. Examples include quantifying global synchronization between time series in electroencephalography (EEG) (Kraskov 2004), evaluating the voltage response of modeled Hodgkin-Huxley-type neurons (Machens 2002), and testing the goodness of neuronal encoding models. (Borst and Theunissen 1999) A particularly successful application of mutual information has been in comparing images, as is done in the application of registration techniques (Collignon, et al. 1994; Pluim, et al. 2003; Viola 1995), and these examples together serve to highlight the potential utility of applying mutual information measurements to fMRI data.

However, calculation of mutual information through estimation of probability density functions presents practical challenges for fMRI data. This stems from the relatively slow temporal sampling frequencies typical of fMRI data (about three orders of magnitude slower than EEG), and the low tolerance of participating subjects for exceptionally long scans. Illustrating this point, note that the examples listed in the previous paragraph either make use of simulated data where temporal sampling is not

actually limited, or involve modalities capable of relatively high temporal sampling rates (kHz in the example of EEG). In the case of calculating spatial mutual information, the number of samples is equal to the number of pixels or voxels in the images and this tends to be very large. In fMRI based functional connectivity analyses, the number of samples in a signal is a function of both the time needed to acquire one image volume (typically in the range of 0.5-2s) and the number of images acquired (on the order of hundreds of images for estimation of mutual information).

It is possible that mutual information may reveal previously undetected functional relationships between regions of the brain measured at rest. The challenge presented by the requirement for so many images to be acquired at such relatively slow rates can be addressed by steady state imaging, and specifically by imaging in the resting state. Resting state fMRI eliminates issues of fatigue and task tolerance that may limit the requite number of images from being acquired during the performance of more demanding cognitive tasks.

Summary

The studies presented here have two aims. The first aim is to test whether decreasing voxel volume improves measurements of resting state functional connectivity through decreasing partial volume averaging. We hypothesize that it will, representing an improvement in image acquisition for functional connectivity studies. The second aim is to test whether mutual information is useful as a nonlinearly sensitive marker of functional connectivity. We hypothesize that there may be regions of the brain whose

resting state BOLD signals are nonlinearly related, and that these regions will be identified by mutual information.

Methods & Results

Improving Image Acquisition: Partial Volume Effects Measured at 7T

Overview

In order to evaluate the influence of partial volume effects in functional connectivity measurements, we tested whether the distribution of measured functional connectivity values changed within the sensorimotor system. We also evaluated effects of voxel size on overall BOLD contrast in sensorimotor activations.

Subjects / Hardware

Five subjects were imaged on a Philips Achieva 7T MRI scanner with a volume transmit RF coil and a SENSE receive coil (16 channels, Nova Bionics). All subjects were normal and right handed by self report.

Image Acquisition

Each subject had a series of five functional images acquired, in addition to high resolution anatomic images for structural reference. Subjects initially performed a block designed finger tapping task while images were acquired and analyzed in real time for activation (single shot gradient echo EPI, 90 volumes, FOV=192mm, TR/TE = 2000/28ms, flip θ = 69.6°, voxel size = 1x1x2mm, SENSE factor = 3.92). The task consisted of 20s tapping with the left hand (thumb pressed to each finger in order from

index to pinky, back and forth at the quickest comfortable pace), 20s tapping with the right hand (same scheme), and 20s resting with their eyes open. This sequence was repeated three times. This real time analysis was used to locate the left and right primary motor cortices, as well as the supplementary motor area. Seven contiguous slices covering these structures were identified for further imaging. Four functional connectivity experiments were performed covering these seven slices with increasingly larger voxels. Subjects began each connectivity series by repeating the previously described finger tapping task, after which they were instructed to close their eyes and rest. The post-task resting state lasted for 500s. Images were acquired again using single shot gradient echo EPI (680 volumes, FOV = 192mm, flip θ = 53.8°, TR/TE = 1000/28ms, SENSE factor = 3.92, full k-space acquisition). The voxel volumes used were $2mm^3$, $4.5mm^3$, $8mm^3$, and $18mm^3$ corresponding to resolutions of 1x1x2mm, 1.5x1.5x2mm, 2x2x2mm, and 3x3x2mm. Seven slices were imaged at the highest resolution, while all three other resolutions spanned 13 slices with the central seven matching those slices imaged at 1x1x2mm resolution.

Image Analysis: General Comments

Two major analyses were used to test for effects of partial volume averaging in functional connectivity data. The first analysis was a comparison of the contrast between motor and non-motor voxels in seed region functional connectivity maps measured at each resolution. This analysis served to establish whether the motor network was better distinguished from the background of the brain at one resolution versus the other. The second analysis was a comparison of the steady state correlations between the primary

motor cortices at each resolution and served to establish whether the apparent connectivity within the motor network changed as a function of voxel volume.

Prior to either analysis, all images were corrected for slice timing artifacts and motion artifacts using SPM5 (http://www.fil.ion.ucl.ac.uk/spm/software/spm5/). Each voxel's BOLD time course underwent linear regression of the six estimated motion parameters, low frequency cosine basis functions, and the global time course calculated across the whole brain. All voxels' time courses also were low pass filtered at 0.1Hz using a Chebychev Type II filter, linearly detrended, and de-meaned as well.

Image Analysis #1

Seed region functional connectivity maps were calculated for each subject by manually selecting a single activated voxel along the right primary motor cortex as the seed voxel. This voxel was identified through analysis of the block designed data gathered at the the highest resolution, and its location was interpolated in order to identify the corresponding larger voxel at every other resolution. Thus all connectivity maps were constructed from single voxel seed regions, where the only variable between resolutions is the size of the voxels. All available slices were analyzed at each resolution.

Functional connectivity maps were constructed by calculating the Pearson's correlation between every voxel and the seed voxel. Connectivity maps were segmented into two regions: the motor network, and the non-motor voxels within the brain. Motor voxels were identified at the highest resolution through finding voxels significantly activated during either left or right handed finger tapping according to the blocked task portion of the data acquisition using an F-test (FWE corrected, $p<0.05$, no minimum

cluster size), and were interpolated in order to identify the same voxels at every other resolution. The histogram of functional connectivity measurements were calculated at each resolution for both motor and non-motor voxels, where voxel counts were normalized by the total number of voxels activated at each resolution. Finally, the contrast to noise ratio (CNR) between the motor network and the rest of the brain was calculated as defined by equation 5.7.

$$CNR = \frac{\left[\bar{r}_{motor} - \bar{r}_{non\text{-}motor}\right]}{\sqrt{\frac{1}{N_{non\text{-}motor}} \sum_{i=1}^{N_{non\text{-}motor}} \left(r_{non\text{-}motor} - \bar{r}_{non\text{-}motor}\right)^2}} \tag{5.7}$$

Paired t-tests were conducted to identify significant differences between the CNR measured at different resolutions across subjects.

Image Analysis #2

In order to measure changes in the distribution of connectivity values within the motor system, analysis was restricted to the specific set of voxels belonging to the primary motor cortices (PMC). These voxels were defined as the entire connected cluster of voxels significantly activated ($p<0.05$, no minimum cluster size, FWE corrected) covering the left and right PMC respectively, and were identified based on the highest resolution data (that containing 1x1x2mm voxels). Their locations were interpolated to locate corresponding voxels at every other resolution. Analyses of data containing 1.5x1.5x2mm voxels, 2x2x2mm voxels, and 3x3x2mm voxels was restricted to the central seven slices corresponding to the seven slices acquired with 1x1x2mm voxels.

Pearson's correlation coefficients were measured between every possible pair of voxels at each resolution, and were analyzed for changes in their distribution as a function of voxel volume.

Results

Significant activation was measured in the sensorimotor system in all five subjects imaged at 7T with all four resolutions. The motor network was defined based upon activation measured in the highest resolution data, and the location of those voxels in lower resolution images was calculated via linear interpolation, an example of which can be seen in Figure 5.2. Functional connectivity maps were calculated for each subject at each resolution, an example of which can be seen in Figure 5.3.

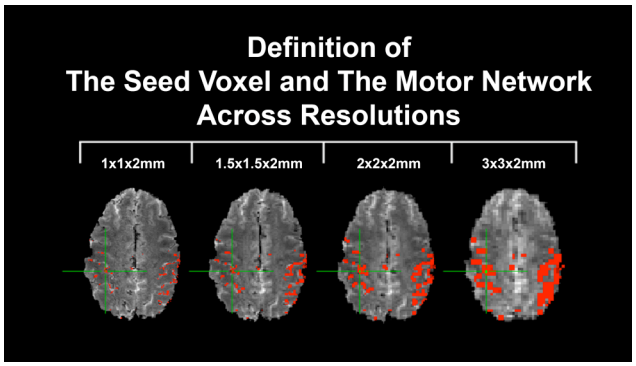

Figure 5. 2 - The seed voxel (green) and the motor network (red) were defined for each subject based on the highest resolution data (representative subject shown). Their locations were interpolated to identify the same voxels across all resolutions.

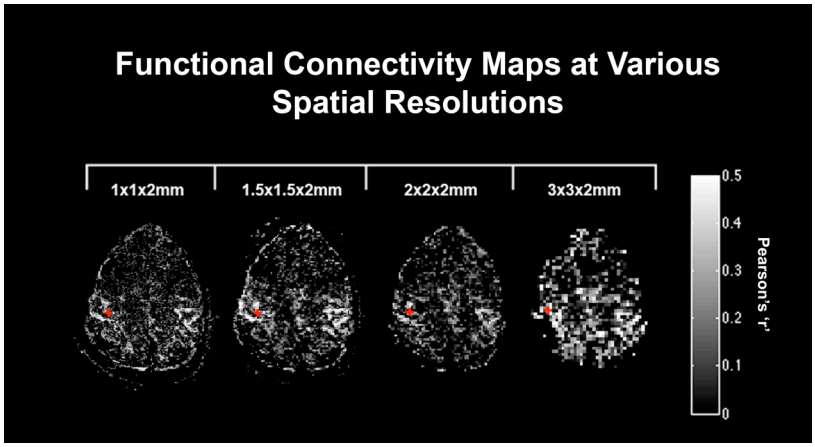

Figure 5. 3 - Examples from one subject of increased specificity associated with functional connectivity mapping with decreasing voxel volumes. The seed voxel is marked with a red '+'.

Described previously as analysis #1, we measured the distributions of correlation measurements among both the motor voxels (red, Figure 5.2) and the non-motor voxels (everything else within the brain, Figure 5.2). Correlations measured within the motor network gradually increased as voxel volume decreased, as shown in Figure 5.4. Correlations measured throughout the rest of the brain remained unchanged as a function of voxel volume (Figure 5.5), and the comparison of the distributions between motor and non-motor voxels can be seen in Figure 5.6. There is increasing separation between the correlations measured in motor voxels verses those measured in non-motor voxels. This separation led to significant differences in the measured CNR between the motor network and the rest of the brain, as shown in Table 5.1. With respect to Table 5.1, note that when the Bonferroni correction for six tests is applied, the differences between the highest and lowest resolution images (3x3x2mm vs. 1x1x2mm) remains significant.

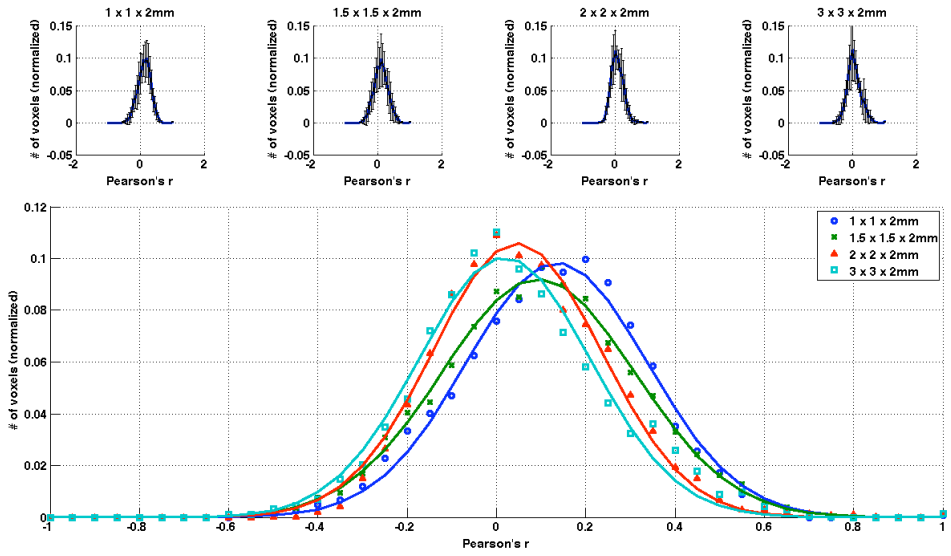

Figure 5. 4 - These are the distributions of functional connectivity (correlation) among MOTOR voxels at each resolution. (Top) The average distribution across subjects, with error bars representing the standard deviations across subjects. (Bottom) The distribution across subjects fit with a Gaussian curve at each resolution.

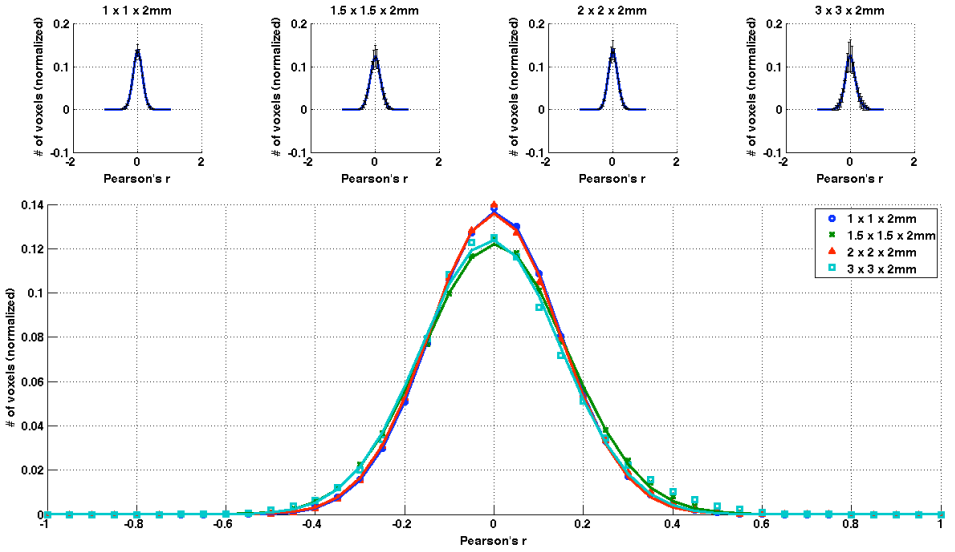

Figure 5. 5 - These are the distributions of functional connectivity (correlation) among NON-MOTOR voxels at each resolution. (Top) The average distribution across subjects with error bars representing the standard deviations across subjects. (Bottom) The distribution across subjects fit with a Gaussian curve at each resolution.

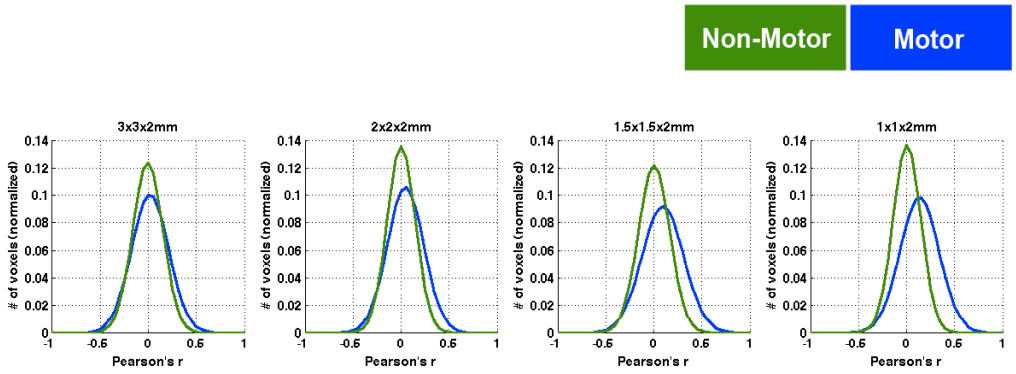

Figure 5. 6 - A comparison of the distributions of correlation among motor and non-motor voxels at each resolution. These curves correspond to those shown in the bottom panes of Figures 5.4 and 5.5.

Table 5.1 - Probability of No Significant CNR Differences Between Resolutions
(p-values from paired t-tests)

	1x1x2mm	1.5x1.5x2mm	2x2x2mm	3x3x2mm
1x1x2mm	-			
1.5x1.5x2mm	0.0396*	-		
2x2x2mm	0.0266*	0.0143*	-	
3x3x2mm	0.0033*	0.0732	0.3172	-

* marks values below 0.05

Previously described as analysis #2, we measured the distribution of all possible pairs of individual voxels in the right and left primary motor corticies, the results of which can be seen in Figure 5.7. As voxel volume decreased, a weak trend towards higher correlations was observed. This is represented by the shifting of the distributions to the right as a function of voxel volume.

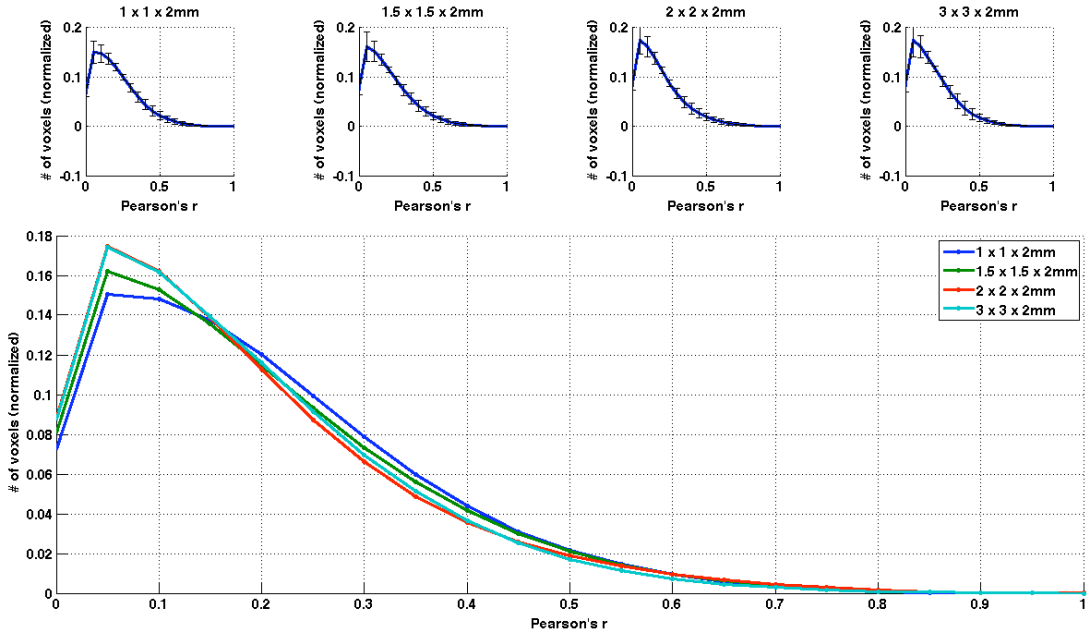

Figure 5. 7 - Pair-wise connectivity measured between all pairs of voxels in the left and right primary motor corticies weakly changes as a function of voxel volume. (Top) The average distributions across subjects at each resolution, with error bars representing the standard deviation across subjects. (Bottom) The average distributions across subjects at each resolution are overlaid for comparison, with smaller voxel volumes showing a slight shift towards higher correlations.

Improving Image Analysis: Mutual Information Measurement of Functional Connectivity

Overview

We used mutual information to measure functional connectivity in the sensorimotor network, and compared the regions identified to those identified by connectivity quantified with Pearson's correlation coefficients. Furthermore, we isolated the nonlinear relationships underlying differences between correlation coefficient and measurements of mutual information through linear regression analyses, confirming that the new regions identified by mutual information were nonlinearly related to the seed region.

Subjects / Image Acquisition

Eight normal subjects were imaged on a Philips Achieva 3T MRI scanner, with a volume transmit and an eight channel SENSE receive coil. One subject was removed from the study due to excessive motion during imaging. In each subject, high resolution T_1 weighted images were acquired for anatomical reference with the same geometry as that used later for functional images.

Each subject had three sets of functional images acquired. First, images were acquired as a localizer for the sensorimotor network during a block designed finger taping task analyzed for activation in real time using IViewBOLD software (TR/TE=2000/35ms, θ_{flip}= 79°, SENSE factor =1.8, FOV=200mm, 2.5mm isotropic voxels). This analysis was used to identify a subset of slices to be imaged more quickly with limited through plane coverage. The finger tapping task consisted of left handed

finger tapping and right handed finger tapping, finishing with a resting period. All three conditions were for 20s each, and the group was repeated three times (180s total).

Focusing on the final two functional runs, one run consisted of a set of 512 images acquired in the resting state. The other run consisted of a set of 180 matching images acquired during a repeat of the finger tapping task. The imaging parameters for both of these runs were as follows: TR/TE=1000/35ms, θ_{flip}= 79°, SENSE factor =1.8, FOV=200mm, 2.5mm isotropic voxels. Through plane coverage was limited to seven slices in three subjects to match that acquired in a separate spin echo fMRI experiment (not presented here), and was expanded to the maximum allowed by the 1s TR (15 slices) in the remaining four subjects.

Image Analysis

All functional data were corrected for slice timing and motion artifacts using SPM5. (http://www.fil.ion.ucl.ac.uk/spm/software/spm5/) All resting state data underwent linear regression of the six estimated motion parameters, low frequency cosine basis functions, and the global time course calculated across the whole brain. All voxels' time courses also were low pass filtered at 0.1Hz using a Chebychev Type II filter, linearly detrended, and de-meaned.

A seed region was defined in the left primary motor cortex based on GLM analysis of the task data. This region was chosen based on the connected cluster of voxels significantly activated by either right or left handed finger tapping as defined by an F-test of both conditions versus rest ($p<0.05$, FWE corrected).

Three maps of functional connectivity were calculated in the resting state data. First, a simple map of Pearson's correlation coefficients was calculated. Second, a map of mutual information, sensitive to linear and non-linear relationships, was calculated according to equation 5.6. Lastly, a map of mutual information sensitive only to nonlinear relationships was calculated. The latter was obtained by linearly regressing the seed region's time course from every voxel's individual time course, and calculating the mutual information between the individual voxel's residual variance and the seed region. These maps will be referred to as 'nonlinear mutual information maps' throughout the rest of this manuscript. All three connectivity maps were thresholded to include only the top 5% of the values within the brain in order to minimize the effects of differences between the distributions of Pearson's correlations and measurements of mutual information, and with a minimum cluster size of ten voxels.

Due to differences between subjects in the number of slices imaged and limited coverage across all subjects, functional connectivity maps were analyzed on the individual subject level, they were not spatially normalized, but were instead individually assessed for similarities/differences between functional connectivity maps across subjects. Specific emphasis was placed on determining whether regions related to the sensorimotor system were identified as being nonlinearly related to the seed region in the left primary motor cortex.

Results

In all seven subjects imaged at 3T, significant activation was measured during the finger tapping task, as was functional connectivity in the resting state. Examples of these

results can be seen in Figure 5.8. Functional connectivity maps measured with mutual information revealed regions that were not identified by Pearson's correlation coefficients along the middle frontal gyrus. These voxels also were identified after linear regression across the brain of the seed region's time course, suggesting that they have a non-linear relationship to the seed region. Their consistency across subjects is evidenced by the lateral-frontal clusters seen in nonlinear mutual information maps shown in Figure 5.9.

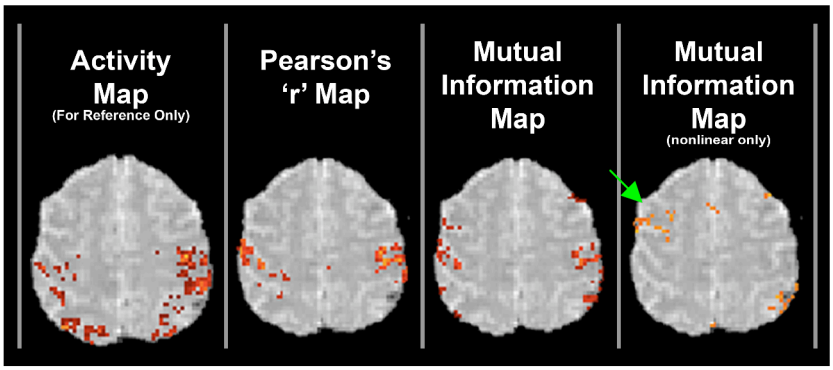

Figure 5. 8 - These are four maps of the sensorimotor network. On the left is a typical activity map, which is compared to three maps of functional connectivity measured in resting state data. The green arrow identifies a region along the middle frontal gyrus that is identified as being nonlinearly related to the left primary motor cortex.

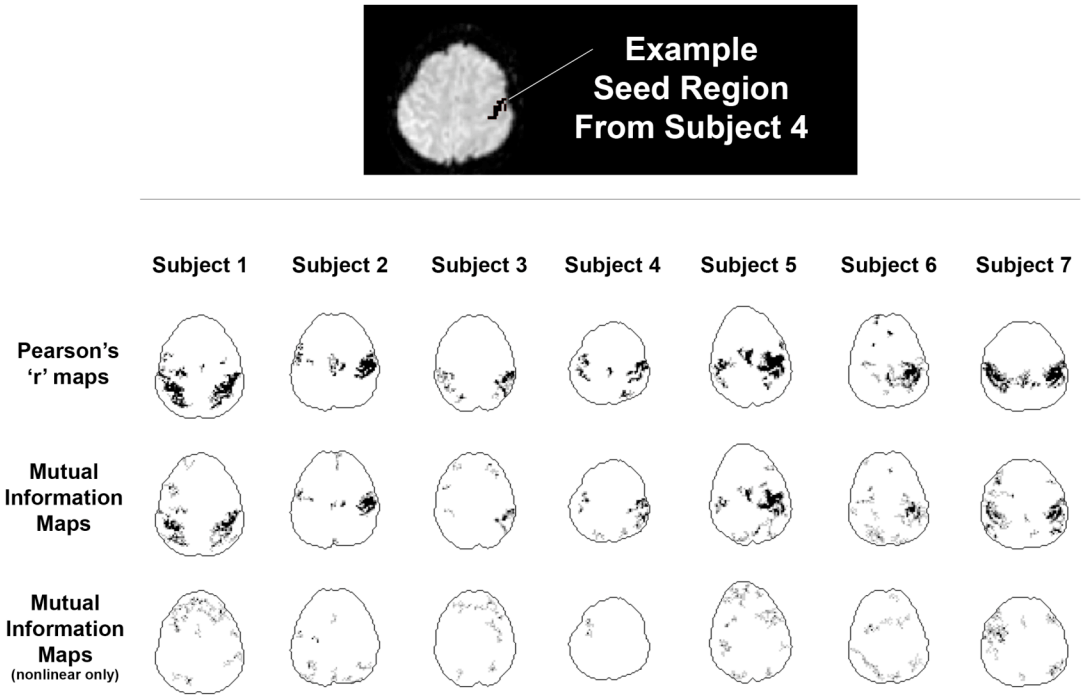

Figure 5. 9 - These are through-plane projections of three functional connectivity maps measured in each subject. Note that lateral frontal regions consistent with the middle frontal gyrus are identified in maps of mutual information that are not identified in maps of correlation coefficients in many subjects. These regions remain after linear regression of the seed region's time course, highlighting the utility of nonlinear sensitivities.

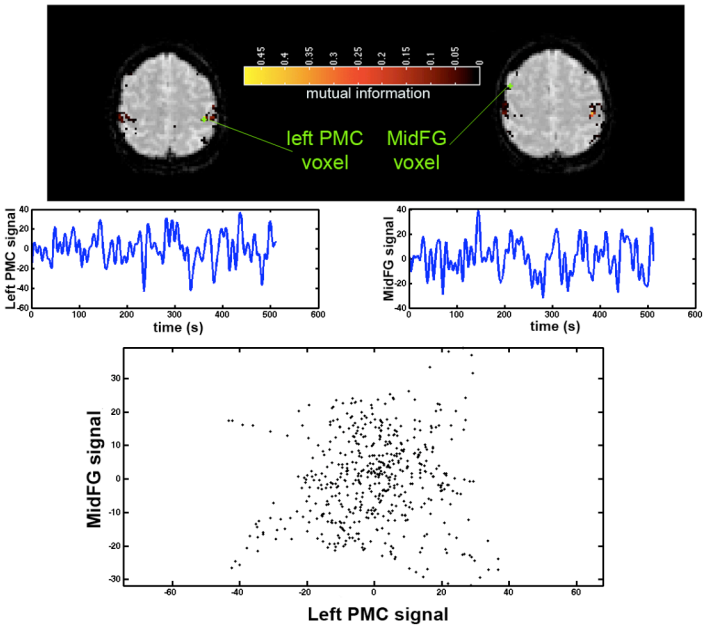

Figure 5. 10 - The signals from two nonlinearly related voxels, as identified via mutual information, were compared with a scatter plot. PMC - primary motor cortex; MidFG - middle frontal gyrus.

Discussion

Here we have demonstrated two methodological advances that may be used in the future to improve functional connectivity analyses performed with fMRI data. In our first experiment, we showed that by acquiring images at 7T and decreasing voxel volume, we were able to reduce detrimental partial volume effects and increase the sensitivity and specificity of functional connectivity measurements. In our second experiment, we demonstrated the potential utility of measures of connectivity by using mutual information to identify the middle frontal gyrus as participating in the motor network. This region is not commonly identified using Pearson's correlation coefficients.

The effects of partial volume averaging have been described in a variety of MRI applications, and our data serve to shed light on this issue in the context of functional

connectivity measurement. Partial volume effects have been described in many different contexts such as classifying multiple sclerosis lesions (Firbank, et al. 1999), tissue segmentation (Bullmore, et al. 1995), and T_2 measurements of vasculature (Stainsby and Wright 1998), and are not unique to MRI data. (Fazio and Perani 2000) With respect to the role of partial volume averaging on measurements of connectivity, most attention has been paid to structural connectivity measurements using diffusion tensor imaging and fiber tracking analyses. (Alexander, et al. 2001; Frank 2001; Tuch DS 1999) In those studies, voxel volume is larger than the axonal fibers of interest. Where fibers of different orientations cross, partial volume effects can cause an apparent decrease in diffusion anisotropy that hides the underlying reality that diffusion is very anisotropic in two or more distinct directions. Our data serve to extend the discussion of partial volume effects in connectivity measurements into measurements of functional connectivity as well.

Our finding that resting state functional connectivity maps more closely mirror typical activity maps as images are acquired at higher spatial resolutions suggests that the activity is more focal may be revealed using lower resolution images. This idea is supported by mounting evidence of functional organization of the brain on spatial scales approaching 1mm, observed in imaging studies of the subdivisions of the thalamus (Gilbert, et al. 2001), optical dominance columns of the visual cortex (Yacoub, et al. 2008), and recently in the digit separation of the somato-sensory cortex. (Stringer EA 2009)

Transitioning functional connectivity studies towards being performed in very large magnetic fields (7T) may provide benefits beyond simply providing access to

higher spatial resolutions. It has been suggested that as B_0 increases, physiological variations in MR signals may increase relative to thermal noise, potentially allowing BOLD variance to dominate temporal signals. (Triantafyllou, et al. 2005) Any increase in physiological BOLD variations relative to thermal noise potentially improves functional connectivity measurements (as it would all fMRI) through increasing temporal SNR. However, physiological noise also includes signals that are not neuronally based, cardiac and respiratory signals being the most dominant, and increases in the power of these signals highlights the importance of removing variance that is not of interest. Reliable mapping of functional connectivity necessitates the separation of variance unique to specific cognitive networks from all the other sources of temporal variance. It is possible that the quality of functional connectivity measurements made at 7T will continue to improve as methods for isolating the 'intrinsic' variance also improve.

By measuring functional connectivity with mutual information, we also have presented evidence of nonlinear relationships between the middle frontal gyrus and the left primary motor cortex, suggesting that the middle frontal gyrus may participate in the sensorimotor network. That this is a nonlinear relationship is supported by two pieces of evidence. First, the middle frontal gyrus is not identified in maps of correlation coefficients, which we know are sensitive only to linear relationships. Second, maps of mutual information retain lateral frontal regions consistent with the middle frontal gyrus after linear relationships to the left primary motor cortex have been removed through linear regression. Given the evidence that there is a nonlinear relationship between these regions, the question becomes whether there is reason to believe that these regions are actually functionally related. Lesion studies have implicated the middle frontal gyrus as

underlying deficites in apraxia patients (Haaland, et al. 2000), and voluntary movement of the right index finger has been shown to induce the Bereitschaftspotential, or the 'readiness potential', originating from a source along the left middle frontal gyrus with corresponding increases in perfusion measured along the middle frontal gyrus with positron emission tomography. (Pedersen, et al. 1998) Middle frontal gyrus has also been implicated in some attention demanding motor tasks. (Lang, et al. 1988) All of these provide support for a functional link between the middle frontal gyrus and primary motor cortex, as implicated by our measurements of mutual information.

Nonlinear relationships can be identified by methods other than through measurement of mutual information, though other methods may not be as sensitive to the variety of nonlinear relationships. Nonlinear curve fitting usually requires a priori definition of a model for the relationship between signals, which may not be known. A common voxel's nonlinear relationship to other voxels may be variable, and those differences mean that parametric curve fitting to one curve may be more appropriate some places than others. Analysis of the full cross correlation function can capture some nonlinear relationships between signals, though this is really limited to phase shifts.

Conclusions

We have demonstrated that measurements of functional connectivity may be improved through acquisition of higher resolution images, and through implementation of data analyses sensitive to nonlinear couplings. Our studies at 7T show that smaller voxels, which decrease partial volume effects, help separate the sensorimotor network from the rest of the brain in typical maps of functional connectivity and increase r values.

Implementing mutual information as a nonlinear metric of functional connectivity identified regions of the sensorimotor network that were not identified by Pearson's correlation coefficients, namely the middle frontal gyrus.

References

Aczél J. DZ. 1975. On Measures of Information and Their Characterizations. New York: Academic Press. 234 p.

Alexander AL, Hasan KM, Lazar M, Tsuruda JS, Parker DL. 2001. Analysis of partial volume effects in diffusion-tensor MRI. Magn Reson Med 45(5):770-80.

Biswal B, Yetkin FZ, Haughton VM, Hyde JS. 1995. Functional connectivity in the motor cortex of resting human brain using echo-planar MRI. Magn Reson Med 34(4):537-41.

Borst A, Theunissen FE. 1999. Information theory and neural coding. Nat Neurosci 2(11):947-57.

Bullmore E, Brammer M, Rouleau G, Everitt B, Simmons A, Sharma T, Frangou S, Murray R, Dunn G. 1995. Computerized brain tissue classification of magnetic resonance images: a new approach to the problem of partial volume artifact. Neuroimage 2(2):133-47.

Collignon A, Vandermeulen D, Suetens P, Marchal G. 1994. Registration of 3d Multimodality Medical Images Using Surfaces and Point Landmarks. Pattern Recognition Letters 15(5):461-467.

Cordes D, Haughton VM, Arfanakis K, Wendt GJ, Turski PA, Moritz CH, Quigley MA, Meyerand ME. 2000. Mapping functionally related regions of brain with functional connectivity MR imaging. AJNR Am J Neuroradiol 21(9):1636-44.

Darbellay GA. 1999. An estimator of the mutual information based on a criterion for independence. Computational Statistics & Data Analysis 32(1):1-17.

Darbellay GA, Vajda I. 1999. Estimation of the information by an adaptive partitioning of the observation space. Ieee Transactions on Information Theory 45(4):1315-1321.

Eckhorn R, Popel B. 1974. Rigorous and Extended Application of Information-Theory to Afferent Visual System of Cat .1. Basic Concepts. Kybernetik 16(4):191-200.

Fazio F, Perani D. 2000. Importance of partial-volume correction in brain PET studies. J Nucl Med 41(11):1849-50.

Firbank MJ, Coulthard A, Harrison RM, Williams ED. 1999. Partial volume effects in MRI studies of multiple sclerosis. Magn Reson Imaging 17(4):593-601.

Frank LR. 2001. Anisotropy in high angular resolution diffusion-weighted MRI. Magnetic Resonance in Medicine 45(6):935-939.

Gilbert AR, Rosenberg DR, Harenski K, Spencer S, Sweeney JA, Keshavan MS. 2001. Thalamic volumes in patients with first-episode schizophrenia. Am J Psychiatry 158(4):618-24.

Haaland KY, Harrington DL, Knight RT. 2000. Neural representations of skilled movement. Brain 123:2306-2313.

Hampson M, Peterson BS, Skudlarski P, Gatenby JC, Gore JC. 2002. Detection of functional connectivity using temporal correlations in MR images. Hum Brain Mapp 15(4):247-62.

Kiviniemi V, Kantola JH, Jauhiainen J, Tervonen O. 2004. Comparison of methods for detecting nondeterministic BOLD fluctuation in fMRI. Magn Reson Imaging 22(2):197-203.

Kraskov A. 2004. Synchronization and Interdependence Measures and their Applicatoins to the Electroencephalogram of Epilepsy Patients and Clustering of Data [thesis]: University of Wuppertal. 106 p.

Kraskov A, Stogbauer H, Grassberger P. 2004. Estimating mutual information. Phys Rev E Stat Nonlin Soft Matter Phys 69(6 Pt 2):066138.

Lang W, Lang M, Podreka I, Steiner M, Uhl F, Suess E, Muller C, Deecke L. 1988. DC-potential shifts and regional cerebral blood flow reveal frontal cortex involvement in human visuomotor learning. Exp Brain Res 71(2):353-64.

Lowe MJ, Dzemidzic M, Lurito JT, Mathews VP, Phillips MD. 2000. Correlations in low-frequency BOLD fluctuations reflect cortico-cortical connections. Neuroimage 12(5):582-7.

Lowe MJ, Mock BJ, Sorenson JA. 1998. Functional connectivity in single and multislice echoplanar imaging using resting-state fluctuations. Neuroimage 7(2):119-32.

Machens CK. 2002. Adaptive sampling by information maximization. Phys Rev Lett 88(22):228104.

Pedersen JR, Johannsen P, Bak CK, Kofoed B, Saermark K, Gjedde A. 1998. Origin of human motor readiness field linked to left middle frontal gyrus by MEG and PET. Neuroimage 8(2):214-20.

Pereda E, Quiroga RQ, Bhattacharya J. 2005. Nonlinear multivariate analysis of neurophysiological signals. Prog Neurobiol 77(1-2):1-37.

Pluim JP, Maintz JB, Viergever MA. 2003. Mutual-information-based registration of medical images: a survey. IEEE Trans Med Imaging 22(8):986-1004.

Salvador R, Martinez A, Pomarol-Clotet E, Sarro S, Suckling J, Bullmore E. 2007. Frequency based mutual information measures between clusters of brain regions in functional magnetic resonance imaging. Neuroimage 35(1):83-8.

Salvador R, Suckling J, Schwarzbauer C, Bullmore E. 2005. Undirected graphs of frequency-dependent functional connectivity in whole brain networks. Philos Trans R Soc Lond B Biol Sci 360(1457):937-46.

Shannon CE. 1948. A mathematical theory of communication. Bell System Technical Journal 27.

Stainsby JA, Wright GA. 1998. Partial volume effects on vascular T2 measurements. Magn Reson Med 40(3):494-9.

Stringer EA FR, Gatenby JC, Chen LM, Gore JC. Separation and Reproducibility of Touch Activations in Areas 3b and 1 within the Primary Somatosensory Cortex by High Resolution fMRI at 7T 2009; Honolulu, Hawaii, USA.

Triantafyllou C, Hoge RD, Krueger G, Wiggins CJ, Potthast A, Wiggins GC, Wald LL. 2005. Comparison of physiological noise at 1.5 T, 3 T and 7 T and optimization of fMRI acquisition parameters. Neuroimage 26(1):243-250.

Tuch DS WR, Belliveau JW, Wedeen VJ. High angular resolution diffusion imaging of the buman brain; 1999; Philadelphia, PA. p 321.

Viola P. 1995. Alignment by maximization of mutual information. Boston, PA: Massachusetts Institute of Technology.

Wang Q, Shen Y, Zhang JQ. 2005. A nonlinear correlation measure for multivariable data set. Physica D-Nonlinear Phenomena 200(3-4):287-295.

Yacoub E, Harel N, Ugurbil K. 2008. High-field fMRI unveils orientation columns in humans. Proc Natl Acad Sci U S A 105(30):10607-12.

Yacoub E, Shmuel A, Pfeuffer J, Van De Moortele PF, Adriany G, Andersen P, Vaughan JT, Merkle H, Ugurbil K, Hu X. 2001. Imaging brain function in humans at 7 Tesla. Magn Reson Med 45(4):588-94.